

**LASER SURFACE MODIFICATION OF CR-
MO POWDERS ON GREY CAST IRON FOR
SURFACE PROPERTIES IMPROVEMENT**



ZULHISHAMUDDIN BIN ABD RAHMAN

Doctor of Philosophy (Mechanical Engineering)

UNIVERSITI MALAYSIA PAHANG

UNIVERSITI MALAYSIA PAHANG

DECLARATION OF THESIS AND COPYRIGHT

Author's Full Name : ZULHISHAMUDDIN BIN ABD RAHMAN

Date of Birth : 6 DECEMBER 1979

Title : LASER SURFACE MODIFICATION OF CR-MO POWDERS
ON GREY CAST IRON FOR SURFACE PROPERTIES
IMPROVEMENT

Academic Session : SESSION 2017/18

I declare that this thesis is classified as:

- CONFIDENTIAL (Contains confidential information under the Official Secret Act 1997)*
- RESTRICTED (Contains restricted information as specified by the organization where research was done)*
- OPEN ACCESS I agree that my thesis to be published as online open access (Full Text)

I acknowledge that Universiti Malaysia Pahang reserves the following rights:

1. The Thesis is the Property of Universiti Malaysia Pahang
2. The Library of Universiti Malaysia Pahang has the right to make copies of the thesis for the purpose of research only.
3. The Library has the right to make copies of the thesis for academic exchange.

Certified by:

(Student's Signature)

(Supervisor's Signature)

791206015341
Date:

SYARIFAH NUR AQIDA BINTI
SYED AHMAD
Date:

SUPERVISOR'S DECLARATION

We hereby declare that We have checked this thesis and in our opinion, this thesis is adequate in terms of scope and quality for the award of the degree of Doctor of Philosophy (Mechanical Engineering).

(Supervisor's Signature)

Full Name : DR. SYARIFAH NUR AQIDA BINTI SYED AHMAD

Position : ASSOCIATE PROFESSOR

Date :

(Co-supervisor's Signature)

Full Name : IR. DR. MOHD RASHIDI BIN MAAROF

Position : SENIOR LECTURER

Date :

STUDENT'S DECLARATION

I hereby declare that the work in this thesis is based on my original work except for quotations and citations which have been duly acknowledged. I also declare that it has not been previously or concurrently submitted for any other degree at Universiti Malaysia Pahang or any other institutions.

(Student's Signature)

Full Name : ZULHISHAMUDDIN BIN ABD RAHMAN

ID Number : PMM13005

Date :



UMP

LASER SURFACE MODIFICATION OF CR-MO POWDERS ON GREY CAST
IRON FOR SURFACE PROPERTIES IMPROVEMENT

The logo of the University of Malaysia Pahang (UMP) is a shield-shaped emblem. It features a central white vertical band. The left side of the shield is light blue, and the right side is light purple. At the top, there is a yellow diamond shape with a blue and green circular swoosh above it. The letters 'UMP' are prominently displayed in white at the bottom of the shield.

ZULHISHAMUDDIN BIN ABD RAHMAN

Thesis submitted in fulfillment of the requirements
for the award of the degree of
Doctor of Philosophy (Mechanical Engineering)

Faculty of Mechanical Engineering

UNIVERSITI MALAYSIA PAHANG

JULY 2018

ACKNOWLEDGEMENTS

I would like to express my gratitude to my supervisors Associate Professor Dr. Syarifah Nur Aqida Binti Syed Ahmad and Ir. Dr. Mohd Rashidi Bin Maarof. Their enthusiasm and kindness have inspired me the whole time and were never wasted. They have provided knowledge, guidance, and advice that was invaluable throughout the course of this research. Plus the opportunities given to me during the past years have made my research works more exciting than I have imagined. Also for Dr Izwan Bin Ismail for his support and motivation during my journey.

I gratefully acknowledge the financial support from the Ministry of Higher Education Malaysia.

I thank the laser processing research team Dr. Erween Bin Abd Rahim, Zazuli Bin Mohid and Faizal at Universiti Tun Hussein Onn for their support. I thank all the technical staff in Universiti Malaysia Pahang for sharing and friendly environment.

A special appreciation to my beloved wife and children, Faradizyana, Husna, Imran and Zahra. Their love has made my PhD journey more meaningful and wonderful.

Last but not least, many thanks to my supportive father, mother, brothers, sisters and in laws for their never ending support.



UMP

ABSTRAK

Kebelakangan ini dalam industri, komponen yang dihasilkan daripada besi tuang kelabu (seperti lapisan silinder dan disk brek) mengalami kecatatan kehausan dan kekaratan disebabkan oleh suhu yang tinggi, tekanan dan geseran yang menyumbang kepada pelbagai keadaan yang tegang. Tujuan kajian ini ialah untuk mengenalpasti dan membuat perubahan pada permukaan besi tuang kelabu dengan menggunakan kaedah mod proses laser nadi. Untuk mengukuhkan permukaan tersebut penambahan sebatian Cr-Mo diletakkan di atas permukaan. Hubungan parameter untuk proses ini dianalisis dengan menggunakan analisis statistik. Saringan awal rekabentuk eksperimen telah membawa kepada lebih banyak penemuan untuk mengoptimumkan rekabentuk dengan lebih terperinci. Dalam kajian ini, Laser Nd:YAG sistem model 300HPS dengan panjang gelombang 10.64 μm telah digunakan. Kajian awalan telah dilakukan dengan menggunakan rekabentuk model eksperimen 2 peringkat faktor pada laser cairan permukaan dengan saiz laser 1.0 mm, 1.2 mm, 1.4 mm dan 1.7 mm. Kajian awalan ini adalah untuk mengenalpasti parameter laser yang optimum dan saiz laser yang sesuai untuk menghasilkan bentuk geometri, kekasaran dan kekerasan yang baik pada besi tuang kelabu. Berdasarkan pada pengoptimuman laser parameter dalam laser cairan, saiz laser 1.0 mm dengan P_p , PRF dan S diantara 800 hingga 1200 W, 80 hingga 90 Hz dan 19.2 hingga 21.6 mms^{-1} digunakan. Kemudian, eksperimen yang komprehensif dengan menggabungkan komponen campuran Cr dan Mo bersama faktor proses telah digunakan dalam proses laser pelapisan permukaan. Kedua-dua pemrosesan laser ini dibantu oleh gas argon pada kelajuan malar 10 Lmin^{-1} . Sampel yang telah di laser disediakan untuk kajian metalografi dan dicirikan untuk menentukan sifat fizikal dan mekanikal. Kajian metalografi dan analisis komposisi kimia dijalankan menggunakan mikroskop pengimbas elektron yang disepadukan dengan spektroskopi sinar-x penyebaran tenaga. Sistem XRD dengan radiasi Cu $K\alpha$ dan panjang gelombang 1.54 \AA digunakan untuk mengesan kristal dan fasa permukaan yang telah diubah dengan laser. Profil permukaan diukur menggunakan sistem pengukur profilometri stylus. Manakala sifat kekerasan permukaan yang telah diubah diukur dengan menggunakan lekukan berlian mikro-Vickers. Lapisan permukaan besi tuang kelabu yang telah diubah suai dengan tambahan lapisan campuran Cr-Mo telah menunjukkan penghapusan grafit dan pembentukan struktur baru dendritik dengan saiz pembentukan zarah pada saiz 32 nm. Fasa karbida juga telah dikesan di permukaan yang terdiri daripada M_2C , M_3C_2 and M_{23}C_6 . Kekerasan maksimum yang telah diubah suai pada besi tuang kelabu ialah 1039.7 $\text{HV}_{0.1}$ pada parameter laser 1200 W, 80 Hz dan campuran 32.3% Cr dan 67.7% Mo. Satu lagi penemuan yang penting dalam kajian ini ialah rintangan haus telah meningkat dengan membuat lapisan campuran Cr-Mo di permukaan besi tuang kelabu. Hubungan antara parameter laser dan tambahan campuran Cr-Mo dibangunkan untuk pemahaman lebih lanjut tentang kesan parameter laser pada campuran Cr-Mo. Penemuan ini penting bagi menghasilkan teknik pengerasan permukaan untuk tujuan rintangan haus, pengoksidaan dan rintangan haba terutamanya untuk komponen pelapik silinder dan cakera brek.

ABSTRACT

Recently, in industrial area, grey cast iron component parts (such as cylinder liner and break disc) experienced wear defect and corrosion due to the usage in high temperature, pressure and mechanical friction, which contribute to multifaceted, high-stress condition. The purpose of this research is to develop a modified surface layer on grey cast iron using laser melting and laser cladding. To strengthen the surface, Cr-Mo powder were added on the surface. The parameter on this process were analyzed using statistical analysis. The presented work is an investigation and modification of the laser surface of grey cast iron using pulse laser processing mode. Initial screening experimental designs was conducted and lead to more optimized detailed designs. A laser Nd:YAG system 300HPS model with 10.64 μm wavelength was used. Preliminary experiment of design of experiment 2-level factorial model were conducted in laser surface melting grey cast iron with spot size 1.0 mm, 1.2 mm, 1.4 mm and 1.7 mm to investigate optimized laser parameter and suitable spot size for the surface geometry, surface roughness and hardness. Based on the optimization laser parameter in laser surface melting, laser spot size of 1.0 mm with PP, PRF and S in range of 800 to 1200 W, 80 to 90 Hz and 19.2 to 21.6 mms^{-1} were used in laser surface cladding respectively. A comprehensive experiment that combines mixture components of Cr and Mo with process factor were used in laser surface cladding. The laser processing was constantly assisted by in line argon gas at 10 Lmin^{-1} . Laser processed samples were prepared for metallographic study and were characterized for physical and mechanical properties. The metallographic study and chemical composition analysis were conducted using scanning electron microscope integrated with energy dispersive x-ray spectroscopy. The crystallinity and phase detection of the modified surface were conducted using an XRD system with Cu K α radiation and wavelength of 1.54 \AA . The surface profile was measured using stylus profilometry measuring systems. The hardness properties of the modified surface were measured by micro-Vickers diamond indentation. A modified surface layer (Cr-Mo mixture added) had shown the elimination of graphite and a new structure of dendritic with the formation of particles in size of 32 nm had developed. A new phase of carbide was also detected on the surface which mainly contained of M_2C , M_3C_2 and M_{23}C_6 . A maximum hardness modified grey cast iron of 1039.7 $\text{HV}_{0.1}$ is achieved at laser surface cladding parameter at 1200 W, 80 Hz and mixture of 32.3 % Cr and 67.7 % Mo. Another important finding was that wear resistance increases by adding the mixture of Cr and Mo on the grey cast iron surface. A relationship between laser surface parameter and mixture of Cr and Mo was established for further understanding of the effects of the laser parameters. These findings are significant to the establishment of surface hardening technique for wear resistance, oxidation and thermal resistance for cylinder liner and break disc.

TABLE OF CONTENT

DECLARATION	
TITLE PAGE	
ACKNOWLEDGEMENTS	ii
ABSTRAK	iii
ABSTRACT	iv
TABLE OF CONTENT	v
LIST OF TABLES	ix
LIST OF FIGURES	xi
LIST OF SYMBOLS	xv
LIST OF ABBREVIATIONS	xvi
CHAPTER 1 INTRODUCTION	1
1.1 Research Background	1
1.2 Problem Statement	3
1.3 Research Objective	5
1.4 Research Scope	6
1.5 Thesis Outline	6
CHAPTER 2 LITERATURE REVIEW	8
2.1 Introduction	8
2.2 Grey Cast Iron Advancement	8
2.2.1 Failure in Grey cast iron	10
2.2.2 Cladding with Cr and Mo	14

2.3	Advanced Surface Modification on Grey Cast iron	20
2.3.1	Laser Surface Melting of Grey cast Iron	24
2.3.2	Laser Cladding of Grey Cast Iron	28
2.4	Laser Surface Modification Parameter	32
2.4.1	Laser Beam Density and Interaction Time	32
2.4.2	Laser Spot Size	38
2.4.3	Laser Power and Traverse Speed	40
2.4.4	Laser Nd:YAG System	44
2.5	Pre-Placed Powder on Substrate Surface	45
2.6	Design of Experiment	49
2.7	Summary	51
CHAPTER 3 METHODOLOGY		54
3.1	Introduction	54
3.2	Material Preparation	56
3.3	Preliminary Experiment: Laser Surface Melting	57
3.4	Experiment for Laser Surface Cladding	59
3.4.1	Sample Preparation for Laser Cladding	60
3.4.2	Mixture Design of Experiment	61
3.5	Laser Nd:YAG System	63
3.6	Laser Spot Size	64
3.7	Characterizations Techniques	65
3.7.1	Sample Preparation	66
3.7.2	Metallographic Study	67
3.7.3	Microhardness Test	68
3.7.4	Surface Profilometry	69

3.7.5	X-ray Diffraction Analysis (XRD)	69
3.7.6	Energy Dispersive Spectrometer (EDS)	70
3.8	Sliding Wear Experiment	70
3.9	Statistical Analysis	72
CHAPTER 4 RESULT AND DISCUSSION		75
4.1	Introduction	75
4.2	Preliminary Findings of Laser Surface Melting on Grey Cast Iron	77
4.2.1	Metallography Study	78
4.2.2	Surface Geometry	80
4.2.3	Surface Properties of Laser Melted Grey Cast Iron	83
4.2.4	X-ray diffraction for laser surface melting	87
4.2.5	ANOVA for Laser Surface Melting of Grey Cast Iron	89
4.3	Laser Surface Cladding of Grey Cast Iron	93
4.3.1	Metallographic Study	94
4.3.2	X- ray diffraction for laser surface cladding	97
4.3.3	Energy Dispersive Spectrometer Analysis	100
4.3.4	Hardness Properties	103
4.3.5	Surface Profile	106
4.4	Statistical Analysis	108
4.4.1	ANOVA for Laser Cladding	108
4.4.2	Optimization Laser Cladding	112
4.5	Laser Surface Cladding from Optimisation Parameter	115
4.5.1	Sliding Wear Test	115
4.6	Summary Result and Findings	120

CHAPTER 5 CONCLUSION	123
5.1 Introduction	123
5.2 Conclusion	123
5.3 Future Work	125
REFERENCES	127
APPENDIX A LASER SURFACE MELTING PARAMETER AT SPOT SIZE 1.0 MM AND 1.2 MM	137
APPENDIX B LASER SURFACE MELTING PARAMETER AT SPOT SIZE 1.4 MM AND 1.7 MM	138
APPENDIX C ARDUINO PROGRAMME	139
APPENDIX D DESIGN SOLUTION IN DOE LASER SURFACE MELTING AT SPOT SIZE 1.0 MM AND 1.2 MM	142
APPENDIX E DESIGN SOLUTION IN DOE LASER SURFACE MELTING AT SPOT SIZE 1.4 MM	143
APPENDIX F DESIGN SOLUTION IN DOE LASER SURFACE MELTING AT SPOT SIZE 1.7 MM	144
APPENDIX G LIST OF PUBLICATIONS	145

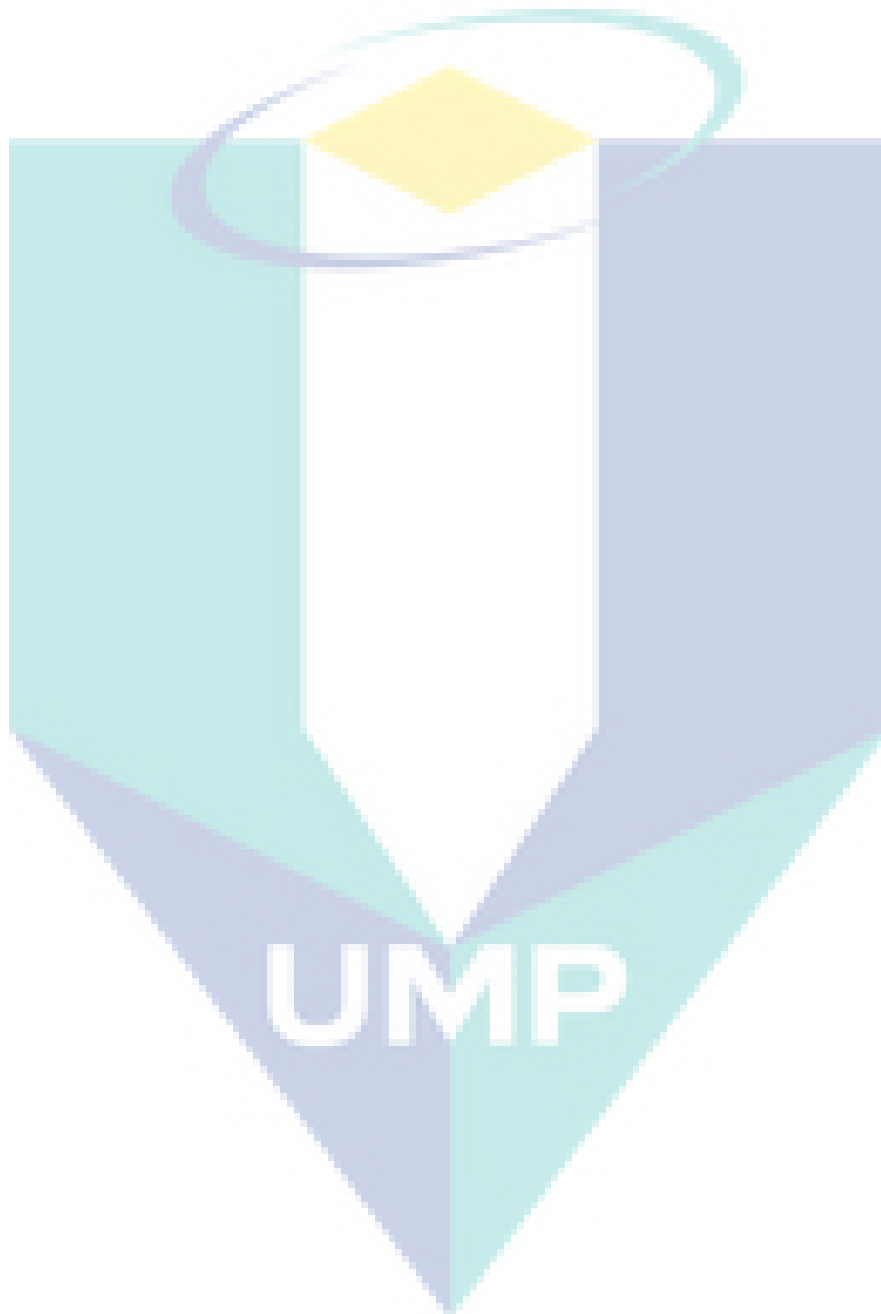
The image features a large, semi-transparent watermark of the UMP logo. The logo consists of a stylized 'U' and 'M' shape in shades of blue and green, with the letters 'UMP' in white, bold, sans-serif font centered within the 'U' shape.

UMP

LIST OF TABLES

Table 1.1	Summary report on gray cast iron failure.	4
Table 2.1	Characteristics of alloy carbide in steels.	15
Table 2.2	Advantage laser surface melting and laser cladding in cast iron.	23
Table 2.3	Previous researcher used laser surface melting at different setting for cast iron.	28
Table 2.4	Dimensions and average hardness of laser surface melting processed at different conditions.	44
Table 2.5	Paint technique used from previous researcher.	46
Table 2.6	Summary Literature review findings in grey cast iron modification with Cr and Mo.	53
Table 3.1	Chemical composition of HT250 grey cast iron.	56
Table 3.2	Summary of parameter settings for laser melting in low and high range for each laser spot size.	59
Table 3.3	Parameter setting for laser surface cladding of grey cast iron at spot size 1.0 mm.	62
Table 3.4	Laser Nd:YAG system 300HPS specification.	64
Table 3.5	Technique used to characterise the laser processed samples.	66
Table 3.6	Sliding wear test parameter setting.	72
Table 4.1	Molten pool radius on grey cast iron surface resulted from different laser.	82
Table 4.2	Microhardness and cooling rate of the melting zone laser surface melting range at four different spot sizes.	87
Table 4.3	ANOVA results for modified surface roughness response.	90
Table 4.4	ANOVA results for modified surface hardness response.	91
Table 4.5	Constraints in design optimization for laser surface melting.	92
Table 4.6	Processing parameter setting based on high desirability for spot size 1.0 mm, 1.2 mm, 1.4 mm and 1.7 mm.	93
Table 4.7	Chemical composition of the gary cast iron substrate analysed from selected area.	100
Table 4.8	Composition analysis for laser clad samples.	102
Table 4.9	Microhardness of cladding zone at spot sizes 1.0 mm.	105
Table 4.10	Surface roughness of clad zone at spot sizes 1.0 mm.	107
Table 4.11	ANOVA results for modified surface roughness response laser cladding.	109
Table 4.12	ANOVA results for modified surface hardness response laser cladding.	111

Table 4.13	Constraints in design optimization with microhardness were maximized and surface roughness was minimized.	113
Table 4.14	Predicted parameters for laser cladding of grey cast iron.	113
Table 4.15	Summary of laser parameters setting ranges and characterization results for factorial model and mixture model.	122



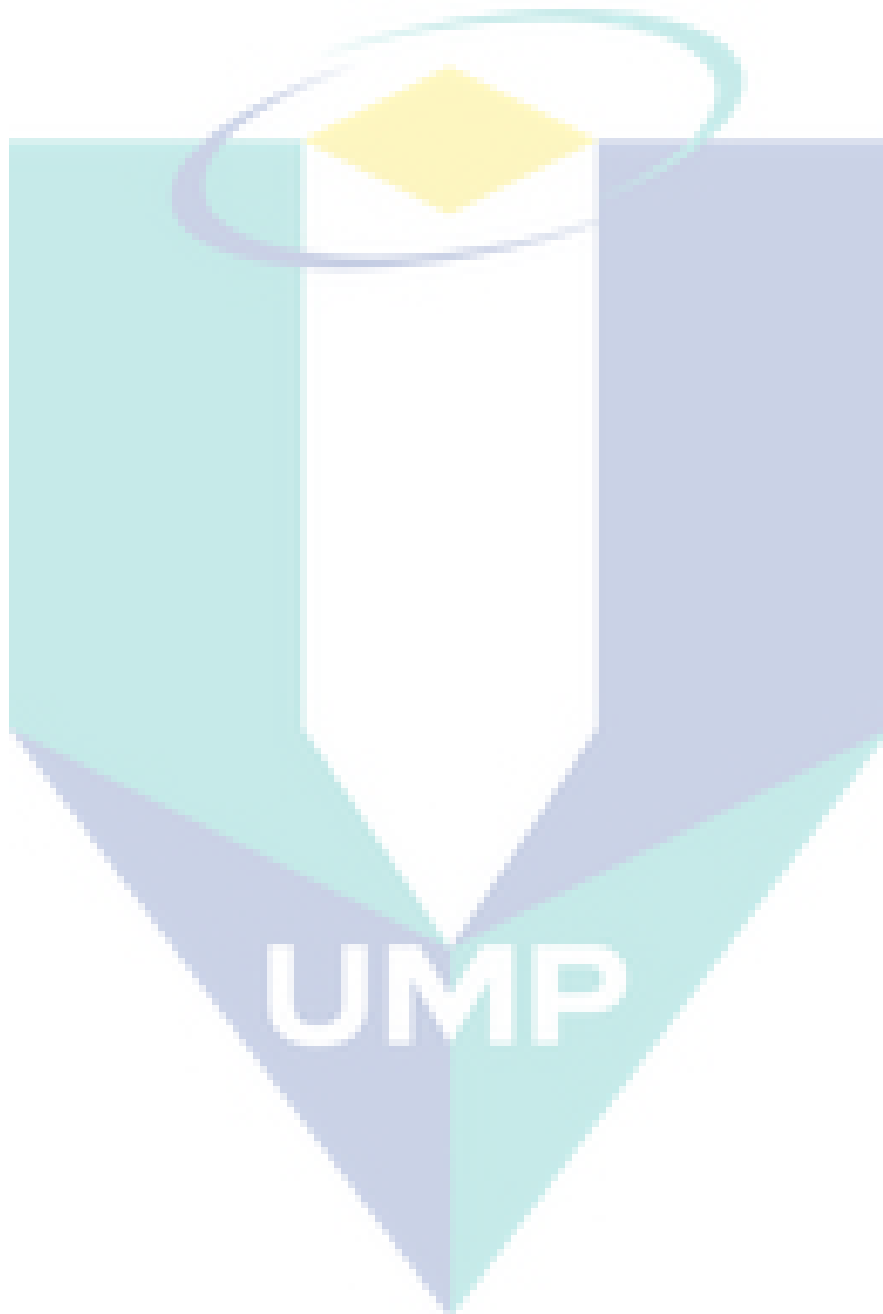
LIST OF FIGURES

Figure 2.1	Microstructure of the HT250 grey cast iron. (a) Unetched and (b) etched.	9
Figure 2.2	Presence of the worn surface on grey cast iron surface.	11
Figure 2.3	Morphology of the worn surface of cast iron with squeeze phenomena (indicated by the small arrow) and the escape of graphite to the surface.	12
Figure 2.4	Microcosmic place of crack (a) initiation and (b) propagation.	12
Figure 2.5	Front view of the crack found in cylinder liner engine diesel.	13
Figure 2.6	Fe-Cr-C liquid projection.	16
Figure 2.7	X-ray diffraction laser cladding Cr addition.	17
Figure 2.8	Wear resistance of grey cast iron with % wt. of molybdenum additions.	18
Figure 2.9	SEM images of the worn surface (a) before wear test and (b) after wear test.	18
Figure 2.10	Pin-on-disc test and hardness test result for the modified cast iron alloys with addition of chromium and molybdenum.	19
Figure 2.11	(a) Thermal shock resistance and (b) ultimate tensile strength of the alloyed grey cast iron as a function of alloyed composition.	20
Figure 2.12	Spectrum of laser application in surface processing.	22
Figure 2.13	The microstructure of melting zone in cast iron.	25
Figure 2.14	The microstructure of molten zone at different energy (a) 5.22 J, (b) 7.09 J, (c) 9.26 J, (d) 12.54 J and (e) 10.87 J.	26
Figure 2.15	(a) The microhardness in depth, (b) the equiaxed crystal grains at the top of molten pool and (c) the columnar crystal grains at the bottom of molten pool.	27
Figure 2.16	Schematic steps involved during the laser surface cladding.	30
Figure 2.17	Cross section of single (a) double (b) triple and (c) clad layer made by overlapping of single laser tracks.	31
Figure 2.18	The range of laser process mapped against laser beam density and interaction time. The diagonal lines represent the lines of constant temperature for the boiling and melting point of iron.	33
Figure 2.19	Laser beam power density (irradiance) treatment parameter variants that caused remelting/alloying in the surface layer of grey cast iron.	34
Figure 2.20	Variation of melt depth with power and time of laser material interaction.	34
Figure 2.21	Transverse cross-section of melted tracks for the following laser processing parameter: $P = 780 \text{ W}$, $d = 0.6 \text{ mm}$, $\tau = 0.01 \text{ s}$ and (a) $V = 0.8 \text{ mm/s}$, (b) $V = 1.6 \text{ mm/s}$, (c) $V = 5 \text{ mm/s}$ and (d) 40 mm/s .	35

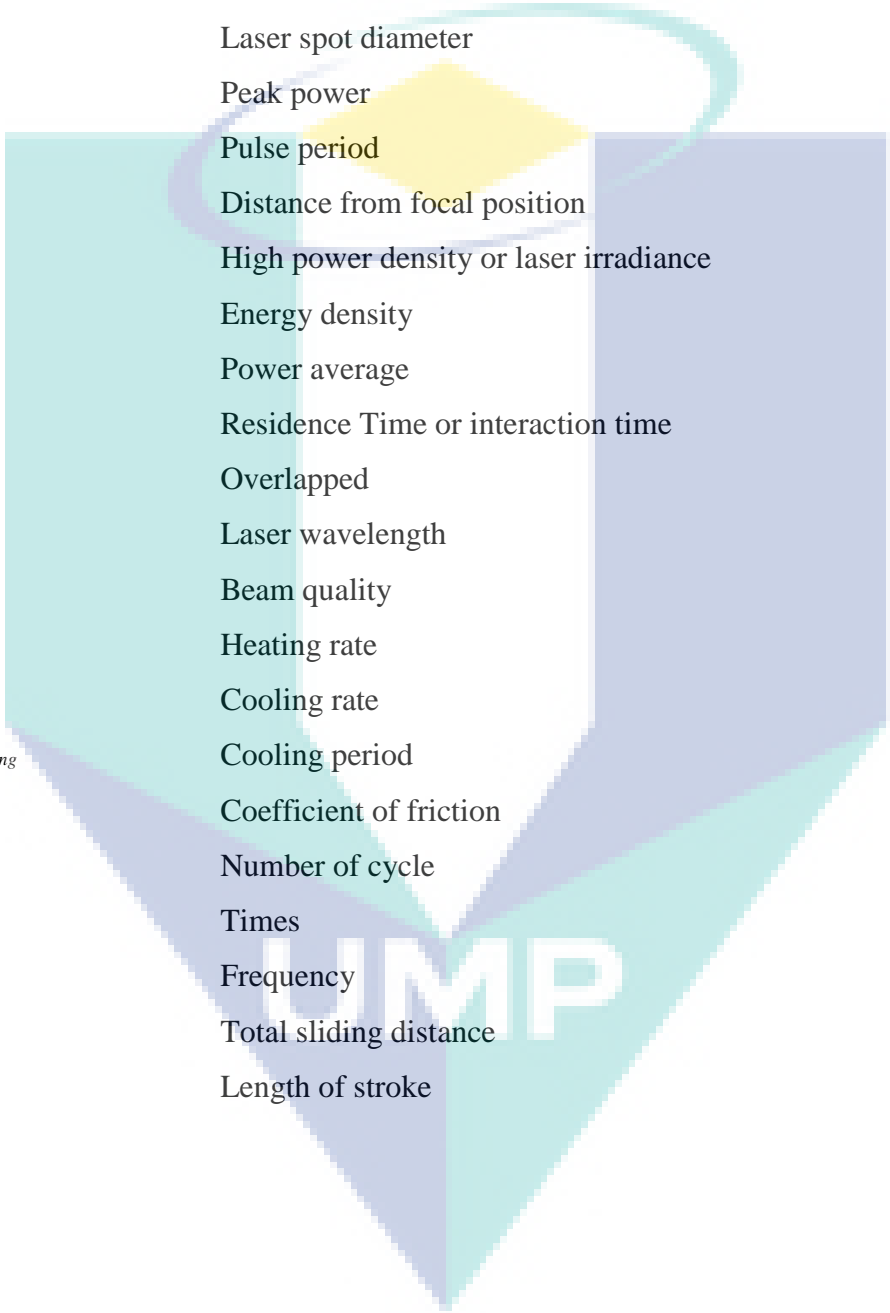
Figure 2.22	The microstructure of laser surface melting (a) (c) (e) and laser surface alloying (b) (d) (f) at different energy density 10.7 Jmm^{-2} , 6.84 Jmm^{-2} and 4.75 Jmm^{-2} .	36
Figure 2.23	Effect of incident energy intensity on surface hardness properties.	37
Figure 2.24	Microhardness of laser melting (LSM) and laser alloying (LSC) in various energy density at load of 0.2 kg and a dwell time of 10 s.	38
Figure 2.25	Gaussian irradiance profile.	39
Figure 2.26	Growth in beam diameter as a function of distance from beam waist.	40
Figure 2.27	Calculated surface temperature and cooling rate as function of laser power and energy density.	41
Figure 2.28	Effect of heat input on the depth of modified layer and the surface roughness of the laser modified surface.	42
Figure 2.29	Laser tracks cross section for side cladding on grey cast iron. Combined parameter of laser power and fed material per unit track length (F/S).	43
Figure 2.30	Nd:YAG laser diagram.	45
Figure 2.31	SEM images of cross section the coatings: (a) 0.47 mm, (b) 0.74 mm, (c) 0.92 mm, (d) 1.09 mm, (e) 1.36 mm and, (f) 1.62 mm.	48
Figure 2.32	The space factor for a mixture experiment with three components in it.	51
Figure 3.1	Overall research methodology flowchart.	55
Figure 3.2	Sample size for (a) laser surface processing and (b) sliding wear test.	57
Figure 3.3	Linear sample movement in laser surface processing.	58
Figure 3.4	SEM image for (a) chromium powder and (b) molybdenum powder.	60
Figure 3.5	The schematic drawing of the preparation process of the preplaced layers.	61
Figure 3.6	Laser Nd:YAG machine.	63
Figure 3.7	Laser spot size at peak power 1 W on black paper, (a) 1 mm, (b) 1.2 mm, (c) 1.4 mm and (d) 1.7 mm.	65
Figure 3.8	Schematic indentation of Vickers hardness test.	68
Figure 3.9	Arithmetic average roughness value Ra.	69
Figure 3.10	Schematic diagram sliding wear test.	71
Figure 4.1	Outline of order of results presented in this chapter.	76
Figure 4.2	Pulse energy as a function of residence time for laser surface melting of grey cast iron at different laser spot sizes.	77
Figure 4.3	Comparison of previous work's in pulse energy versus laser spot size with this research.	78
Figure 4.4	Micrograph of grey cast iron with graphite and pearlite microstructure.	79

Figure 4.5	Micrograph of cross section (a) laser surface melting layer and (b) microstructure of grey cast iron surface melting zone.	80
Figure 4.6	Surface geometry of samples processes at spot size (a) 1.0 mm; (b) 1.2 mm; (c) 1.4 mm and (d) 1.7 mm.	82
Figure 4.7	High energy setting in laser surface melting effect at different spot size on surface roughness of melting zone.	84
Figure 4.8	Average hardness properties as a function of distance from surface for samples processed using spot size of 1.0 mm, 1.2 mm, 1.4 mm and 1.7 mm.	85
Figure 4.9	Residence time effect on hardness of laser surface melting grey cast iron at different laser spot sizes.	86
Figure 4.10	(a) X-ray diffraction as-received grey cast iron and (b) surface melting of grey cast iron.	88
Figure 4.11	Micrograph of laser cladding grey cast iron microstructure with addition of (a) Cr powder, (b) Mo powder and (c) Cr-Mo mixture powder.	95
Figure 4.12	Particle analysis in clad zone of grey cast iron with addition of (a) Cr, (b) Mo and (c) Cr-Mo mixture.	97
Figure 4.13	X-ray diffraction pattern for (a) grey cast iron substrate, (b) Cr-added clad, (c) Mo-added clad and (d) Cr-Mo mixture clad zone.	99
Figure 4.14	Selected area in grey cast iron substrate.	101
Figure 4.15	EDS qualitative analysis spectrum of phase for grey cast iron substrate.	101
Figure 4.16	Selected area in laser clad zone of (a) Cr, (b) Mo and (c) Cr-Mo mixture.	102
Figure 4.17	EDS qualitative analysis spectrum of phases for modified layer (a) Cr clad, (b) Mo clad and (c) Cr-Mo mixture clad.	103
Figure 4.18	Hardness properties of laser cladding surface with addition of Cr, Mo and Cr-Mo mixture as a function of distance from surface all cladding samples were processed at spot size 1.0 mm.	104
Figure 4.19	Micrograph of formation clad layer on grey cast iron substrate.	107
Figure 4.20	Contour plot of peak power and mixture component on surface roughness of clad zone at constant (a) 80 Hz and (b) 90 Hz.	110
Figure 4.21	Contour plot of peak power and mixture component on microhardness at constant (a) 80 Hz and (b) 90 Hz PRF.	112
Figure 4.22	Counter plot of design for laser surface cladding process optimization of grey cast iron at 1.0 mm laser spot size.	114
Figure 4.23	As-received grey cast iron and laser surface cladding layers result in (a) coefficient of friction (b) surface roughness and (c) weight loss.	117
Figure 4.24	Micrograph of the worn surface after the wear sliding test at 17.5 N. (a) as-received grey cast iron and (b) Cr-Mo mixture clad zone.	118

Figure 4.25 Wear rate at different load on as-received grey cast iron and laser clad sample.



LIST OF SYMBOLS



E_P	Pulse energy
τ	Pulse width or pulse duration
S	Scan speed
d	Laser spot diameter
P_P	Peak power
T	Pulse period
z	Distance from focal position
I	High power density or laser irradiance
F	Energy density
P_{ave}	Power average
T_R	Residence Time or interaction time
η	Overlapped
λ	Laser wavelength
M^2	Beam quality
H_R	Heating rate
C_R	Cooling rate
$t_{cooling}$	Cooling period
μ	Coefficient of friction
N	Number of cycle
t	Times
f	Frequency
x	Total sliding distance
L	Length of stroke

LIST OF ABBREVIATIONS



ASTM	American Society for Testing and Materials
ANOVA	Analysis of variance
Ar	Austenite
COD	Crystallography open database
CoF	Coefficient of friction
DOE	Design of experiment
EDS	Energy dispersive spectrometer
GCI	Grey cast iron
HV	Hardness Vickers
HAZ	Heat affected zone
LSM	Laser Surface Melting
LSC	Laser surface cladding
Nd:YAG	Neodymium-doped yttrium aluminium garnet
PRF	Pulse repetition frequency
RZ	Remelting zone
RPM	Revolution per minutes
RSM	Response Surface Methodology
SEM	Scanning electron microscopy
TZ	Transform zone
TEM	Transverse electromagnetic mode
UV	Ultraviolet
XRD	X-ray diffraction

CHAPTER 1

INTRODUCTION

1.1 Research Background

Recent advances in materials design emphasize on sustainability and low cost consumption. Conventional material like grey cast iron is among the cheapest metal and the most common engineering materials with wide range of applications in automotive component such as brake disc, cylinder liner, cylinder head, engine block and gear box. In previous industry reports and researches, these automotive parts usually experienced wear defects and corrosion (Keller, Fridrici, Kapsa, Vidaller, & Huard, 2007; Zhong, Liu, & Zhang, 2006). The operational conditions of these parts involved high temperature, pressure and mechanical friction, which contribute to multifaceted, high-stress condition (Ghasemi & Elmquist, 2014). Previous studies had reported, failure of the components made of grey cast iron occurred near-surface graphite phase and acted as a source of crack nucleation under high impact condition and caused crack growth (Chen, Zhou, Zhang, Yang, & Zhou, 2015a). In automotive application, cylinder liner of engines experienced high friction at elevated temperature that requires such properties that can prevent crack and can increase the life of the cylinder liner. In long cycle operation, high wear rate leads to corrosion and produce sulphur in the fuel during operation (Jeong & Kim, 2001). Therefore elimination of graphite phase near the surface is an option. With the presence of hard phase on the surface, corrosion and wear can be avoided (Nadel & Eyre, 1978).

To date, various conventional and advanced processing methods have been used to produce hardened layer for high wear resistance including laser surface melting (LSM) and laser cladding. Laser surface melting can improve surface properties with the formation of hard, homogenous and ultrafine structure of the material surface layer without changing its chemical composition (Kusinski *et al.*, 2012). Meanwhile, laser cladding can improve surface properties by forming a new alloy layer with new chemical composition that resulted a formation of hard, homogenous and also ultrafine structure of the material layer (Sun, Zhou, Li, Feng, & Zhang, 2011). This method also has been proven to change the surface layer to enhance surface hardness, corrosion resistance, thermal fatigue and wear resistance by elimination graphite on the surface and form a new structure (Yang, Zhang, Wang, & Ren, 2015; Zhong *et al.*, 2006).

Laser cladding shows significant advantage compared to the melting method since it can modified layer surface with variety of alloying elements. Alloying with chromium and molybdenum can form complex carbides with the carbon in the cast iron, which significantly enhances the strength, hardness and wear resistance (Amirsadeghi & Sohi, 2008; Tong *et al.*, 2008). Modifying surface using tungsten inert gas (TIG) on cast iron surface with chromium and molybdenum formed structure of cementite, martensite, retained austenite and primary carbides structure of M_7C_3 and M_3C (Amirsadeghi & Sohi, 2008). The alloyed surface has higher hardness compared to the melting surface because of the carbide formation.

The important processing parameters for the laser surface modification include laser power, laser spot size, heat intensity distribution across the beam, absorptivity of the beam energy by the treated material surface, scanning rate of the laser beam across the substrate surface and the thermal properties of the treated material (Kusinski *et al.*, 2012). Melting surface versus the intensity of energy produced a distinct linear relationship for melting zone, transformation zone and incipient melting at the surface followed by a predominantly transformed zone (Hwang, Lee, Kim, & Youn, 2002).

Controlled laser power and traverse speed can melt the grey cast iron and increase the hardness properties of the melting zone. At different spot sizes, parameters such as residence time, scan rate, PRF and energy density were varied corresponding to the preferred laser spot size to prevent material vaporization and irregular surface

morphology (Aqida, Naher, & Brabazon, 2011). Smaller spot size will allow greater scattering of the laser beam, thus limiting its penetration, while larger spot size penetrate more deeply into the substrate due to less scattering (Allemann & Kaufman, 2011). Previous researchers used laser surface at different setting of laser spot size such as 0.6 mm, 0.8 mm and 1.5 mm. Using the same laser parameter at different laser spot size will produce different results. Further investigation on laser surface melting in different spot size is necessary. Thus, there is a need to optimize the laser surface processing of grey cast iron at different spot sizes for maximum hardness properties and minimum surface roughness. The surface roughness were unexpectedly decrease with the decreasing of the peak power and the increasing of the traverse speed (Fazliana, Aqida, & Saidin, 2014). Meanwhile, the increment of the laser beam size reduced the laser irradiance and increase the residence time and also increased the grain diameter for H13 steels (Aqida *et al.*, 2011).

The purpose of this study is to develop a modified layer on grey cast iron substrate with new metallurgical properties and phase using laser melting and laser cladding. In order to strengthen the surface properties, Cr-Mo powders were added to the surface. The parameters on this process were analyzed using statistical analysis to obtain the relationship between laser parameter and mixture element of Cr and Mo.

1.2 Problem Statement

Nowadays, increasing power output in automotive engine could cause difficulty to maintain an adequate oil film between the piston and cylinder liner surface. Increasing the surface properties becomes important when marginal lubrication metal to metal contact occurs. Failure or damage such as crack, wear and fatigue can happen on components or part of automotive that is made of grey cast iron. Grey cast iron is brittle and has low corrosion resistance where these can cause stress corrosion and corrosion fatigue (Espadafor, Villanueva, García, & Trujillo, 2010). Besides, with low melting point of 1400°C compared to steel, when involves with high thermal wear, grey cast iron component surface experiences surface fatigue, crack and abrasion. For example, the surface of cylinder liner initiated cracks on the surface due to the friction during operation. Moreover a prolong cycles at maximum service temperature of 250°C increases the crack length (Branco, Infante, Sousa e Brito, & Martins, 2002). A few

reports had been published regarding the failure of grey cast iron in automotive part as shown in Table 1.1. Therefore, these defects caused surface failure and decreased the life of the automotive parts.

Table 1.1 Summary report on gray cast iron failure.

Num.	Components	Type of Failure	References
1.	Brake discs material grey cast iron (EN GJL 250)	Fatigue failure at temperature 700 °C.	(Pevec, Oder, Potrč, & Šraml, 2014)
2.	Diesel generator cylinder	The piston and liner cracked and broken after 80000 service hours (operating mainly at full load).	(Espadafor <i>et al.</i> , 2010)
3.	Maritime diesel engines wet liners (ASTM grade 40 equivalent to HT 250)	The liner had shown cracks and extensive corrosion after about 1200 service hours.	(Branco <i>et al.</i> , 2002)
4.	Diesel engine cylinder head	A crack was initiated from the interior wall and propagated towards the exterior surface of the cylinder head.	(Xu & Yu, 2006)

Meanwhile, grey cast iron has the advantage of properties compared to the steel such as good machinability and excellent damping capacity. Enhancing the properties of grey cast iron has been done by many researcher, especially by chemical composition modification during casting (Imurai, Thanachayanont, Pearce, Tsuda, & Chairuangri, 2015). Modifying the entire bulk material is inefficient for wear resistance purposes, while elements like Cr and Mo are costly in abundance usage. By conducting laser processing, the substrate properties are remained while the surface properties can be tailored with additional elements. Several works have been conducted on laser cladding of grey cast iron to enhance the hardness and wear resistance with addition of carbon and Fe-based powder (Chen *et al.*, 2015b; Yi, Xu, Fan, Li, & Shi, 2015). However, few studies reported on the laser cladding of grey cast iron with Cr and Mo powder and in fact cladding of cast iron surface can be difficult to design (Hussein, Kamarul, & Ayof, 2013). The main difficulty is related to substantial differences in laser beam absorptivity at the cast iron surface. The graphite flakes act as heat sources area due to their high laser beam absorption when was direct illumination by the laser beam, therefore non-

homogeneous thermal fields may be formed (Ocelik, Oliveira, Boer, & Hosson, 2007). Adding Cr and Mo in grey cast iron can resist the softening effect caused by the heat and protect it against oxidation.

Very few papers dealt with the relationship of laser parameter and mixture elements on the metallographic properties; and these have not been found to be consistent (Ocelik *et al.*, 2007). This relationship is crucial to design the laser energy and laser spot size to melt the surface. Energy from laser beam influence the dimension, hardness and surface roughness on the surface. High energy of laser beam can cause defects such as porosity, crack, bubble and depression in the surface (Aqida, 2011). In this research, a systematic study on laser cladding of grey cast iron with addition of Cr and Mo powder was conducted using mixture design of experiment to develop a new metallurgical property and phase. The relationship between laser parameters, powder ratio addition and cladding surface properties was determined and optimized for maximum hardness and wear resistance properties. The consistency of parameters in laser processing of grey cast iron was investigated at different focal distances and pulse energy. The wear behaviour of Cr/Mo surface modified grey cast iron was investigated in order to enhance the cylinder liner life and prevent premature failure of friction.

1.3 Research Objective

The main objective of this research is to modify grey cast iron surface using Nd:YAG laser system for enhanced surface hardness and wear resistance. To meet the main objective, the research addresses three separate goals:

- i. To develop a modified surface layer on grey cast iron substrate with new metallurgical properties and phase using laser surface melting and laser cladding.
- ii. To strengthen surface properties of grey cast iron through laser cladding by adding chromium and molybdenum particle.
- iii. To analyse relationship between laser parameters, mixture element of chromium and molybdenum.

1.4 Research Scope

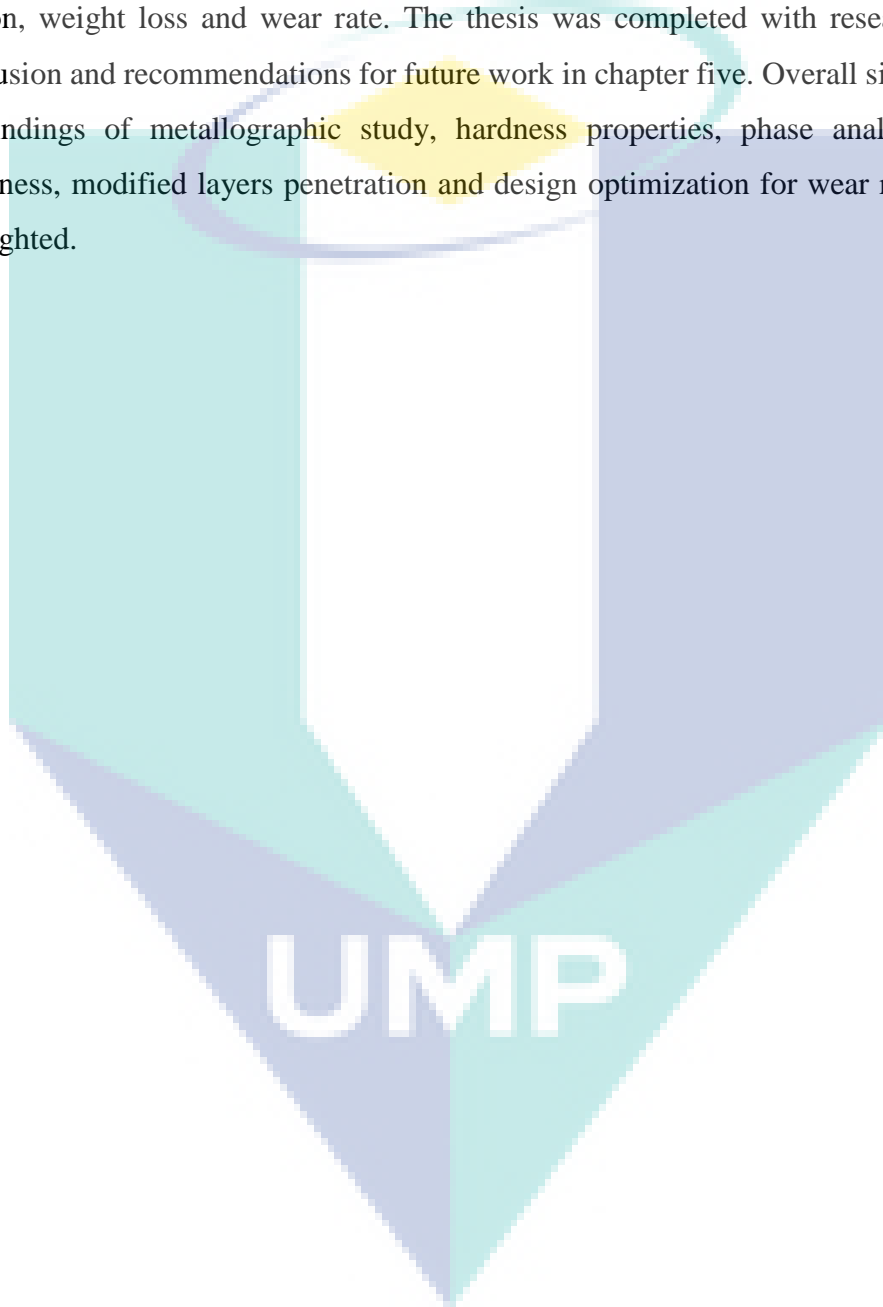
There are six scopes for this research which are related to the objective:

- i. Conduct preliminary experiment on laser surface melting of grey cast iron grade HT250 using design of experiment (DOE) at laser spot sizes of 1.0, 1.2, 1.4 and 1.7 mm.
- ii. Develop a design of the experiment for laser surface melting of grey cast iron using factorial model with three processing factor; peak power (Pp), scan speed (S) and pulse repetition frequency (PRF).
- iii. Develop a design of experiment (DOE) for laser cladding of grey cast iron with Cr/Mo powders addition using mixture design experiment with two laser parameters; peak power (Pp) and pulse repetition frequency (PRF) and two components of mixture; chromium (Cr) and molybdenum (Mo).
- iv. Conduct laser surface melting and cladding based on the respective DOE.
- v. Characterization of laser surface melting and cladding samples for metallographic study, surface morphology, hardness properties, surface roughness, chemical composition and phase transformation.
- vi. Conduct wear test on laser cladding samples using sliding wear test machine referring to ASTM G133-05.

1.5 Thesis Outline

In chapter one, a brief research background was presented including the introduction of grey cast iron defect in automotive application and surface modification followed by prior knowledge of problem statement and objectives. In chapter two, present previous works on laser surface modification of grey cast iron, pre-placed technique in cladding and design of experiment (DOE). The literature review includes failure material of grey cast iron and Cr/Mo affect in grey cast iron cladding. The ability of laser surface melting and cladding in grey cast iron surface was presented based on controlled parameter and parameter effects on surface properties. The research methodology is presented in chapter three and comprises: materials and sample preparation, preliminary study on laser surface melting and laser cladding process, design of experiments for both process, sliding wear experiment and characterization techniques. Chapter four presents the characterization results and discussion of the as-received grey cast iron and laser

surface modified samples. The modified samples results were presented and discusses in two section that is preliminary experiment on laser surface melting and laser cladding. The surface dimension, XRD and EDS for laser cladding were discussed with comparison Cr, Mo and Cr-Mo cladding. At the end of laser cladding, optimization samples were analysis on wear characterize. The sliding wear results were discussed in a coefficient of friction, weight loss and wear rate. The thesis was completed with research findings conclusion and recommendations for future work in chapter five. Overall significance of the findings of metallographic study, hardness properties, phase analysis, surface roughness, modified layers penetration and design optimization for wear resistance are highlighted.



CHAPTER 2

LITERATURE REVIEW

2.1 Introduction

In this chapter, the literature review encompassed grey cast iron advancement, laser surface processing advancement, failures in automotive components, surface modification of cast iron through melting and cladding, sliding wear on cast iron surface and design of experiment (DOE). Substantial literature has been studied on surface properties of grey cast iron, laser processing parameter, transformation structure on melting surface, phase formation by laser cladding and wear on grey cast iron surface. The review is organized chronologically to offer insight on how the past research have laid the groundwork for subsequent studies, including the present research. The review is detailed so that the present research effort can be properly tailored to complete the present body of literature as well as to justify the scope and direction of the present research effort.

2.2 Grey Cast Iron Advancement

Cast iron is one of engineering material that widely used in manufacturing components based on ferrous metal other than steel. Grey cast iron is used particularly in automotive components like brake disc, cylinder blocks and piston liner due to its wear resistance. There are various types of cast iron such as grey cast iron, white cast iron and

nodular cast iron. Grey cast iron is one of the cast iron that is produced by casting and normally characterized by a microstructure of graphite flake in a ferrous matrix. This graphite flake made grey cast iron has unique properties such as good machinability, excellent damping capacity and high in wear resistance (Ghasemi & Elmquist, 2014). However, high percentage of graphite in grey cast iron directly decreased the elastic modulus and elongation and caused failure to the grey cast iron. Length of graphite flake affects the fatigue resistance of grey cast iron due to the micro-cracks which initiated at the tip of the flake graphite (Collini, Nicoletto, & Konečná, 2008). Figure 2.1 shows the microstructure of HT250 grey cast iron made for cylinder blocks. The matrix of the pearlitic HT250 is mainly composed of lamellar pearlite with traces of ferrite and was produced by gravity casting technology (Fan *et al.*, 2014).

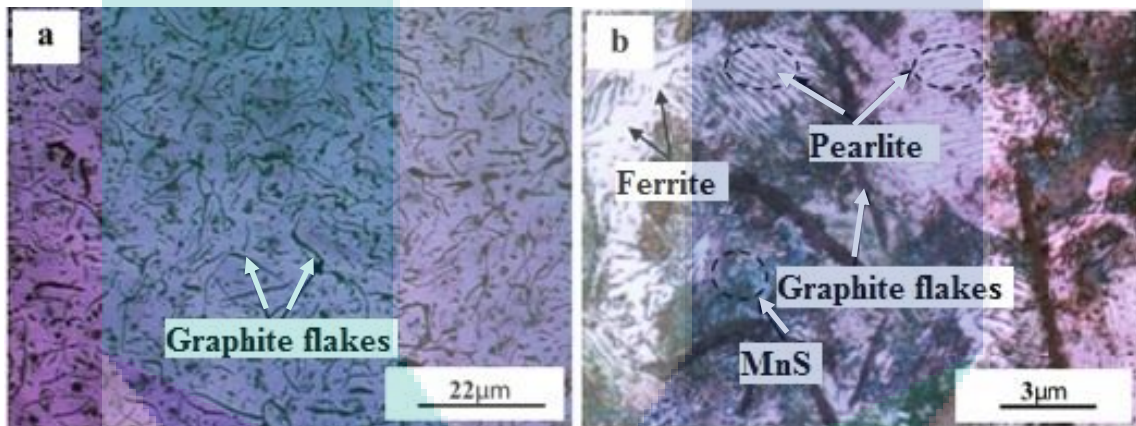


Figure 2.1 Microstructure of the HT250 grey cast iron. (a) Unetched and (b) etched.
Source : Fan *et al.* (2014)

It is well known that grey cast iron grade HT250 contains 2.5 to 4.2 % of carbon and 1.0 to 3.0 % of silicon plus manganese, sulphur and phosphorus. Each of the element in grey cast iron gives different impact to the mechanical properties. Carbon and silicon can change the graphitization of the iron as well as castability. High carbon content increases the amount of graphite. Carbon is very important in heat treatment process. To increase the overall strength of grey cast iron is by reducing total carbon content or by adding alloying elements (Seidu, 2014).

Overall, grey cast iron material grade HT250 has been used to manufacture engineering components specifically automotive parts because of its properties. However, its low strength caused surface of grey cast iron components easily cracks and lead to

failure. Reducing the carbon contents by adding alloying elements on the grey cast iron surface can increase the strength and prevent them from crack.

2.2.1 Failure in Grey cast iron

The factor that influence the properties of grey cast iron are the chemical composition, the size, dispersal, volume fraction and morphology of the single microstructure constituents (Alp, Wazzan, & Yilmaz, 2005). Besides that, the properties of grey cast iron depend on chemical composition which is influenced by major elements (carbon and silicon), minor elements (manganese, sulphur and phosphorus) and alloying addition such as chromium, molybdenum and tungsten. These composition give advantage to the properties of grey cast iron where it is good in hardenability and castability, high thermal conductivity, convenient machining property, better wear resistance and very good in vibration damping (Balachandran, Vadiraj, Kamaraj, & Kazuya, 2011; Collini *et al.*, 2008). Since demands for high performance and durability in automotive appliances are continuously, advancing further attempts are required to improve the hardness and wear resistance of engine parts by formatting new layer (Hussein, Asri, & Shamsuri, 2014). Furthermore, mechanical properties of cast iron can also be enhanced by several heat treatment process such as tempering (Balachandran *et al.*, 2011).

However, grey cast iron had limited application because of low tensile strength and poor in terms of fatigue resistance especially low ductility which is caused by the presence of thick graphite flake in a pearlite matrix (Atmadja, Sulardjaka, Nugroho, Adnan, & Cahyono, 2013). Under rolling contact condition in grey cast iron, plastic deformation would lead to the generation of concentration stress which generally was preferred to occur at the tip of the graphite. Hence, the fatigue crack must preferentially emerged at the graphite tip (Chen *et al.*, 2016). This also supported by Ghasemi and Elmquist (2014) that plastic deformation of the matrix grey cast iron during the wear processes results in closing the graphite flakes (Ghasemi & Elmquist, 2014).

Most of the graphite will be deformed by other impingement and caused the end of the deformed graphite to behave as crack nucleation. Some of the crack may originate within the matrix and initiates other crack at the matrix graphite interface. This is usually

at the edge of graphite, which act as the stress risers. The crack is initiated at the soft graphite matrix interface and propagate in the matrix during the process of subsequent erosion. These crack joined together to form craters, dislodging the fragmented graphite. Hence, the surface of untreated sample was pitted and full of dimples all over (Alabeedi, Abboud, & Benyounis, 2009). These resulted scuffing, grooving and lip formation type failure to the grey cast iron due to the direct metal-to-metal contact. This is also proven by dark areas of oxidation produced at high contact temperature as shown in Figure 2.2 (Alabeedi *et al.*, 2009; Blarasin, Corcoruto, Belmondo, & Bacci, 1983). According to Jensen *et al.* (2002), scuffing failure can cause material loss and shorten the material life. Thus, the grey cast iron surface which are high oxidation resistance and high hardness are suitable to be used for engine's components (Jensen, Böttiger, Reitz, & Benzon, 2002).

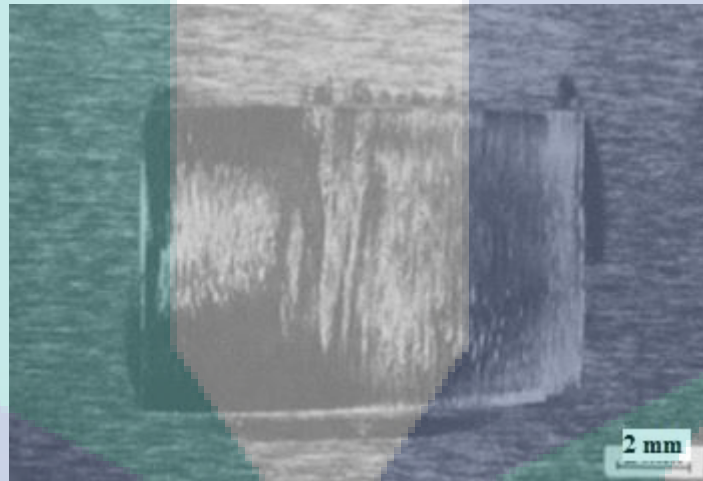


Figure 2.2 Presence of the worn surface on grey cast iron surface.

Source: Blarasin *et al.* (1983)

For many years, wear rate in piston and cylinder liners made by grey cast iron in engine diesel were attributed by corrosion and Sulphur in the fuel. In high wear rate these components resulted scuffing that produced metallic plates of debris by a process of delamination (Nadel & Eyre, 1978). Wear mechanisms in diesel engine is operated either separately or together with corrosion, scuffing and abrasion. Grey cast iron components with operated without lubricant will increase the wear loss and friction torque because of the embedded graphite release, as a result of removing the deformed surface material and the formation of a squeeze film (Sugishita & Fujiyoshi, 1982). Figure 2.3 shows the squeeze phenomenon and the escape of graphite to the surface.

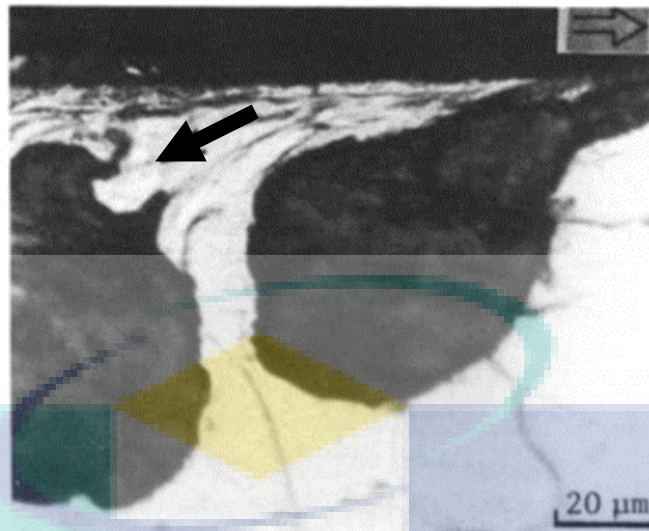


Figure 2.3 Morphology of the worn surface of cast iron with squeeze phenomena (indicated by the small arrow) and the escape of graphite to the surface.

Source: Sugishita & Fujiyoshi, (1982)

High wear rate can cause shear stress which could cause plastic deformation. Concentrated stress resulted from plastic deformation drove the generated cracks to nearly closed or entirely closed. Subsequently, the portion surrounded by cracks would fall off or torn from the surface which contributed to the fatigue failure (Chen *et al.*, 2015a). This crack occurs because of the dispersal of the graphite in the structure as show in Figure 2.4. Then, it is necessary to optimize the surface contacts to enhance the wear resistance by modifying the surface properties (Chen *et al.*, 2015a).

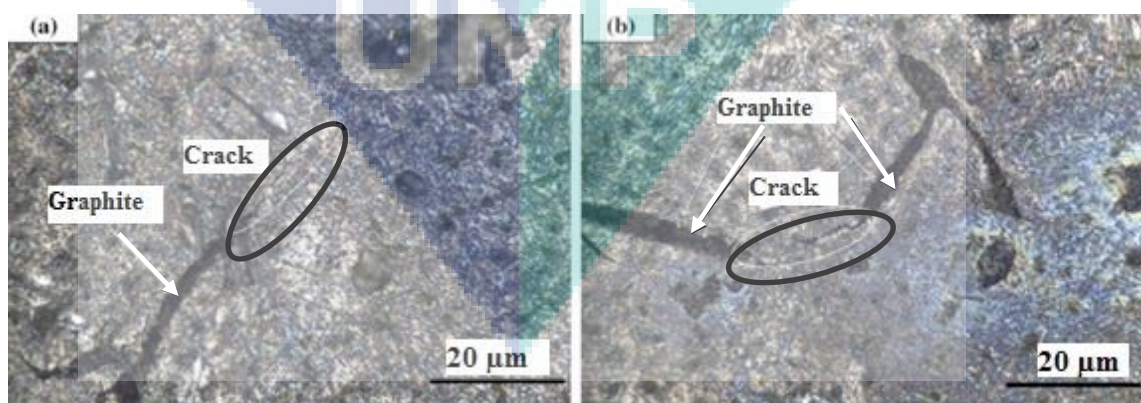


Figure 2.4 Microcosmic place of crack (a) initiation and (b) propagation.

Source: Chen et al. (2015a)

Another properties of grey cast iron is brittle. This is cause by the graphite morphology and small stress cracking that can be initiated on grey cast iron surface and become fatigue failure (Tong *et al.*, 2008). For example, cylinder liners in diesel engine are subjected to low cycle fatigue, mainly due to starts and stops of engine and resulted a crack on the surface. Cracking occurred in cylinder liners in diesel engines because of the stress attributed by corrosion as show in Figure 2.5.

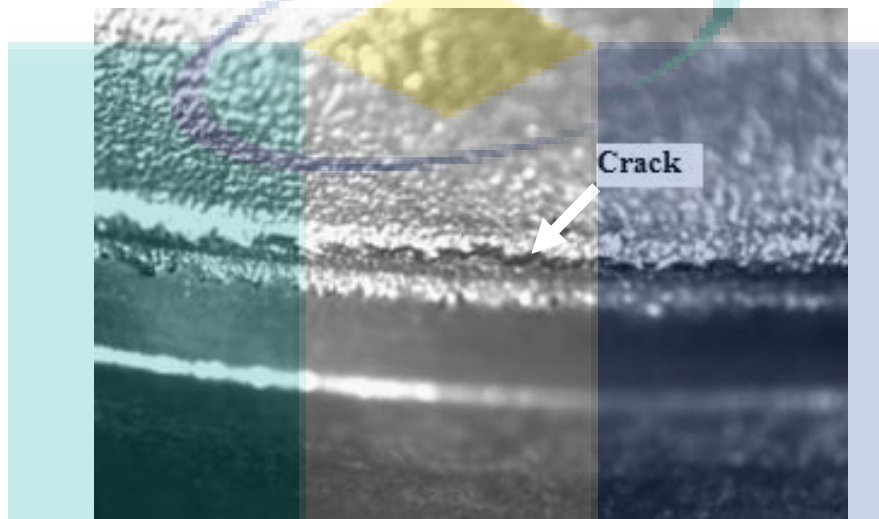


Figure 2.5 Front view of the crack found in cylinder liner engine diesel.

Source : Branco *et al.* (2002)

In laser hardening of grey cast iron surface, the wear rate is high at an initial stage and it gradually decreases. This is attributed to the fact that increasing the contacting area with progressing wear phenomena reduces the pressure per unit area. According to Hwang *et al.* (2002), wear on cylinder liner and piston ring in automotive engine is in linear at the same time, the wear life of laser hardened layer was determined to be almost doubled than the untreated one. From the study, untreated material shows both the nature of the metallic wear formed by the material transfer phenomenon and the adhesive wear features such as plastic flow and tearing damage, which are caused by the effect of severe contact wear, whereas in the modified surface material, tearing damage occurred only around graphite flakes by the mild wear resulting from the higher hardness (Hwang *et al.*, 2002).

Mechanical properties of grey cast iron can be improved by adding elements such as chromium, molybdenum and tungsten. These elements can promote hardness same like low alloy steel if proper amounts added in grey cast iron. As we know, chromium and molybdenum are transition metals that can form carbide in the structure. In steel, the transition metal carbides attain very high hardness and thus contribute significant wear resistance, which is alloy that contains large volume of carbide fractions (Krauss, 2005). However, there is no reliable evidence proving that the additional elements on the grey cast iron surface showed phase formation and mechanical properties as bulk materials.

A number of studies have found that rapid solidification through surface modification process showed the formation of several types of structure depending on the additional elements on the surface. This new structure is proven enhance the properties of grey cast iron. For example, Sohi et al. (2012) found that surface melting and surface alloying with Cr addition had improved the hardness because of the formation of ledeburite structure and carbides phase on the alloying layer (Sohi, Ebrahimi, Ghasemi, & Shahripour, 2012). The research study by Chen et al. (2015) also found cladding with additional elements can be improved the grey cast iron fatigue wear resistance by eliminating the graphite and formation of carbide on grey cast iron surface (Chen *et al.*, 2015b).

2.2.2 Cladding with Cr and Mo

Chromium and molybdenum are known as transition metal that can form carbide in the structure. Besides that, alloying with Cr and Mo will form various carbides in iron matrix (Nagai, Inoue, & Utsunomiya, 2002). In steel, the transition metal carbides attains very high hardness and thus contribute significant wear resistance, which is alloy, that contains large volume of carbides fractions (Krauss, 2005). As shown in Table 2.1, Cr and Mo elements yield characteristics of alloy carbide in steels.

Table 2.1 Characteristics of alloy carbide in steels.

Type of carbide	Lattice type	Remarks
M_3C	Orthorhombic	This is a carbide of the cementite (Fe_3C) type, M. Maybe Fe, Mn, Cr with little W, Mo, V.
M_7C_3	Hexagonal	Mostly found in Cr alloy steels. Resistant to dissolution at higher temperatures, hard and abrasion resistant. Found as a product of tempering high speed steels.
$M_{23}C_6$	Face-centered cubic	Present in high-Cr steels and all high speed steels. The Cr can be replaced with Fe to yield carbides with W and Mo.
M_6C	Face-centered cubic	Is a W or Mo rich carbide. May contain moderate amounts of Cr, V, Co. Present in all high speed steels. Extremely abrasion resistant.
M_2C	Hexagonal	W or Mo rich carbide of the W_2C type. Appears after temper. Can dissolve a considerable amount of Cr.

Source : Krauss, (2005)

Recent evidence show that chromium carbide is the most suitable to be added in metal matrix as hard phase as for their high hardness, good in oxidation resistance and good in wetting capability with iron matrix (Shang-ping, He-Li, Di, Xu, & Xi-e, 2009). Chromium can promote a pearlitic matrix and assist the increment of hardness. Suitable percentage of chromium can resist the softening effect of heat and protect against oxidation. According to Amirsadeghi et al. (2008), when the surface was alloyed with chromium added more than 10 %, eutectic carbides of the M_7C_3 type is formed. Lower than that the M_3C type will be formed. Because of the solidification characteristic, hypoeutectic irons containing M_7C_3 carbides are normally stronger and tougher than irons containing M_3C carbides (Amirsadeghi, Sohi, & Bozorg, 2008). Research by Kagawa and Ohta (1998) also found that the carbide layer formation can increase the hardness and wear resistance with the increment of Cr content on coating layer (Kagawa & Ohta, 1998).

Surface melting temperature is also important, based on Fe-Cr-C liquid projection in Figure 2.6, at high percentage of chromium and carbon content in alloy grey cast iron, the phase transforms into M_3C_2 , M_7C_3 and $M_{23}C_6$ carbide phases at melting temperature of $1726^\circ C$, $1575^\circ C$ and $1530^\circ C$ respectively. These results are also supported by Wiengmoon (2011) that the present of carbide in the high chromium cast iron are M_7C_3 , M_3C , $M_{23}C_6$

and M_6C , with the increment of carbon and carbide ratio. Furthermore, the $M_{23}C_6$ contains Cr is with around 60 wt% and carbon of 5.3 – 5.7 wt% (Wiengmoon, 2011). It is conclusively been shown that the formation of carbide phase due to the high amount of Cr can prevent the formation of martensite and decrease the graphite, which can reach the hardness of more than 1000 HV. Besides that, surface with carbide phase formation reduced the wear rate up to 70 %. (Atanda, Okeowo, & Oluwole, 2010) (Amirsadeghi & Sohi, 2008).

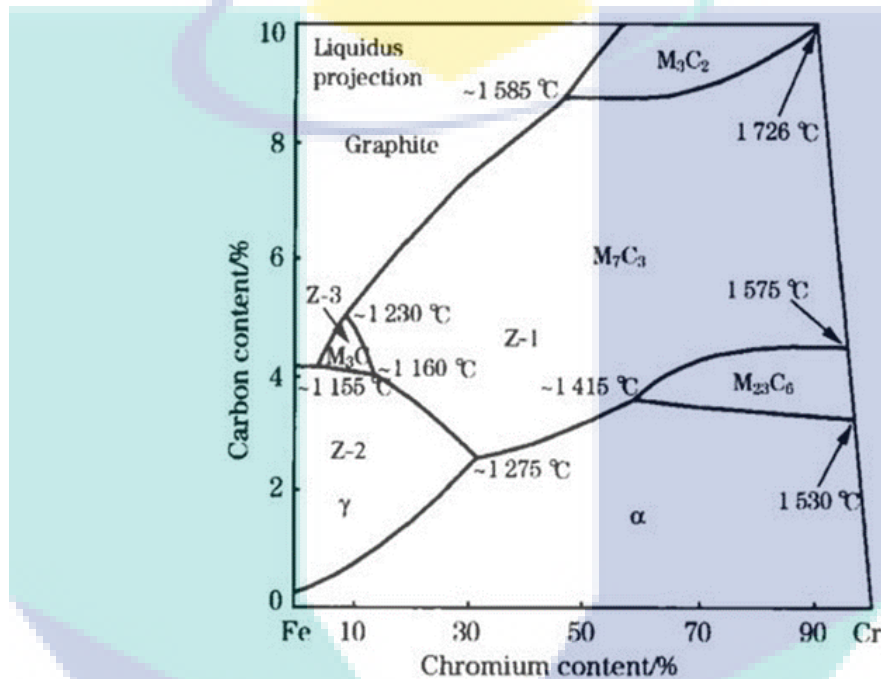


Figure 2.6 Fe-Cr-C liquid projection.

Source: Amirsadeghi et al. (2008)

Similarly, Chen et al. (2016) found in laser surface cladding with addition of Cr in pre-coating, new phases such as $(Fe,Cr)_x C_y$, $Cr_x C_y$, $\alpha-(Fe-Cr)$ and Cr were formed on the surface of grey cast iron as shown in x-ray diffraction in Figure 2.7. It is proven that Cr atom can be dissolved into α -Fe and subsequently detached out during solidification. Moreover, graphite was not found in Figure 2.7, to show that it is completely dissolved during laser processes (Chen *et al.*, 2016). According to Chen et al. (2016) formation of $Cr_x C_y$ and Cr at the interior of dendritic crystal is due to the combination of Cr and C in high temperature period, while in low temperature period carbonization reaction would not take place at the formation (Chen *et al.*, 2016).

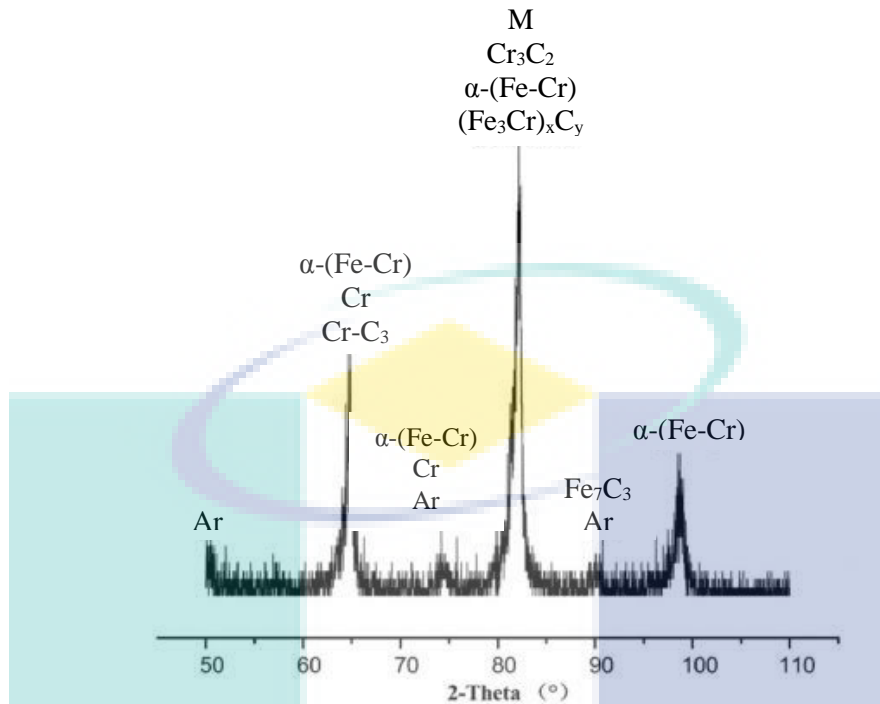


Figure 2.7 X-ray diffraction laser cladding Cr addition.

Source: Chen et al. (2016)

Recent years, about 86% molybdenum is used in metallurgical applications such as alloys, with the rest of molybdenum used as compounds in chemical application. Molybdenum can withstand extreme temperature without significantly expanding or softening which makes it useful in application that involves intense heat. Besides that, molybdenum in grey cast iron promotes high hardness and can improve heat resistance and corrosion resistance (Branco *et al.*, 2002; Maluf *et al.*, 2009; Moonesan, raouf, Madah, & zadeh, 2012). Nagai *et al.* (2002), found that surface coating with Mo added increases the surface hardness of grey cast iron due to the formation of cementite and complex carbides (Nagai *et al.*, 2002). Besides increasing the hardness, alloy with Mo also can increase the wear resistance. The researchers have been studied the effect of alloying Mo in grey cast iron on wear resistance. The result revealed that the volume loss decreased as the percentage of molybdenum in cast iron increased. As shown in Figure 2.8, wear resistance of grey cast iron increased when % w.t of Mo increases at different speed rotation disc. This behavior is due to the type of phases present in grey cast iron

such as molybdenum carbide appears in grey cast iron structure (Agunsoye, Bello, Talabi, Hassan, & Moumoh, 2014).

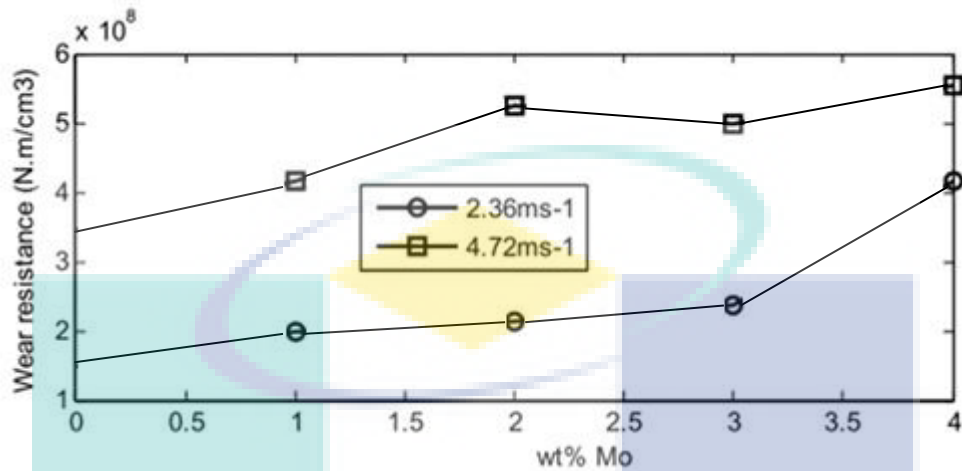


Figure 2.8 Wear resistance of grey cast iron with % wt. of molybdenum additions.

Source: Agunsoye et al. (2014)

Previous studies have been reported that alloying with Mo in cast iron produced carbide phase such as M_2C and M_6C and improved the wear resistance of cast iron which is shown in white needle carbide and white block carbide. According to Liu and Zhou (2012) the M_6C has higher wear resistance compared to the M_2C , where some big pores appear in the worn surfaces at M_2C carbide as shown in Figure 2.9 (Liu & Zhou, 2012).

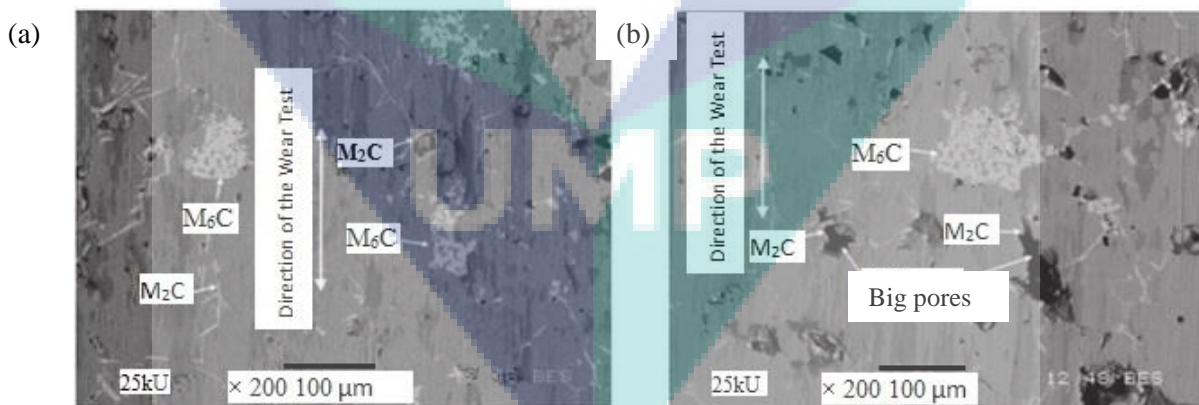


Figure 2.9 SEM images of the worn surface (a) before wear test and (b) after wear test.

Source: Liu & Zhou, (2012)

Mixture of Cr-Mo also can increase the wear resistance where the volume loss of the cast iron decreases as the carbide forming elements were added, which should be mainly attributed to the increment of hardness. This is due to the introduction of fine

carbide and microstructure refinement (Chung, Tang, Li, Hinckley, & Dolman, 2013). The finding is consistent with findings studied by Sulardjaka et al. (2013), where alloying with Cr and Mo improved fatigue strength at room temperature where Cr and Mo can hinder graphite precipitation and increase the inclination to form iron carbide in grey cast iron (Atmadja *et al.*, 2013). Figure 2.10 shows the comparison result between pin-on-disc test and hardness test in alloying cast iron with chromium and molybdenum. These results proved that alloy of chromium and molybdenum increase the hardness, wear resistance and oxidation in grey cast iron material.

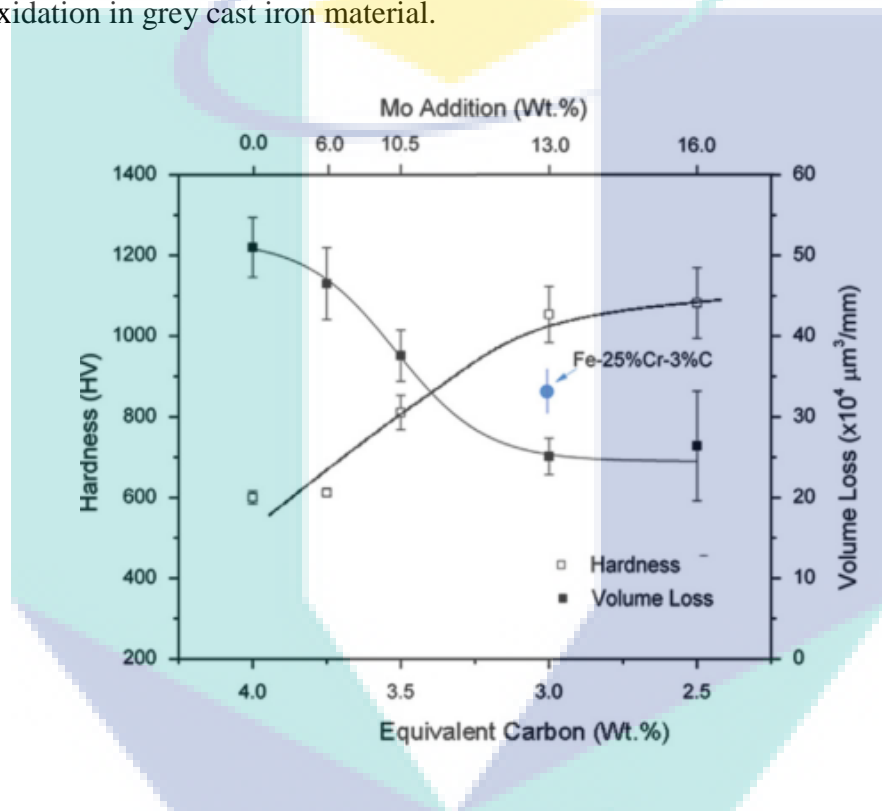


Figure 2.10 Pin-on-disc test and hardness test result for the modified cast iron alloys with addition of chromium and molybdenum.

Source: Chung et al., (2013)

In other different study, Moonesan et al. (2012) examined alloying Cr and Mo in grey cast iron and it shown that it can enhance the thermal shock resistance and tensile strength. Grey cast iron without Cr and Mo alloy resulted major crack on the surface after two cycles of thermal shock test. The finding suggests that increasing Mo content will increase the thermal shock resistance, while increasing the Cr will increase the tensile strength in grey cast iron. It is obvious that Mo have high thermal conductivity, which can minimize the thermal stress and increase the thermal shock resistance. According to Moonesan et al. (2012), alloying with Cr will reduce the decomposition of pearlite and

stabilize the structure which is enhancing the tensile strength (Moonesan *et al.*, 2012). Based on Figure 2.11, increasing the alloying Cr and Mo will increase the number of thermal shock cycle and tensile strength in grey cast iron.

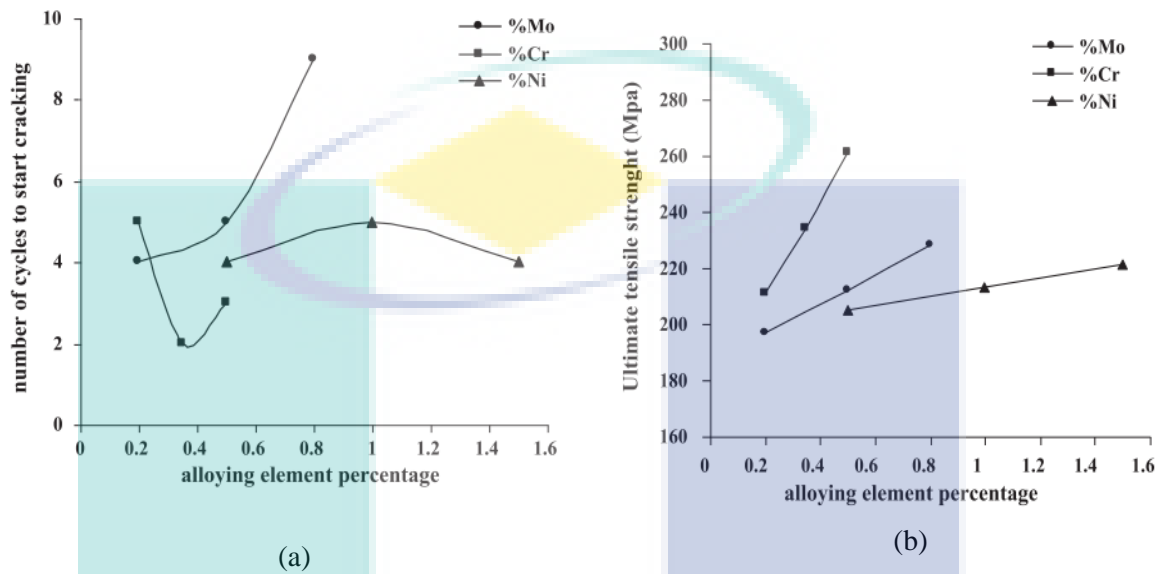


Figure 2.11 (a) Thermal shock resistance and (b) ultimate tensile strength of the alloyed grey cast iron as a function of alloyed composition.

Source: Moonesan *et al.*, (2012)

In other words, it is proven that additional elements such as Cr and Mo improved the hardness, wear resistance and corrosion resistance in grey cast iron. These elements also will enhance the heat resistance and tensile strength. These enhanced properties are due to the carbide phase formation and microstructure refinement. So far, alloying with Cr and Mo has only been applied on casting process, which involved bulk material. Special attention should be paid to modify the surface of grey cast iron with addition of Cr and Mo without involving the bulk material.

2.3 Advanced Surface Modification on Grey Cast iron

Grey cast iron is widely used in components with extreme pressure and wear such as brake disc, piston liner and cylinder liner. While the components is being used, usually defect will be formed on the surface of grey cast iron. Many researches have been done to improve the surface properties of the grey cast iron by changing their composition or

performed additional process such as heat treatment. These processes involved bulk materials and some time there are not suitable because of the size and not economical.

Nowadays, there are some advanced technology that can change the surface properties of grey cast iron, through laser processing which can modify only the surface of it without involving bulk material. Therefore, it can reduce the manufacturing cost compared to the traditional method using casting and it is flexible in its operation (Hussein *et al.*, 2013; Montealegre *et al.*, 2010). The purpose of surface modification is to enhance surface properties since the surface experience wear, high load and heat at elevated temperature (Kusinski *et al.*, 2012). For many engineering applications especially tooling industry, enhanced surface properties are significant to endure high temperature, wear and friction (Jhavar, Paul, & Jain, 2013).

Laser processing have been used in many applications such as cutting, drilling, welding, surface hardening, alloying, cladding, rapid prototyping, ablation and shot peening. The laser manufacturers stated that the laser beam is delivered in wavelength, in the range from the ultraviolet (UV) to infrared radiation and may vary either high continuous or pulsed power density with spatial as well as temporal coherence, low divergence and monochromaticity (Kusinski *et al.*, 2012). Previous reported show the laser processing have been proven to be capable of producing adherent, hard, wear, corrosion, fatigue and fracture resistant coating on a diverse range of materials (Aqida, Naher, Maurel, & Brabazon, 2008). Although there are various advanced materials with significant properties have been developed, but when it concerns about a particular surface for engineering appliances, a material's physical properties is one of the factor that need to be considered, which include practicality, energy saving, cost and time (Rao, 2013). The advantage of the laser surface processing is the possibility of accurate control at the area where laser radiation should be delivered, as well as the amount and the rate of energy deposition (Kusinski *et al.*, 2012). Besides that, laser surface processing have benefits compared to other methods including fine grained and homogeneous microstructures, low thermal damage to the underlying substrate, reduced grain growth and distortion, non-equilibrium and amorphous structures; and extension of the solid solubility of alloying elements (Aqida *et al.*, 2008).

As shown in Figure 2.12, laser surface melting is one of the process that can be used to modify the material's surface. This process requires high laser power to melt the surface at proper temperature and usually it is used in surface melting, glazing, cladding, welding and cutting (Kusinski *et al.*, 2012). Compared to other process such as heating and shock hardening, which require low power that can change the hardness of the surface without eliminating the graphite and this produce new phase (Monteiro, Silva, & Rossi, 2009).

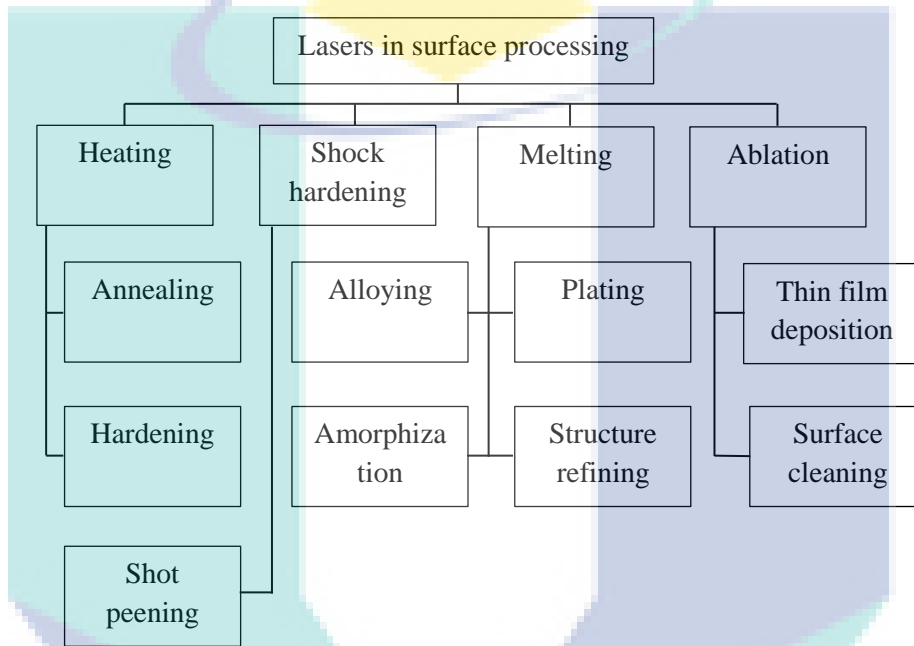


Figure 2.12 Spectrum of laser application in surface processing.

Source: Kusinski *et al.*, (2012)

There are a few reports produced to investigate on how to improve the surface of grey cast iron using laser CO₂, laser Nd:YAG, and tungsten inert gas (TIG) welding which are considered as rapid solidification processes (Alabeedi *et al.*, 2009; Benyounis, Fakron, Abboud, Olabi, & Hashmi, 2005; Chen *et al.*, 2015b). These techniques have been proven to increase hardness and wear resistance by transforming structure into martensite, retain austenite and cementite (Fe₃C). Besides that, grey cast iron surface modification can involve a range of processes including epitaxial regrowth of the substrate, nucleation of crystallites throughout the undercooled melted region, material reheating due to the release of the latent heat of solidification, or formation of an amorphous surface structure (William & Leonid, 2007). This formation is due to the high cooling rate during laser processing. This is supported by Yilbas *et al.* (2016) study which

revealed that the high cooling rate in laser surface processing exhibited enhanced wear resistance due to the lubrication effect and optimized impact toughness which contributed to the formation of oxide film consisting of low nitrogen compound and iron oxidation (Yilbas, Akhtar, Karatas, & Boran, 2016).

There is also a report to enhance surface properties by adding powder metal on the surface to change the surface composition. This technique has been used by many researchers when material surface involved with high temperature during operation (Hussein *et al.*, 2013; Ocelik *et al.*, 2007; Yaoa *et al.*, 2017). Usually transition metal such as chromium, molybdenum and tungsten are used because of these elements have properties advantage such as high temperature strength, improved toughness, hardenability and corrosion resistance. Previous report showed modifying surface using TIG in cast iron surface alloying with chromium and molybdenum will form structure of cementite, martensite, retained austenite and primary carbides structure of $(Fe,Cr)_7C_3$ and $(Fe,Mo)_3C$ (Amirsadeghi & Sohi, 2008). As a result, the alloying surface showed higher hardness and high temperature strength compared to the melting surface because of the carbide formation. However, as show in Table 2.2, laser surface melting and laser cladding process have advantages compared to other laser surface processing.

Table 2.2 Advantage laser surface melting and laser cladding in cast iron.

Laser surface melting	Laser surface cladding
High depth of penetration in melting zone.	Can increase their resistance properties such as corrosion, wear, oxidation, and extreme temperature, as well as the ability to provide lubricant.
Minimizing the total amount of material affected.	Cost effective in the enabling salvage of expensive parts, which were damaged during service.
Can improve their properties such as wear, erosive and corrosive resistances due to formation of hard, homogenous and ultrafine structure of the material surface layer, without changing its chemical composition.	Allow to obtain the porosity and cracking free surface coating containing uniformly distributed hard particles in the softer and tough matrix.
Can form of grain refinement, supersaturated solid solution and fine dispersion of particles.	Have strong bonding in comparison to the thermal spray coating.

Source: Kusinski *et al.*, (2012)

2.3.1 Laser Surface Melting of Grey cast Iron

To date, various conventional and advanced processing methods have been used to produce hardened layer for high wear resistance including laser surface melting (LSM). This technique improves surface properties by forming of hard, homogenous and ultrafine structure of the material surface layer without changing its chemical composition (Kusinski *et al.*, 2012). This method has been proven to change the surface layer enhance surface hardness and wear resistance by eliminating graphite on the surface (Chen *et al.*, 2015b; Cheng, Hu, Song, & Xiong, 2014).

For many years, surface properties of metal has been improved by laser surface melting and this improvement is commonly discussed in surface technology. Generally the surface properties improvement involved the microhardness, corrosion, wear and fatigue wear, where failure could happen on the material surface. The previous work showed most of the laser surface modification cast iron used laser melting to modify the surface properties and some of them used laser heating to harden the surface without changing the phase. This processes depend on the laser parameter setting. It has been proven that this processes can enhance the surface properties because of the high cooling rate during the processes (Fazliana *et al.*, 2014).

Previous result shows that laser melting can improve wear resistance by considering beam size, traverse speed and power. The combined effect established the temperature field in the interaction area between laser beam and material and determined the cooling rate of the surface layers (Blarasin *et al.*, 1983). High cooling rate of laser surface on grey cast iron can transform the surface structure into martensite, cementite (Fe_3C), retain austenite (Ar) and smaller crystals which contributed to the enhancement of microhardness (Amirsadeghi *et al.*, 2008; Blarasin *et al.*, 1983; Chen *et al.*, 2015a). Figure 2.13 shows the melting zone with white bone microstructure and phase of reticular carbides (Fe_3C), and the appearance of needle martensite mixed with retain austenite (Ar) and a complete dissolution of the graphite in the space of Fe_3C .

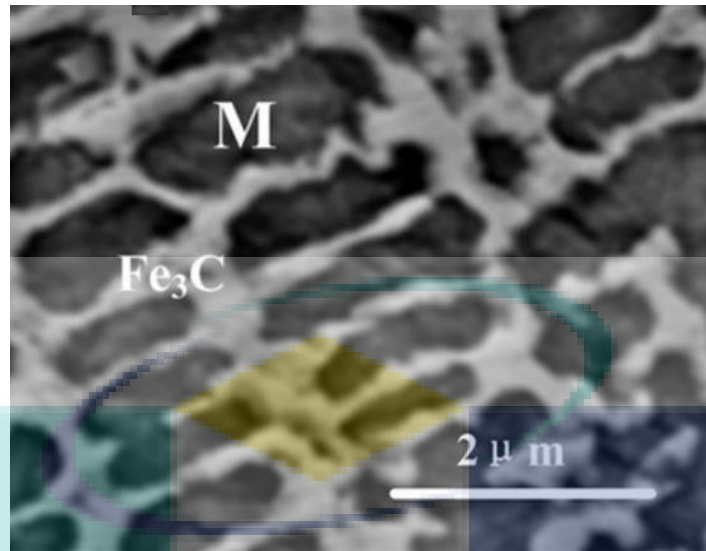


Figure 2.13 The microstructure of melting zone in cast iron.

Source: Chen et al., (2015a)

In addition, ferrite in the grey cast iron matrix is in random dispersion and only a portion of ferrite that which is close to cementite or graphite can be transformed into austenite during surface melting, and subsequently into martensite and retained austenite when the surface is chilled in room temperature. In contrast, owing to a small amount of solute trapping of carbon, the ferrite structure which is far from cementite or graphite cannot be transformed into austenite, resulting in retained ferrite (Chen *et al.*, 2015b).

Various laser power, frequency and pulse duration at different laser spot size influenced the dimension of grey cast iron surface. High energy from laser beam and relatively longer pulse duration produced deep and narrow melted zone with high hardness (Benyounis *et al.*, 2005). During the laser process, the light and heat energy exchanged between laser and grey cast iron to obtain the molten zone. The light energy was absorbed, the surface of grey cast iron was melted and then solidified by conduction (Pang *et al.*, 2015a).

A researcher from Chen and co-workers (2015) used pulse energy of 5.37 J at three different focal distances of 10, 12 and 14 mm for cladding with carbon powder, while in 2016, he reported laser processes of grey cast iron with W/Cr powder addition using pulse energy of 4.5 J at focal distance of 15 mm (Chen *et al.*, 2016; Chen *et al.*, 2015b). The usage of different energy in laser processing directly change the surface

cooling rate. It would influence the size of the microstructure where more energy can be absorbed by the surface of grey cast iron and increase the cooling rate and make the microstructure more compact. From Figure 2.14, it shows that graphite is completely dissolved and re-solidification of the dendrite structure. The dendritic structure is proeutectic austenite and the white reticulate parts are cementite (Pang *et al.*, 2015a). The small interdendritic spacing resulted in the higher microhardness.

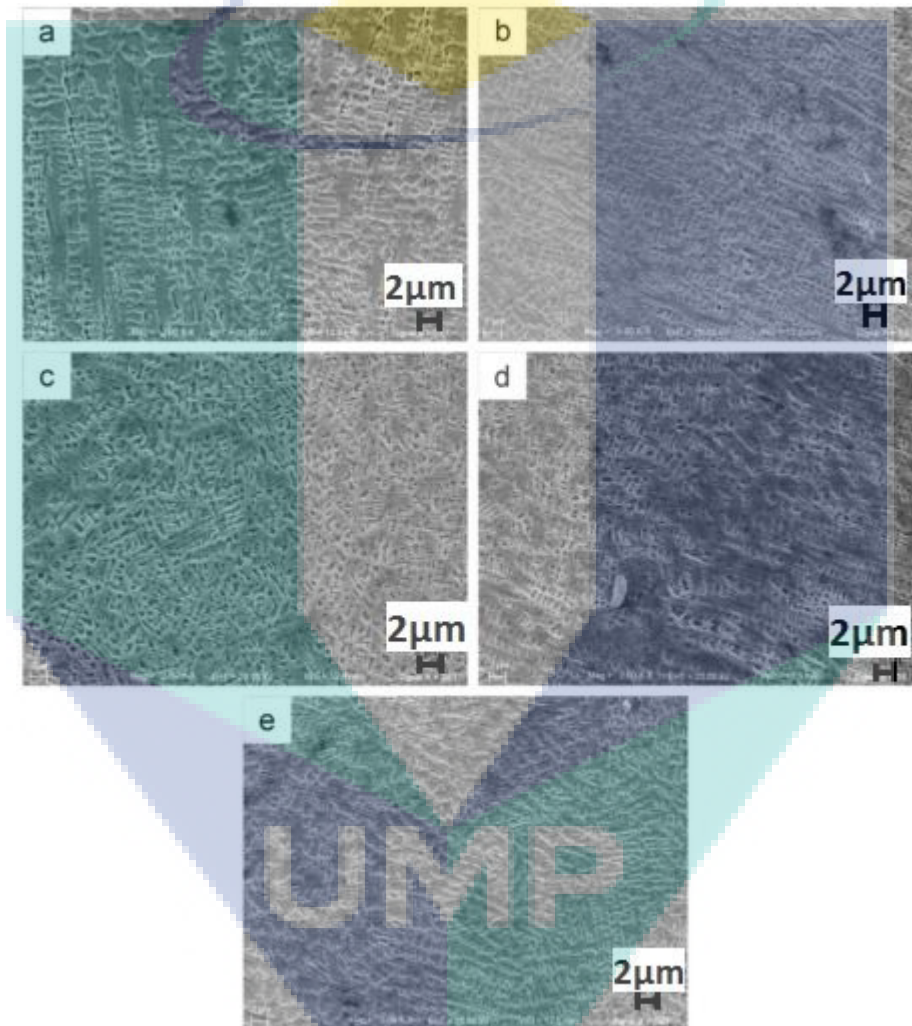


Figure 2.14 The microstructure of molten zone at different energy (a) 5.22 J, (b) 7.09 J, (c) 9.26 J, (d) 12.54 J and (e) 10.87 J.

Source: Pang *et al.*, (2015a)

Laser surface melting on grey cast iron produced three different zones which were distinguished by distinct phase characteristics, remelting zone (RZ), transform zone (TZ) and substrate. Transform zone has low hardness compared to the remelting zone because the coarse martensite and incomplete melted graphite were found as shown in Figure 2.15.

According to Figure 2.15 (a), the measurement of microhardness on the top was markedly larger than that at the bottom of remelting zone, almost at 900 HV. At RZ microstructure, the equiaxed crystal grain were presented at the top, while the columnar crystal grains were investigated at the bottom because of the distinct cooling rate (Chen *et al.*, 2015a). This phenomenon occurred when the laser irradiate move, so the heat was transmitted from the top to bottom with gradient temperature and the heat, however, was not able to adequately melt the material to retain some untransformed pearlite in transform zone.

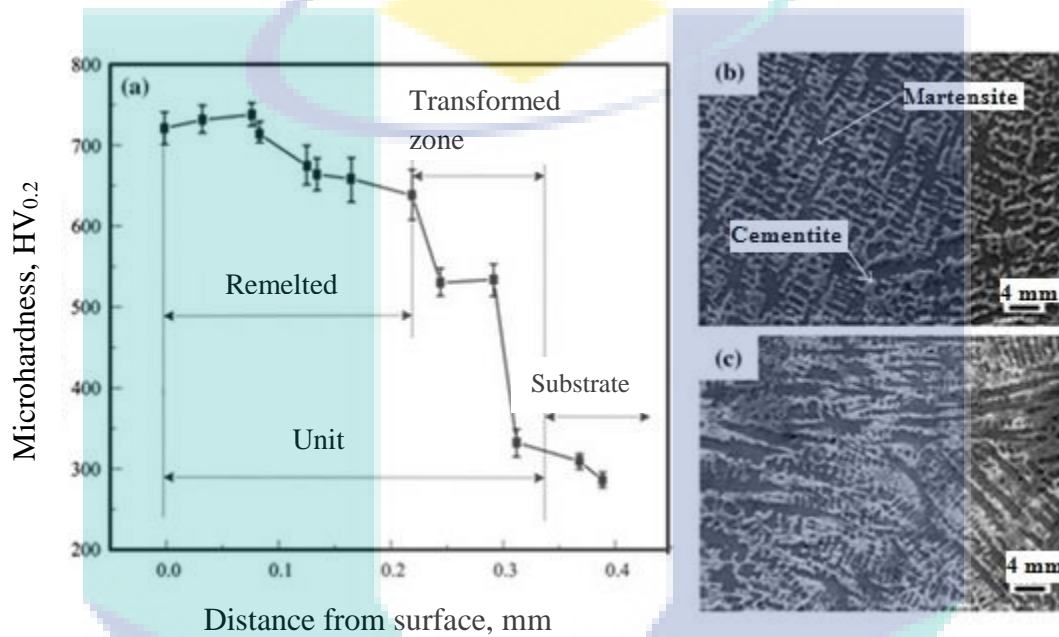


Figure 2.15 (a) The microhardness in depth, (b) the equiaxed crystal grains at the top of molten pool and (c) the columnar crystal grains at the bottom of molten pool.

Source: Chen *et al.*, (2015a)

Development of laser surface melting to improve the wear resistance of grey cast iron has been done in 1983 and continued by other researchers until now. They found the increment of the surface hardness influenced the wear resistance of grey cast iron. However, the laser parameter that they used were not consistent and different among each other's. For example, they used the same laser Nd:YAG system to melt the grey cast iron surface, but the laser spot size were different and it directly change the laser parameter setting. Table 2.3 show the previous researchers used laser surface melting at different setting for cast iron.

Table 2.3 Previous researcher used laser surface melting at different setting for cast iron.

Reference	Spot Size (mm)	Pulse Energy (J)	Pulse width (mm/s)	Scan speed (mm/s)	PRF (Hz)
(Zhou <i>et al.</i> , 2014)	1.5	2.75	5	0.5	7
(Fazliana <i>et al.</i> , 2014)	0.6	0.72 - 1	Not specify	16.67 – 23.33	50 - 70
(Chen <i>et al.</i> , 2015a)	1.3	5.37	5	Not specify	9
(Pang <i>et al.</i> , 2015a)	1.0	5.22	Not specify	0.5	4
	1.3	7.09			6
	1.5	9.26			8
	1.6	12.54			4
(Chen <i>et al.</i> , 2016)	12 (focus distance)	2.28	3	0.5	7

The most important processing parameters for the laser surface modification include laser beam power, laser spot size, heat intensity distribution across the beam, absorptivity of the beam energy by the treated material surface, scanning rate of the laser beam across the substrate surface and the thermal properties of the treated material (Kusinski *et al.*, 2012). Previous report showed that melting surface versus the intensity of energy will produce distinct linear relationship for melting zone, transformation zone and incipient melting at the surface followed by a predominantly transformed zone (Hwang *et al.*, 2002). Although by controlling laser power and traverse speed can melt the grey cast iron and increase the microhardness. Little information was found on optimization of the laser melting of grey cast iron at different laser spot sizes for maximum hardness properties and minimum surface roughness. The surface roughness is sharply decreases with the decreasing of the peak power and the increment of traverse speed (Fazliana *et al.*, 2014).

2.3.2 Laser Cladding of Grey Cast Iron

Nowadays, various conventional and advanced processing methods have been used to produce hardened layer for high wear resistance including laser surface cladding (Chen *et al.*, 2015b; Norhafzan, Aqida, Chikarakara, & Brabazon, 2016). Comparing between laser cladding and laser alloying, these two processes involved introducing

additional elements to the laser melted surface. In alloying, the composition of the surface change while in cladding, only bonding with minimal mixing of the additional elements and melted surface involved (Aqida, 2011). The purpose of laser cladding in grey cast iron is to improve wear, impact, corrosion resistance properties of surfaces, by generating a protective layer for different material. This method is similar to the laser surface melting where the purpose is to melt the surface at high cooling rate (Fazliana *et al.*, 2014). Furthermore, laser surface cladding used desired elements that being added to the melt pool to modify the surface chemical composition. However, the different in thermal properties of added elements affect the cooling rates and solidification in the laser surface modification, particularly in the close region of the hard particles. This modifies the microstructure around the hard particles in the surface region while modifying the residual stress, microhardness, and coefficient of friction of the resulting surface (Yilbas *et al.*, 2016).

During laser processing, pre-placed layer and substrate are melted and both liquid phases are intensively mixed and therefore the solidification of a new desirable surface alloy is formed. In addition, rapid solidification on the surface layer is the feature for the laser cladding process and in some conditions the coating formed by cooling rates in range of 10^3 to 10^5 Ks^{-1}/s shows very fine, non-equilibrium or even amorphous microstructure (Ocelík, Oliveira, & Hosson, 2009). The process sequences are shown in Figure 2.16. The factor that contributes to successful alloying of the surface is the temperature gradient that can influenced the intensity of the convective movement in the melted pool and cause the distribution of the alloying elements in the molten pool (Kusinski *et al.*, 2012).

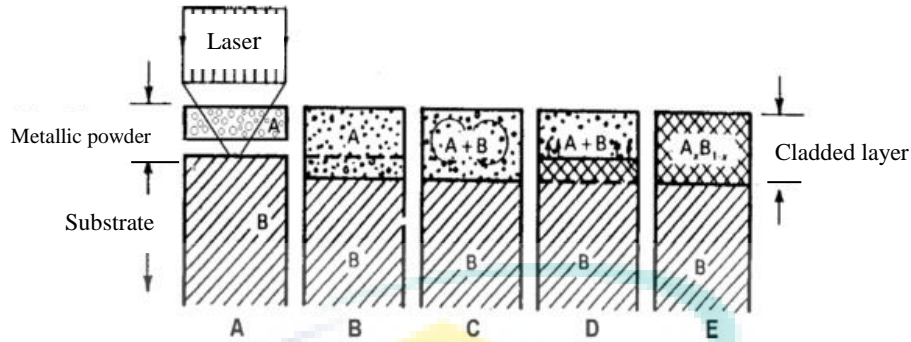


Figure 2.16 Schematic steps involved during the laser surface cladding.

Source: Kusinski et al., (2012)

Laser processing using laser cladding technique is usually defined in terms of laser power P_p (W), traverse speed S (mms^{-1}), laser spot size, laser beam energy distribution, sort and amount of shielding and carrier gas, size, speed and feeding direction of power particles (Hussein *et al.*, 2014). However, the important effect in laser cladding is to have excellent bonding between powder and the substrate. Important performance parameter to evaluate the quality of the laser cladding is the dilution rate. An excessively large dilution rate will lead to the degradation of inherent properties of the coating. An excellent fusion bond may not be formed between clad powder and substrate if the dilution rate is too small. As a result, the coating is easy to spill out from the substrate when subjected to an external force and a dramatic change in temperature (Qu *et al.*, 2015). However, laser cladding by an overlap of single track can reduced the dilution rate due to the laser beam energy is consumed by remelting clad material at the side in the previous laser track (Ocelik *et al.*, 2007). According to Ocelik et al. (2007), laser cladding by an overlap of single laser tracks deposited side by side with displacement can minimize the surface roughness and maximize the depth of the clad layer. This technique creates a coating which usually 20-35 % thicker than the depth of single laser track as shown in Figure 2.17 (Ocelik *et al.*, 2007).

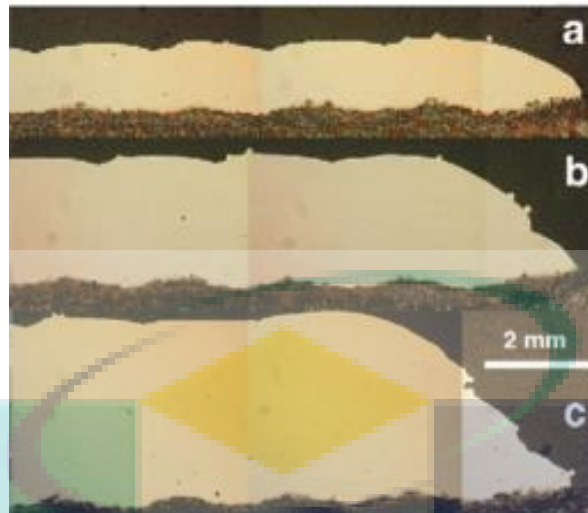


Figure 2.17 Cross section of single (a) double (b) triple and (c) clad layer made by overlapping of single laser tracks.

Source: Ocelik et al., (2007)

Laser cladding improves surface properties by forming a new alloy layer with new chemical composition of hard, homogenous and ultrafine structure (Sun *et al.*, 2011). This method has been proven to change the surface layer to enhance surface hardness, corrosion resistance, thermal fatigue and wear resistance by eliminating the graphite on the surface and form a new structure (Sun *et al.*, 2011; Yang *et al.*, 2015; Zhong *et al.*, 2006). This method shows significant advantage compared to the melting method because it can modify layer surface with variety of alloying elements. Alloying with chromium and molybdenum can form complex carbides with the carbon in the cast iron, which significantly enhances the strength, hardness and wear resistance (Amirsadeghi & Sohi, 2008; Tong *et al.*, 2008). For instance, Amirsadeghi and Sohi (2008) research show alloying with chromium and molybdenum will increase the hardness up to 1000 HV_{0.2} and reduced the wear rate up to 60 %. This is because a new hard phase consist of M₇C₃ and M₃C carbide is formed on the surface of cast iron. In addition, heat input during the process of alloying the surface affects the formation of carbide on the surface of cast iron.

Researchers have studied the effect of laser energy to the laser cladding dimensions. In laser cladding with constant input energy, the width dimension increases as the laser spot is increased, while the depth dimension rapidly decreases in contrast. However, the area decreases in inversed proportion to the size of the laser spot. According to Chen et al. (2015), this is due to the energy density noticeably declines with the

amplification of the laser spot, which causes a decrement in temperature at the centre of heat source, leading to a wider but shallower and smaller area as response (Chen *et al.*, 2015b). Comparing between laser surface melting and laser cladding, the width in laser cladding are smaller because the surface is covered with powder coating, so the heat conductivity of powder material is much smaller than the uncoated grey cast iron. Thereby, heat cannot spread rapidly in abundant carbon direction. However, the depth of laser clad is greater than the laser surface melting. The factor that contributes to this different dimension in laser surface melting and laser cladding is the existence of the powder layer in laser cladding, where the absorbance of laser beam is increased. As the absorbance increases, the subsequently increased energy density caused the melted materials to reach higher temperature, which in turn leads to the further spreading of heat and deepening of the unit (Chen *et al.*, 2015b). In other words, for laser cladding processing, the effective heat affected on substrate was much less than the heat absorbed by coating (Chen *et al.*, 2016).

2.4 Laser Surface Modification Parameter

Grey cast iron composition and properties are different with steel. It is important when laser surface modification is considered. The value of density, melting temperature point and thermal conductivity are extremely varies within ferrous alloys. Therefore, if the same laser parameter conditions such as laser beam size, laser power and irradiance are applied, there will be changes on the surface layer, therefore, the importance of laser parameter will be discussed in the next section.

2.4.1 Laser Beam Density and Interaction Time

Laser parameter is an important factor to enhance the surface properties in laser surface modification especially for grey cast iron which have low melting point. The crucial parameter in generating the temperature in the surface layer of treated material is laser beam density or irradiance and interaction time. Consequently, different temperature effect in the surface layer can be reached like melting zone. However, at high temperature over boiling point, evaporation could be occurred and it will affect the shape of the surface and properties of material (Paczkowska, 2016). As show in Figure 2.18, laser beam density and interaction time can affect the thermal on the surface layer such as remelting,

alloying, hardening and tempering for grey cast iron. In addition, the material properties such as density, melting temperature and specific heat capacity are extremely varied within metal alloy and even within ferrous alloys. Therefore, if the same laser parameter are applied, final properties in surface layer could be different in steel and cast iron.

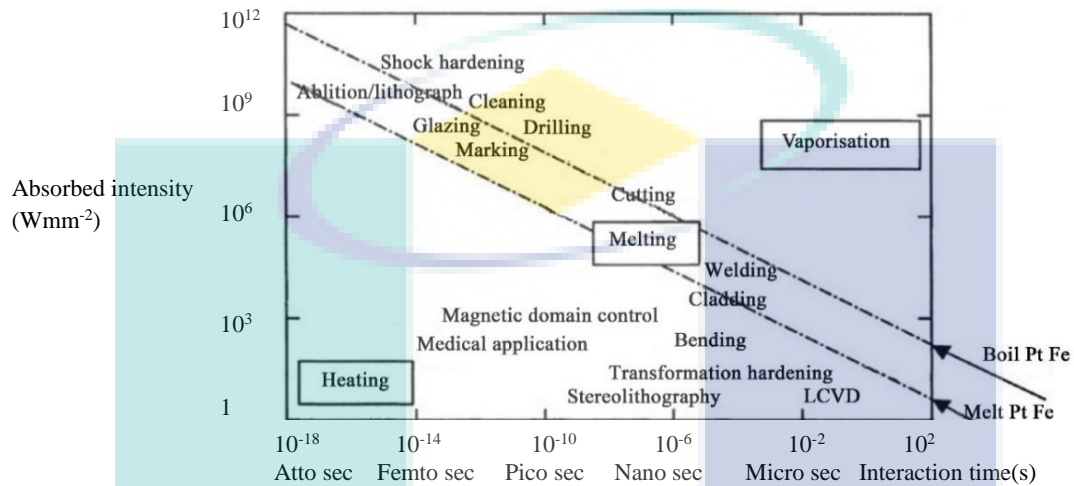


Figure 2.18 The range of laser process mapped against laser beam density and interaction time. The diagonal lines represent the lines of constant temperature for the boiling and melting point of iron.

Source: Chen et al., (2016)

It has been suggested that, melting on the surface of grey cast iron could be obtained at the value of the laser beam power density of at least 10 to 20 Wmm^{-2} , where the laser interaction time had to be longer than 0.2 s . While applying a shorter laser interaction time requires higher values of the laser beam power density as shown in Figure 2.19 (Paczkowska, 2016).

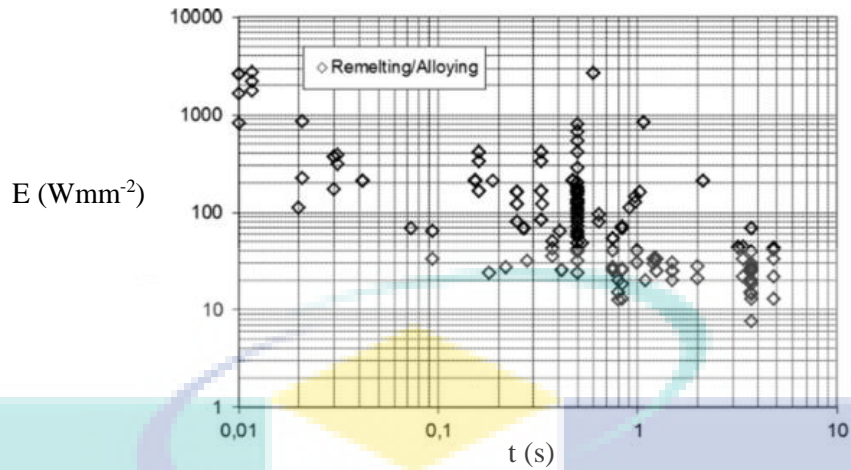


Figure 2.19 Laser beam power density (irradiance) treatment parameter variants that caused remelting/alloying in the surface layer of grey cast iron.

Source: Paczkowska, (2016)

Blarasin et al. (1983), observed the combination of laser beam size, scan speed and laser power effect established the temperature field in the area interaction between laser beam and material and determined the cooling rate of the surface layers (Blarasin *et al.*, 1983). High cooling rate is necessary to eliminate graphite and formation of grain structures. High irradiance and short interaction time combination are usually ideal for faster cooling rate to be achieved. According to Figure 2.20, increasing interaction time produced deeper penetration in the melt zone and it also increases the cooling rate where the amount of retained austenite is increased (Gadag, Srinivasan, & Mordike, 1995).

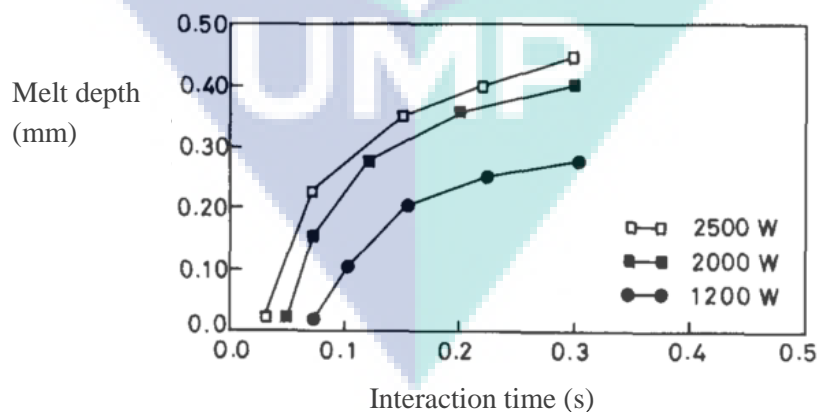


Figure 2.20 Variation of melt depth with power and time of laser material interaction.

Source: Gadag et al., (1995)

Furthermore, for interaction time lower than 0.1 s, periodic cracks could occur across the melt track, as number of speed increased as interaction time decreased until it is too short to produce surface melting as shown in Figure 2.21 for interaction time at 0.01 s. According to Fouquet and Szmatura, (1998) at scan speed above 6 mm/s the martensite is present in the melted zone at which the interaction time became too short to obtain homogeneous melting and deeper penetration; part of the austenite could have a lower carbon content and transform to martensite at room temperature (Fouquet & Szmatura, 1998).

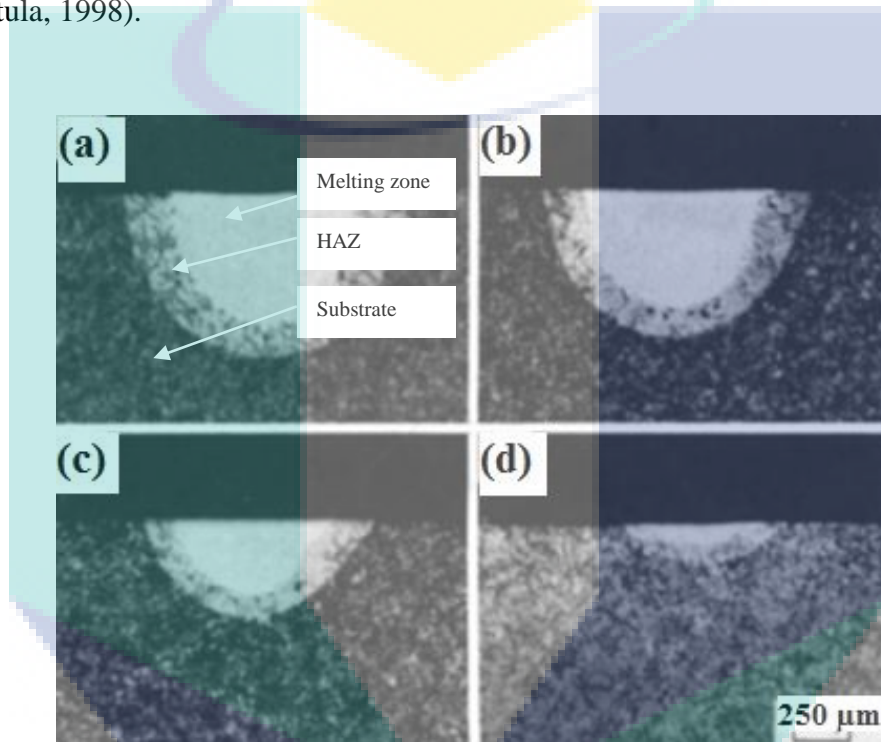


Figure 2.21 Transverse cross-section of melted tracks for the following laser processing parameter: $P = 780 \text{ W}$, $d = 0.6 \text{ mm}$, $\tau = 0.01 \text{ s}$ and (a) $V = 0.8 \text{ mm/s}$, (b) $V = 1.6 \text{ mm/s}$, (c) $V = 5 \text{ mm/s}$ and (d) 40 mm/s .

Source: Fouquet & Szmatura, (1998)

Increasing the energy density resulted an increment of area cross section at laser surface modification. In addition, the area of laser surface alloying is larger than the laser surface melting due to laser beam absorbance increment (Chen *et al.*, 2015b). Energy density also can affect the dimensions of the crystal. From the laser surface melting microstructure, it can be seen that the dimensions of the crystal increases as the energy density decreases, and the result of solidification rate declined. These effects can improve the fatigue wear resistance of surface grey cast iron. The increment of amount columnar

crystal also occur in laser surface alloying when the energy density decreases (Chen *et al.*, 2015b). However, comparing the microstructure of laser surface melting and laser surface alloying shows that the laser surface alloying is finer and more compact, as show in Figure 2.22.

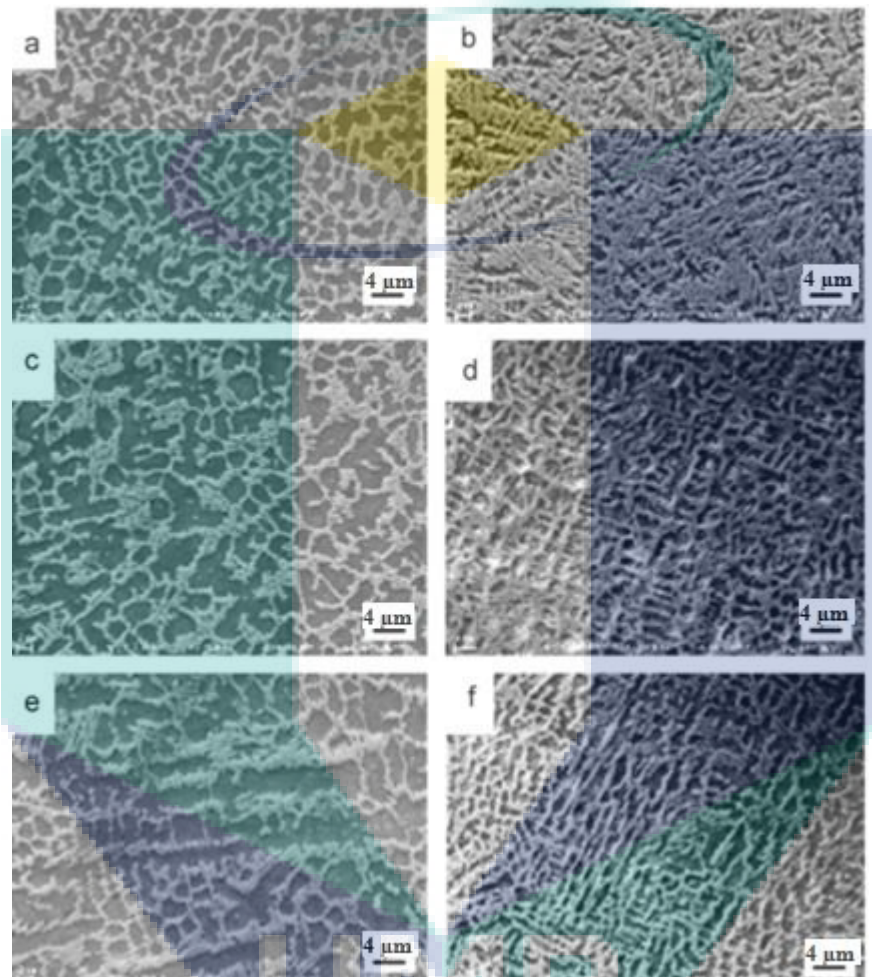


Figure 2.22 The microstructure of laser surface melting (a) (c) (e) and laser surface alloying (b) (d) (f) at different energy density 10.7 Jmm^{-2} , 6.84 Jmm^{-2} and 4.75 Jmm^{-2} .

Source: Chen *et al.*, (2015b)

Gadag *et al.* (2015) also found that the hardness of modified layer is linear with energy density as shown in Figure 2.23 and also shown that the hardness surface modification increases from substrate to the surface. This is due to the increment of energy density that caused variation of the cooling rate and more carbon being dissolved in the initial stage due to the extended solid solubility and partly which had generated different structures (Gadag *et al.*, 1995).

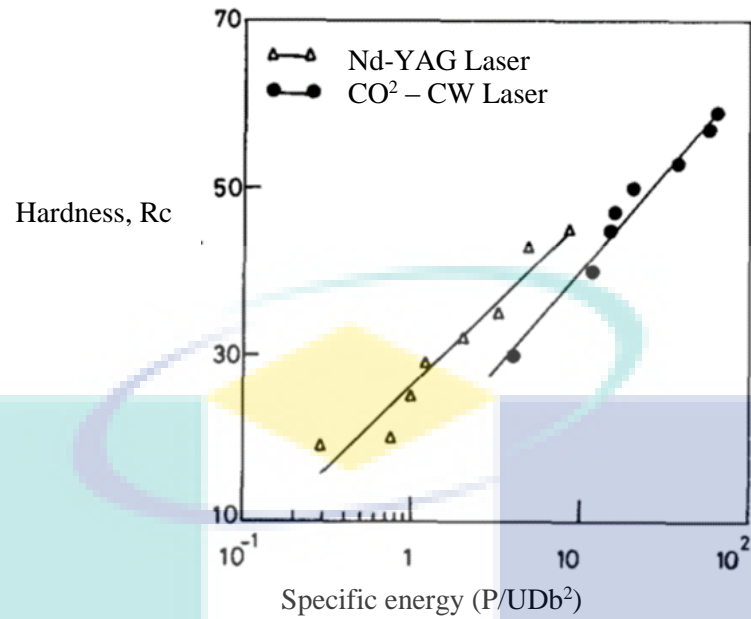


Figure 2.23 Effect of incident energy intensity on surface hardness properties.
Source: Gadag et al., (1995)

High energy density can reduce the hardness of laser surface modification. Laser surface alloying has higher hardness compared to laser surface melting because of the finer and more compact crystal. Besides that, percentage of ledeburite in laser surface alloying is higher than laser surface melting as show in Figure 2.24. Based on the quantitative analysis, percentage of ledeburite is proportional to the energy density (Chen *et al.*, 2015b).

UMP

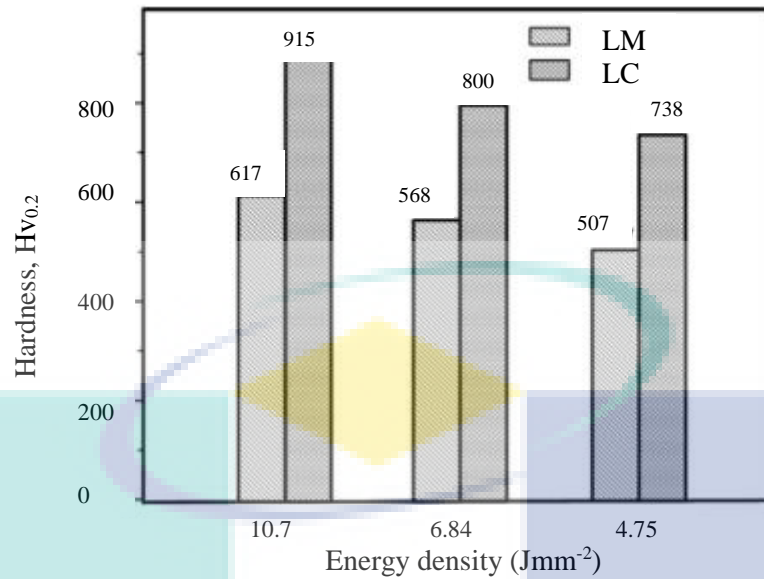


Figure 2.24 Microhardness of laser melting (LSM) and laser alloying (LSC) in various energy density at load of 0.2 kg and a dwell time of 10 s.

Source: Chen et al., (2015b)

2.4.2 Laser Spot Size

Laser spot size is an important parameter in many lasers and can be chosen within a range of possibilities. According to Sands (2011), spot size is not simply based on the size of the targeted area. In fact, the spot size can have a great deal of influence on the depth of penetration of the laser, regardless of wavelength (Sands, 2011). Laser spot size or laser beam diameter are based on a model of a Gaussian distribution of the beam's intensity or irradiance, across its diameter. Basically, the Gaussian model of laser beam characterizes the beam's maximum intensity is at the center of the beam, with intensity falling off in a Gaussian profile as it goes outward as shown in Figure 2.25. The diameter of the beam at which its intensity equals $1/e^2 \times I_{max}$ where e is mathematical constant (approximate 2.7183) and I_{max} is maximum intensity of laser beam. This has turned out that $1/e^2$ approximately equals to 13.5 %.

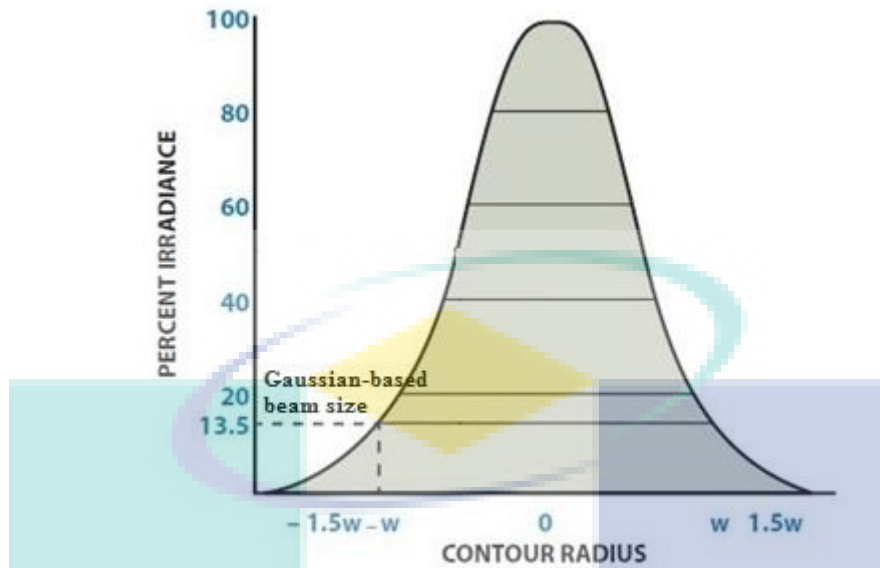


Figure 2.25 Gaussian irradiance profile.

Source: Jacobs, (2006)

According to Jacobs (2006), laser beam diameter varies on the function of its distance from the scanner. Unmodified, the diameter of a laser beam will naturally tend to increase with distance as shown in Figure 2.26 (Jacobs, 2006). Basically, the laser beam diverge and the beam will always increase in width over distance. The least divergent beam is the TEM_{00} beam. In generally, the TEM_{00} is more suitable for most laser application. Furthermore, the melt pool formed by the TEM_{00} mode has the greatest depth and width, and develops more quickly during processing compared to other modes. The beam propagation factor M^2 , is a parameter which describes how much faster a real beam diverges in comparison to a TEM_{00} beam. A beam with an $M^2 = 3.1$ will diverge 3.1 times as fast as a TEM_{00} beam. The M^2 parameter is an important property of the laser beam as it describes how easy it is to focus the beam on a surface. The M^2 is usually calculated by measuring the beam width at several distances from a lens. However, no standardized method for measuring the M^2 parameter exists (Eriksson, 2005).

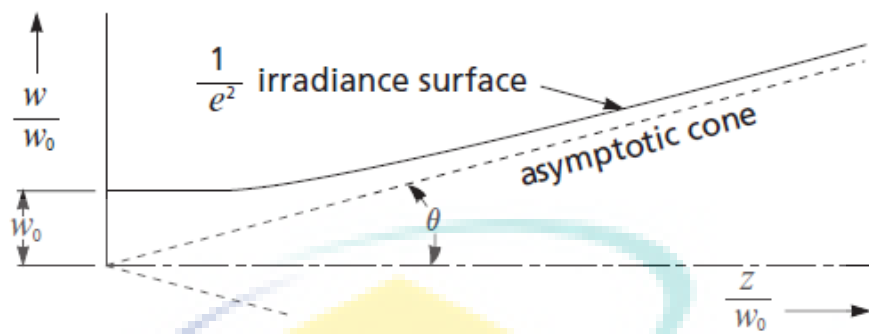


Figure 2.26 Growth in beam diameter as a function of distance from beam waist.

Source: Jacobs, (2006)

Researchers have studied the effect of laser beam diameter on metal surface. It is shown that, using laser beam at larger size have less scattering occurs, while at the same time the penetration is increased and less energy loss with depth of penetration. On the other side, decreasing the spot size by 50 % will increase the irradiance by power of 4. Hence, to maintain the same energy density with a spot size only half the diameter, one would have to reduce the irradiance by a factor of 4. Furthermore, small spot sizes allow for greater scattering of the laser beam, thus limiting its penetration, while larger spot sizes penetrate more deeply into the substrate due to less scattering (Sands, 2011).

2.4.3 Laser Power and Traverse Speed

The increment of laser power influences the heat input in laser beam which increase the surface temperature and affect the surface roughness. Proper combination of laser power and traverse speed during laser processing will affect the surface dimension whether increases or decreases the surface roughness. According to Hwang et al. (2002), the surface roughness of the layer decreases with an increment of traverse speed for given laser power and also increases with a decrement in laser power for a given traverse speed.. However, higher laser power and lower traverse speed can cause the surface to vaporize. There have been several studies in the literature reporting the effect of laser power and energy density on the cooling rate and surface temperature during laser processing (Aqida, 2011). The surface temperature and cooling rate linearly increase with the increment of laser power or energy density as shown in Figure 2.27. Increasing the laser power increases the surface temperature which influences the molten surface solidification rate. The heat transfer mechanism occurs when the surface area is heated

by the absorption of energy delivery by the laser beam. The heat input which is due to a high power laser beam is well confined and very intense. Hence, heating rate in the surface layer is high. The heated layer is self-quenched after the laser beam passed it by diffusion of heat to the cold bulk. The high heating and cooling rates in the surface layer resulted in grain refinement and the formation of metastable phases and transformed microstructures (Schneider, 1998).

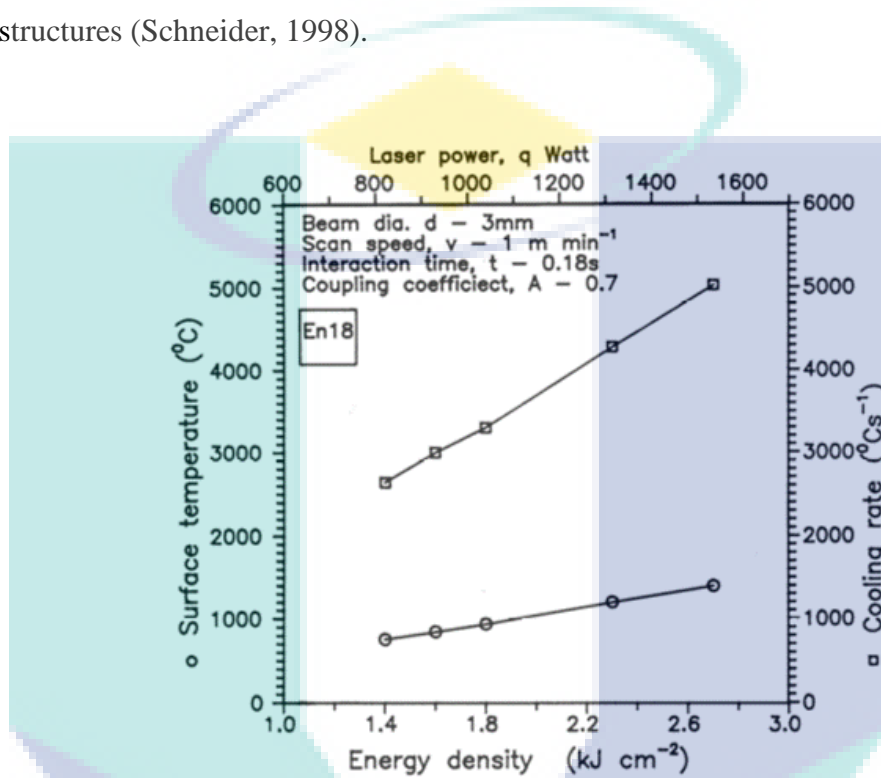


Figure 2.27 Calculated surface temperature and cooling rate as function of laser power and energy density.

Source: Aqida, (2011)

Recently, evidence suggest that depth of clad layer can be increased by decreasing the clad speed (Hussein *et al.*, 2014). Figure 2.28 shows the characteristics of the layer depth and surface roughness at different heat input. The increment of the heat input will increase linearly the depth of modified layers. The surface roughness increase slightly up to a heat input of 45 Jmm⁻¹ and then increase drastically when the heat input is over 45 Jmm⁻¹ (Hwang *et al.*, 2002).

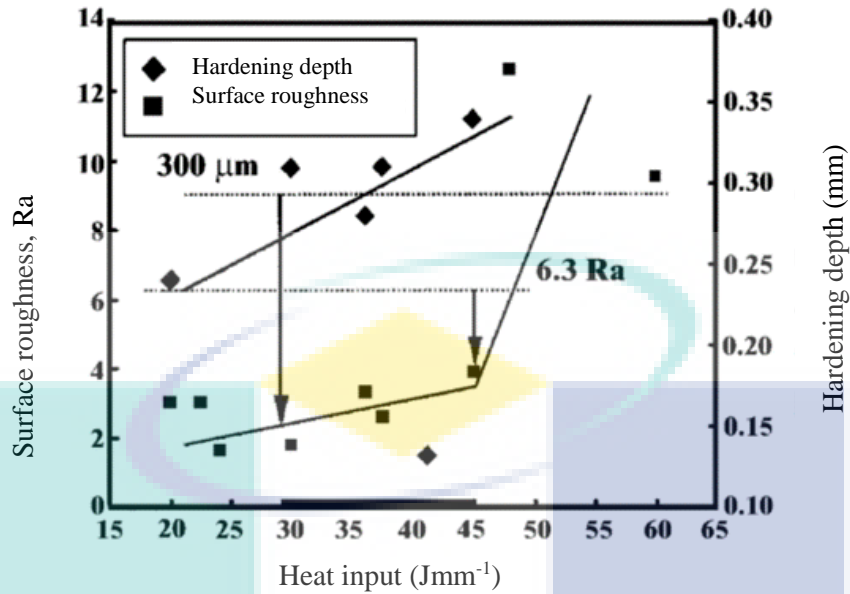


Figure 2.28 Effect of heat input on the depth of modified layer and the surface roughness of the laser modified surface.

Source: Hwang et al., (2002)

A number of studies have found that, when a low laser power is combined with a high amount of clad powder per unit length, almost all the laser power is absorbed by the powder particles and no melt pool can be created in the substrate. In contrast, when a small amount of the powder is clad together with a high laser power, a non-desired amount of dilution happened as shown in Figure 2.29 (Ocelik *et al.*, 2007).

UMP

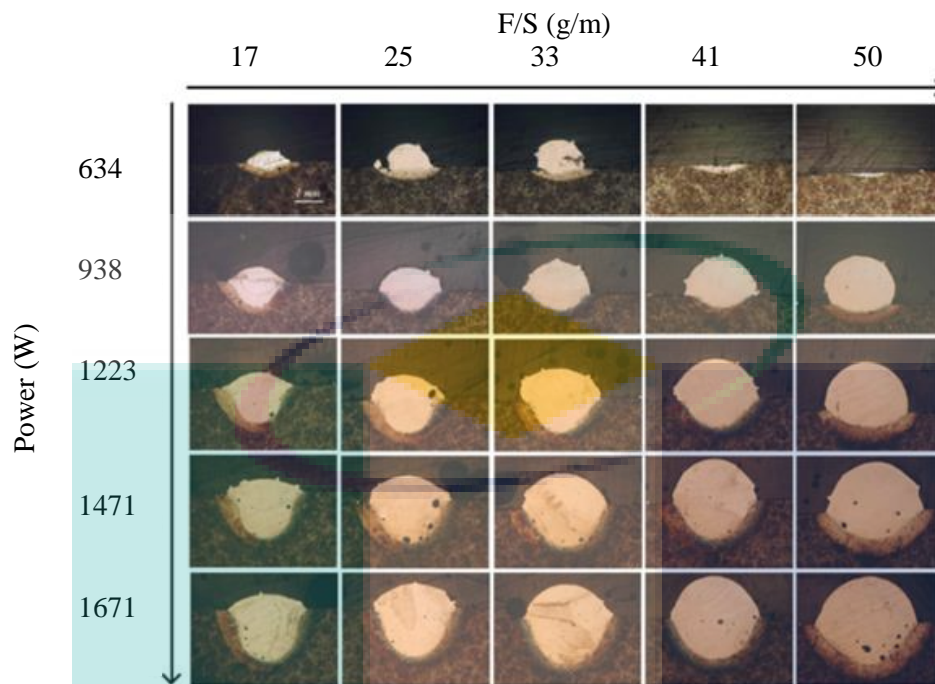


Figure 2.29 Laser tracks cross section for side cladding on grey cast iron. Combined parameter of laser power and fed material per unit track length (F/S).

Source: Ocelik et al., (2007)

The hardness of clad zone is influenced by the laser parameter such as laser power and traverse speed due to the high temperature gradient occurred. These important parameters effect on the shape, quality and boundary of clad zone and heat affected zone (Hussein *et al.*, 2014). Similarly, Benyounis et al. (2005) also found that, to obtain high hardness and depth penetration, high power density above 300 MWm^{-2} and relatively longer pulse duration at 2.5 ms are required. It can produced depth almost at 0.35 mm, narrow melted zone at 0.45 mm and relatively a high hardness at 600 HV. While for processing condition which involve low power density and short pulse duration, wide melt zone and a little penetration with a relatively low hardness will be produced (Benyounis *et al.*, 2005). Laser processing result using different power density and pulse duration with scanning speed at 1 mms^{-1} is shown in Table 2.4.

Table 2.4 Dimensions and average hardness of laser surface melting processed at different conditions.

Specimen no.	Power density (MWm ⁻²)	Pulse duration (ms)	Scanning speed (mms ⁻¹)	Melted depth (mm)	Melted width (mm)	Average hardness (HV)
1	60	0.8	1.0	0.08	0.67	540
2	80	0.8	1.0	0.10	0.67	560
3	100	0.8	1.0	0.13	0.76	600
4	300	2.5	1.0	0.30	0.34	590
5	350	2.5	1.0	0.38	0.45	600

Source: Benyounis et al., (2005)

2.4.4 Laser Nd:YAG System

Laser Nd:YAG is a crystal laser using a Neodymium doped Yttrium Aluminum Garnet with a chemical formula $Y_3Al_5O_{12}$ as a host material. Laser Nd:YAG is an optically pumped solid state laser, working at a wavelength of 1.06 mm for which the matrix is highly transparent. Figure 2.30 shows the Nd:YAG laser diagram. Laser Nd:YAG advantages include its lower reflectivity of the cut material, smaller kerf width, narrower heat affected zone, better cut edge profile, smaller thermal load, the enhanced transmission through plasma, so it is preferred for applications that need a narrow kerf width and a small HAZ width (Abbas, 2014). Moreover, the smaller thermal load of the Nd:YAG laser facilitates the brittle materials machining without crack damage in the manufactured part.

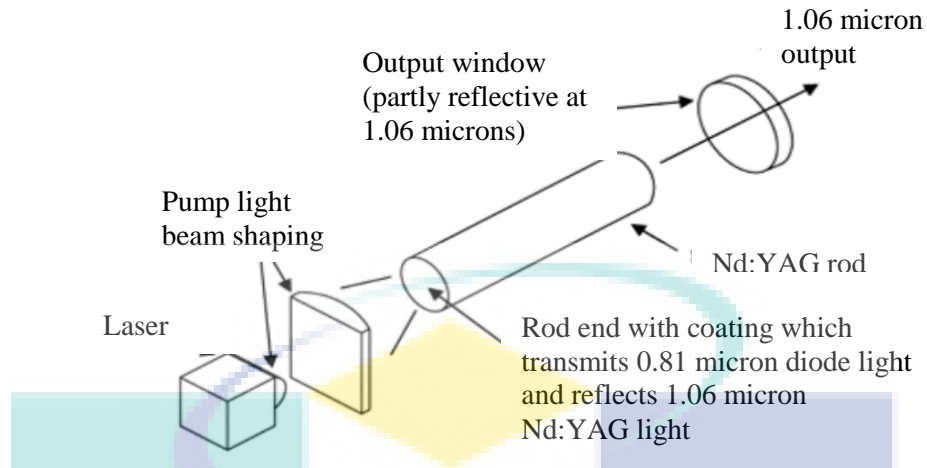


Figure 2.30 Nd:YAG laser diagram.

Source: Abbas, (2014)

Laser Nd:YAG laser is suitable for the processing of metals in general and reflective materials in particular. In addition, the shorter wavelength of Nd:YAG laser have a better absorption in metal due to the glass is transparent to the light from laser thus making it possible to use an optical fiber delivery system thus enabling the laser source to be in a different position to that of the processing point (Eriksson, 2005). Since Nd:YAG laser has many selection of waveforms, it can be applied to various processes such as trimming, repairing, scribing, welding, cutting, annealing, and soldering (Abbas, 2014). However Nd:YAG lasers have low overall efficiency and low beam quality resulting in low focus ability (Wandera, 2010).

2.5 Pre-Placed Powder on Substrate Surface

In laser surface cladding process, cladding material is usually added in powder, wire or plate forms. Among this, powder is the most frequently used. Metal powder is primarily supplied by blown powder or pre-placed powder coating (Kusinski *et al.*, 2012). There are various techniques to pre-place powder on the surface such as spraying and painting. These techniques are commonly used for laser surface alloying and laser cladding. Based on the previous reports, the pre-placed layer method is widely used because a wide range of materials can be easily mixed and used. Besides that, higher laser absorption rate on the rough surface of the pre-placed layer and lower powder loss rate make this method suitable to be used (Qu *et al.*, 2015). Previous works show it used spray technique to pre-place powder on the substrate surface by mechanically mixed the

powder, dissolved in the ethanol liquid and sprayed it to form a pre-layer with the thickness of 20 to 25 μm (Sun *et al.*, 2011). However, this technique needs a small size of particle to prevent the spray nozzle stuffed. Furthermore, with thin surface of layer, the powder can be easily dispersed during laser processing and it might be not suitable for laser surface cladding.

Researchers have been done the studies on the effect of particles' size in surface coating. Using different size of powder particles can influence the surface roughness, porosity, coating surface bonding and microhardness (Chivavibul *et al.*, 2010). Chivavibul *et al.* (2010) suggested that, to decrease the surface roughness, improve splat-splat bonding, increase the hardness and reduce the porosity on surface coating can be achieved by using smaller particle of powder. This is due to the smaller particle tend to be heated and accelerated more quickly to a higher temperature and velocity (Chivavibul *et al.*, 2010).

Now, most of the researchers used painting to pre-placed powder on the substrate surface. Normally, this technique used a binder because of its simplicity, flexibility and no requirement for equipment (Qu *et al.*, 2015). In this technique, the powder is mechanically mixed with binder such as sodium silicate or polyvinyl alcohol to form paste for the ease of painting on the substrate surface. To prevent the powder from being dispersed during laser processing, the powder mixture is dried in furnace at temperature of 200 $^{\circ}\text{C}$ for 2 h to harden the powder on the surface (Chen *et al.*, 2015b; Sohi *et al.*, 2012). Table 2.5 shows the painting technique to pre-place powder on the surface with different thickness by previous researchers.

Table 2.5 Paint technique used from previous researcher.

Reference	Thickness (mm)	Binder	Powder	Method
(Farnia, Ghaini, & Sabbaghzadeh, 2013)	1 \pm 0.1	Sodium silicate	Stellite powder	Paint
(Eroglu & zdemir, 2002)	0.3 – 2	Sodium silicate	chromium, high carbon ferro-chromium graphite	Paint
(Man, Leong, & Ho, 2008)	0.1-0.4	Polyvinyl alcohol	AISI 316 stainless steel	Paint
(Sohi <i>et al.</i> 2012)	0.5 – 3	Sodium silicate	Chromium	Paint

According to the previous researcher, the thickness of the pre-placed layer cannot be controlled precisely (Qu *et al.*, 2015). To have precise thickness of preplaced layer, previous works showed that compacted method is the best method. This method has been used by Qu *et al.* (2015) for laser cladding on the Ti₆Al₄V alloy substrate. The nominal composition of Cr-16, B-4, Si-4, and Ni-balance (wt. %) was selected as the cladding material. The result showed the required pre-placed layer thickness is reduced slightly after compacting around 10%. Compacting the powder is to make sure the fine particle fill in the air gaps and resulting the slight increment in the reduction rate with the increment of the powder contents.

In regard to pre-placed thickness, different thickness will produce in result different morphology, phase formation and mechanical properties. Based on the previous works, the increment in pre-placed layer thickness can cause the coating to become coarsen an irregular (Mezghania *et al.*, 2016; Qu *et al.*, 2015). Some obvious defects can also be observed. If there is an increment of thickness in the pre-placed layer, the profile of the coating which are presented in the arc radius become smaller and smaller. Other than that, the proportion of melting area below the substrate surface presents the downward tendency as shown in Figure 2.31 (Qu *et al.*, 2015). Recent evidence suggests that pre-placed layer thickness should not exceed 1.0 mm because more defect such as pores and unmelted particles will occur on the clad zone (Qu *et al.*, 2015).

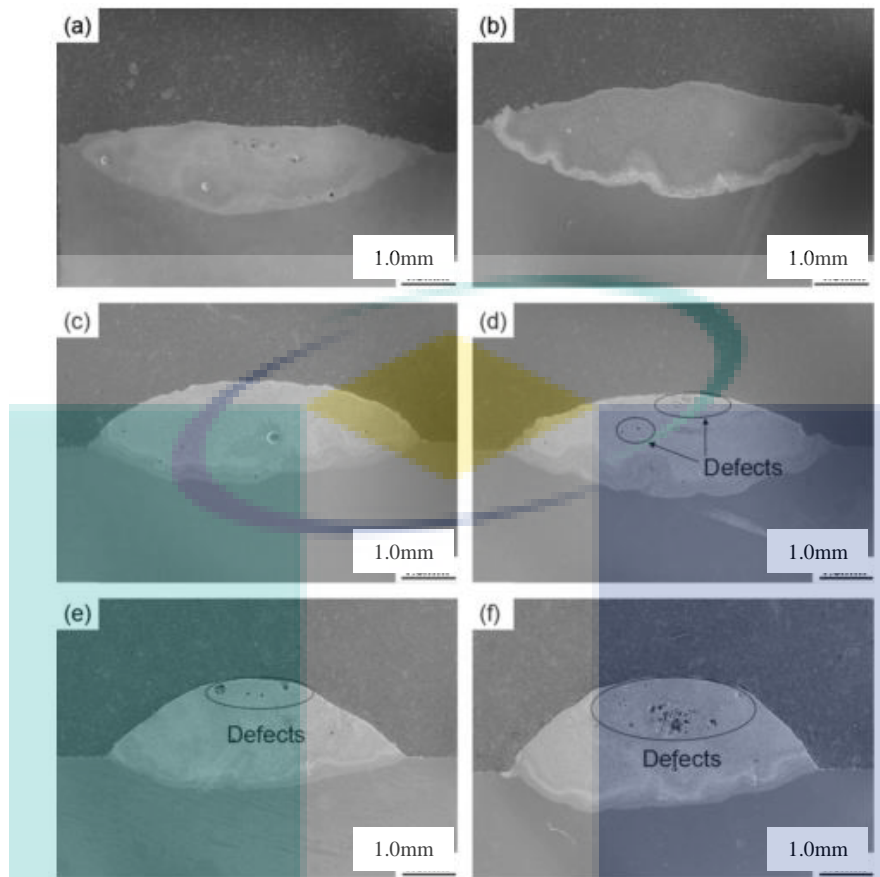


Figure 2.31 SEM images of cross section the coatings: (a) 0.47 mm, (b) 0.74 mm, (c) 0.92 mm, (d) 1.09 mm, (e) 1.36 mm and, (f) 1.62 mm.
Source: Qu *et al.*, (2015)

Pre-placed layer thickness correlated with laser energy, where increasing the thickness will reduce the energy absorbance by the alloy powder per unit volume (Qu *et al.*, 2015). Some particles may not be melted completely and remain in the coating due to the uneven distribution of laser energy. Besides that, the effect of the substrate becomes weak and the alloying elements is gradually predominant. On the other hand, there is more residual gas in the pre-placed layer with the thickness increasing. More gas has no time to escape and exist in the pore form in the coating during laser cladding due to its rapid melting and solidification characteristics (Qu *et al.*, 2015). These defects will deteriorate the microstructure and mechanical properties of the coating.

In addition, alloy powder brightness can influence the absorbance of laser energy. Generally the absorbance is only 20 %, but can reach as high as about 90 % with dark powder (Chen *et al.*, 2015b). High surface absorbance will lead to wider and deeper dimension. However, the alloying particle consumed amount of heat to get melted during

the heat transformation. It means that, the effective heat affected on substrate was much less than the heat absorbed by alloy layer (Chen *et al.*, 2016).

In conclusion, coating powder on the grey cast iron surface using pre-placed powder by painting is easy and economic. This technique used a bonding to prepare the pre-placed layer using binder agent such as sodium silicate or polyvinyl alcohol. However, to have precise thickness on the layer, compacting powder with compressed method can reduce the thickness slightly after compacting around 10%. Moreover, this method can prevent the clad powder from defect such as porosity. The factors that can influence the dimension and properties of clad layer is the brightness of powder, clad layer thickness and the laser energy during laser processing. Therefore, pre-placed powder on the surface of grey cast iron should be done in proper technique.

2.6 Design of Experiment

The purpose of design of experiment (DOE) is to optimize a process or system by performing each experiment and to draw conclusions about the significant behavior of the studied object based on the results of the experiments. With design of experiment, the number of experiments are kept as low as possible and the most informative combination of the factors is chosen. According to Triefenbach (2008), design of experiment is an effective and economical solution (Triefenbach, 2008).

The main distinction between factorial model and mixture model is the construction of their space design. The space design of the factorial model is a set of possible combinations of its independent variables or components. The space design for a mixture model is a set of possible combinations of relative proportion of each component, which usually add up to a certain value. The main objective in a mixture model area is to find the optimal response for any mixture or combination of the components, and to obtain the influence of the response for each component singly and in combination with other components.

Mixture model is a special class of response surface experiments in which the product under investigation is made up of several components. The advantages of response surface experiments are it provides a direct and comprehensive estimate of the

plus or minus prediction errors that experimenters can expect to achieve and to limit the numbers of inputs that are included in the response surface model to those that are identified as the most important using screening sensitivity analysis (Hussein *et al.*, 2014).

According to Henry (1958), who is defined the mixture model, suppose a mixture is composed of q components and the i th components contain x_i of it. Each component proportion can't be negative and the sum of all component proportions must be equal to 1 as shown in Eq. (2.1) (Henry, 1958).

$$\sum_i^q x_i = x_1 + x_2 + \dots + x_q = 1 \quad (2.1)$$

and $x_i \geq 0, \quad i = 1, 2, \dots, q$

The space factor of any mixture experiment is reduced by one dimension due to the restriction of Eq. (2.1) which is different from the factorial experiment. For a q -factor factorial experiment, feasible space factor is a q -dimensional space called q -cuboid. However for a q -component mixture experiment, its feasible region is $(q-1)$ dimensional space called $(q-1)$ simplex. For a mixture experiment with three components in it, its feasible region will be an equal lateral simplex due to the restriction of Eq. (2.1). The feasible region is shown in Figure 2.32.

UMP

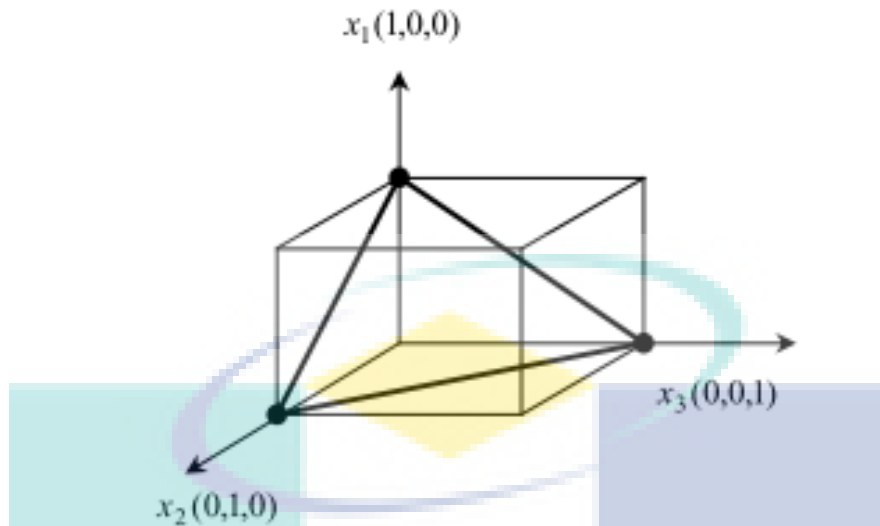


Figure 2.32 The space factor for a mixture experiment with three components in it.

Source: Wang & Fang, (2010)

Wang and Fang, (2010) suggest that the appropriate model for a mixture experiment will be selected through the method of analysis of variance. To accomplish a mixture experiment, one will follow the steps as follows (Wang & Fang, 2010);

- i. Select the design points of the mixture experiment according to the restriction of components among them.
- ii. Select the appropriate model among response variables and components by the method of analysis of variance.
- iii. Execute the confirmation run to verify the fitted model.
- iv. Find the optimal component proportions to get the best result of responses.

2.7 Summary

In the recent decades, laser processing is among the major interesting research subject due to high precision, quick handling and flexibility of parameter to modify surface properties. High energy from laser beam resulted in localized melting on materials surface and rapid cooling formed new refine structure without changing the materials composition. In surface engineering, least attention was focused on grey cast iron modification. Nonetheless, major utilisation of engineering parts involves cast irons. Automotive components, such as cylinder blocks and piston liner are made from grey cast iron type HT250. The composition of this material Laser surface melting can dissolve

graphite phase in grey cast iron that triggers crack nucleation. By adding Cr and Mo on grey cast iron give some advantages to the properties such as corrosion resistance due to the changes of the composition and formation of new hard phase structure. Transition metals like Cr and Mo will form carbides in the structure which can increase the hardness between 517 HV to 2200 HV and wear resistance up to 70%. While in steel, these elements can reduce the carbon content and increase the strength of the steel with the formation of finer grain and formation carbide phase. Laser cladding on grey cast iron surface also can improve the surface properties similar to steel without changing the bulk properties. Previous works indicated that hardness had increased due to the elimination of graphite and high cooling rate above 10^3 Ks^{-1} , but none of the reports determine the relationship between the laser power and focal distance on grey cast iron. To investigate the relationship between the laser parameter and mixture components of Cr and Mo, design of experiment with factorial design and mixture design were used. A new hard phase had been developed in laser surface melting such as martensite, cementite (Fe_3C), retain austenite (Ar) and smaller or finer crystals which contributed to the enhancement of microhardness. Laser cladding with additional of Cr and Mo will produce hard phase of M_3C , M_7C_3 , M_2C , M_6C and retain austenite. A technique called pre-placed powder was used to place the Cr and Mo powder on the grey cast iron surface. Table 2.6 shown the summary literature review findings relative to grey cast iron modification with Cr and Mo.

The logo for UMP (Universiti Malaysia Perlis) is a large, stylized letter 'U' composed of four overlapping triangles in shades of teal and light blue. The letters 'UMP' are printed in white, bold, sans-serif font across the center of the 'U' shape.

UMP

Table 2.6 Summary Literature review findings in grey cast iron modification with Cr and Mo.

Reference	Materials	Hardness properties	Wear properties	Phase formation
(Nagai, Inoue, & Utsunomiya, 2002)	Grey cast iron with Mo addition	In range of 1000 to 1150 HV	Wear amount of the materials decreased.	M_3C , α -ferrite, γ -ferrite and cementite (Fe_3C)
(Amirsadeghi, Sohi, & Bozorg, 2008)	Ductile cast iron with ferrochromium	1. 1078 HV (heat input 11.2 kJcm ⁻¹), 2. 755 HV (heat input 13.7 kJcm ⁻¹) 3. 896 HV (heat input 16.2 kJcm ⁻¹)	Reduced wear rate by 70%, 42 % and 38 %.	M_7C_3 , martensite and γ -ferrite
(Kagawa & Ohta, 1998)	Grey cast iron with chromium carbide hardfacing	In range of 1900 to 2200 HV	Higher wear resistance	M_7C_3 and γ -ferrite
(Chen <i>et al.</i> , 2016)	Grey cast iron with Cr addition	In range of 800 to 840 HV0.2	Mass loss have decrease to 47%.	M_xC_y , Cr_xC_y , α -(Fe-Cr), MC and Cr, martensite, γ -ferrite
(Agunsoye, Bello, Talabi, Hassan, & Moumoh, 2014)	Grey cast iron with Mo addition	Hardness values increased as the % w.t of molybdenum increased	The volume loss decreased as the % w.t molybdenum increases.	α -ferrite, cementite (Fe_3C) and MoSi.
(Liu & Zhou, 2012)	Grey cast iron with Mo addition	In range of 513 to 577 HV.	Wear ratio rises slowly	M_6C and M_2C
(Chung, Tang, Li, Hinckley, & Dolman, 2013)	High chromium cast iron with Mo addition	1082 HV	Improve their wear performance when volume loss has decreased.	M_7C_3 , M_2C , MC and γ -ferrite
(Chen <i>et al.</i> , 2015)	Grey cast iron with Fe powder addition	500 HV	Not specify	Martensite and cementite (Fe_3C)
(Tong <i>et al.</i> , 2008)	Grey cast iron with Cr addition	Not specify	Not specify. However, it has superior resistance to thermal fatigue.	γ -ferrite , martensite, M_7C_3 and $Cr_{23}C_6$.

CHAPTER 3

METHODOLOGY

3.1 Introduction

The research methodology comprises of materials and sample preparation, laser surface modification process, two sets of designs of experiments and characterization techniques. This research work involved two different approaches of laser surface modification of grey cast iron. The first approach was laser surface melting using factorial design of experiment (DOE) where the three factors used were traverse speed (s), peak power (Pp) and pulse repetition frequency (PRF). It was a preliminary experiment to determine the parameter on laser processing at different laser spot size. Design of experiment of combined mixture component was developed subsequently according to the highest hardness and the lowest surface roughness in laser surface melting. Laser cladding is operated using combine mixture component to enhance the grey cast iron properties by adding powder on the surface. Mixture component for laser surface alloying are chromium (Cr) and molybdenum (Mo) and the factor is peak power and pulse repetition frequency. Laser surface melting and laser cladding are conducted using 300 W high power Nd:YAG laser system with wavelength 1064 nm in pulse mode.

For simple explanation on this work, the experiment is divided into four stages as shown in Figure 3.1. In the first stages as-received grey cast iron in round bar was cut into two sample for metallography study and sliding wear test.

In the next stage, preliminary experiment on laser surface melting was conducted using design of experiment factorial model. These design were used for four different laser spot size of 1.0 mm, 1.2 mm, 1.4 mm and 1.7 mm. In factorial design, three process factors used were traverse speed, peak power and pulse repetition frequency. This experiment is to determine the laser parameter processing for grey cast iron with high hardness and low surface roughness. In the third stage, laser cladding was conducted using combined mixture design. The component for this design are chromium and molybdenum and the process factor are peak power and pulse repetition frequency. In the last stage of the research, analyses were conducted to determine the hardness properties, surface geometry, surface roughness, chemical composition, x-ray diffraction for phase analysis and wear properties.

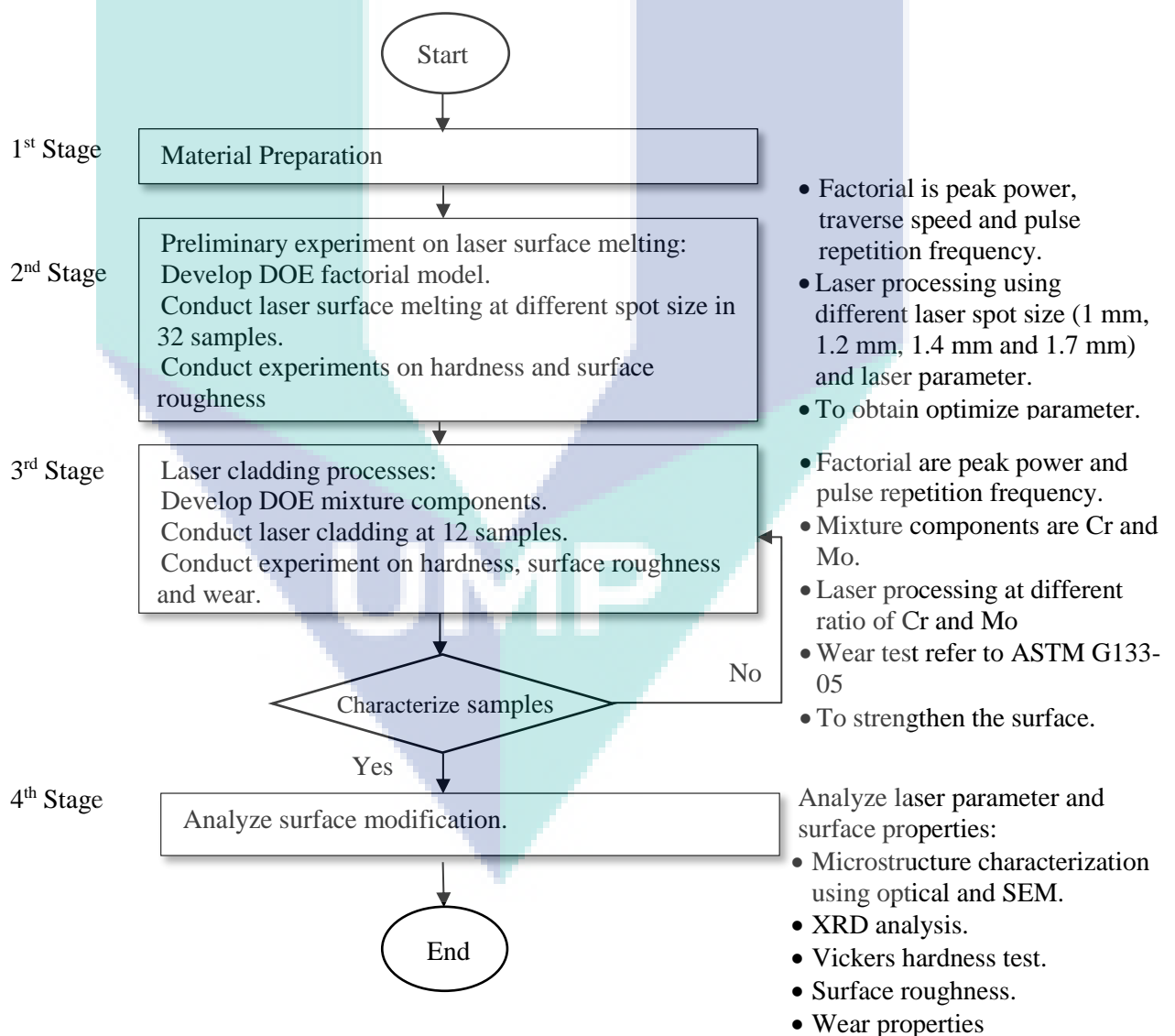


Figure 3.1 Overall research methodology flowchart.

3.2 Material Preparation

The materials used for this research was grey cast iron grade HT250, which is equivalent to ASTM A48 class 40 consists of type D graphite distribution characterized by interdendritic distribution (fully ferritic matrix) and preferred orientation. The structure comprises of graphite lamella and surrounded with α -ferrite and pearlite. The as-received round bar was supplied with 230 HB (235 HV) maximum hardness. The grey cast iron chemical composition grade HT250 is listed in Table 3.1.

Table 3.1 Chemical composition of HT250 grey cast iron.

Material	Elements (wt. %)				
	C	Si	Mn	S	P
Grey cast iron	3.0 – 3.6	2.2 – 3.2	0.7 – 1.0	< 0.10	< 0.08

As-received 40 mm diameter HT250 round bar was sectioned into 15 mm length sample and ground on a flat surface with 250 grit silica sand papers. Sample roughness were 0.094 μm average roughness, Ra. Prepared samples through grinding was used to reduce the laser beam reflectivity and to remove any contaminant on the surface. (Abbouda, Benyounisb, Olabic, & Hashmic, 2007). Samples were laser processed in the as-received condition. For sliding wear test, samples were cut into 27 mm wide as shown in Figure 3.2. Each corner of the sample was drilled with 3 mm hole. These sizes were used to match the sample in the holder and band with the screw at wear test machine. Before the wear test, samples were ground with 600 grit silica sand paper to minimize the surface roughness factor. According to ASTM G133-05, a ground surface roughness of 0.8 μm arithmetic average or less is usually recommended. The surface roughness can affect wear and friction, by the fact that it will increase them when the surface is not even or the surface is too rough (Al-Samarai, Haftirman, Ahmad, & Al-Douri, 2012). However this process need to be conducted carefully, to prevent surface cladding to move out from the surface.

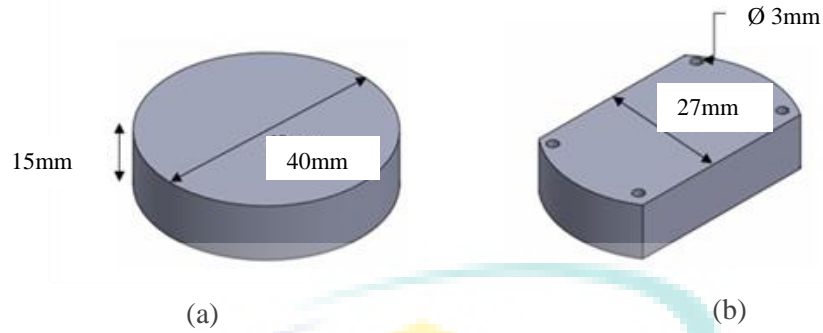


Figure 3.2 Sample size for (a) laser surface processing and (b) sliding wear test.

3.3 Preliminary Experiment: Laser Surface Melting

Preliminary experiment on grey cast iron surface was executed with laser surface melting. This procedure is to investigate the surface geometry, surface roughness and microhardness at different laser spot sizes. Besides that, this experiment was carried out to determine the optimized laser parameter and suitable laser spot size to melt the surface without evaporating the surface. To get the result, design of experiment in 2-level factorial model was used in laser processing.

Laser processing parameter were designed to increase the hardness and to minimize the surface roughness. Laser spot sizes used for this experiment are 1.0, 1.2, 1.4 and 1.7 mm and processed at constant average power of 50 W and 70 % overlap to investigate effect of different laser spot size at different laser parameter settings. The overlap, η can be calculated from Eq. (3.1)

$$\eta = \left(1 - \frac{\Delta}{d}\right) \cdot 100\% \quad (3.1)$$

where, $\Delta = (X_2 - d)$ is the overlap distance between passes, X_2 is the longitudinal length of two subsequent passes and d is the spot diameter. Figure 3.3 shown the linear sample movement to form a continuous processed region in laser surface processing.

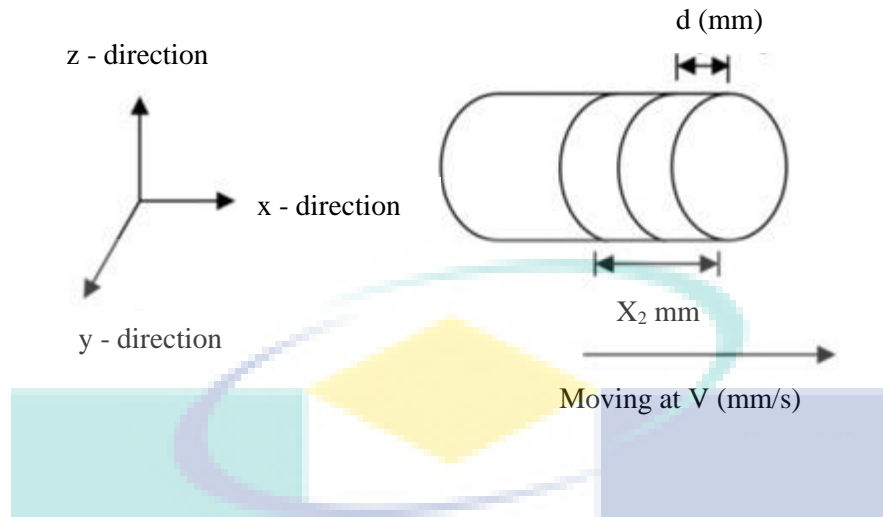


Figure 3.3 Linear sample movement in laser surface processing.

A factorial design of experiment (DOE) at 2-level factorial model was developed and yielded 8 parameters for each spot size. Controlled parameter were peak power, pulse repetition frequency, and traverse speed. Two responses were surface roughness and hardness. The parameter setting and calculated parameters are summarized in Table 3.2 and laser parameter setting for each 32 samples is listed in Appendix A and Appendix B. The calculated parameters from the setting were pulse energy (E_p), residence time (T_R) and irradiance (I). Setting the parameter at different value will produce significant amount of energy and irradiance to melt the sample at different spot size. Pulse energy are measured in Joule (J) and depends on the power average (P_{ave}) and pulse repetition frequency (PRF) as shown in Eq. (3.2).

$$E_p = \frac{P_{ave}}{PRF} \quad (3.2)$$

Residence time is the materials-beam interaction time measured in millisecond (ms). The materials-beam interaction time depends on both laser speed and samples traverse speed. In pulse mode, the materials-laser interaction time is limited by the duty cycle as show in Eq. (3.3), while laser irradiance or high power density is measured in Wmm^{-2} . Laser irradiance are determined from energy density (F), residence time and duty cycle as show in Eq. (3.4). Laser processing was assisted by argon gas at $10 Lmin^{-1}$ to prevent oxidation.

$$T_R = \frac{DC \times d}{s} \quad (3.3)$$

$$I = \frac{F}{T_R} \times DC \quad (3.4)$$

Table 3.2 Summary of parameter settings for laser melting in low and high range for each laser spot size.

Spot size (mm)	Parameter setting			Calculated parameter		
	P _p (W)	PRF (Hz)	s (mms ⁻¹)	E _p (J)	T _R (ms)	I (Wmm ⁻²)
1.0	Low: 800	Low: 80	Low: 19.2	Low: 0.56	Low: 1.9	15.28
	High: 1200	High: 90	High: 21.6	High: 0.63	High: 3.3	
1.2	Low: 800	Low: 40	Low: 13.6	Low: 1.00	Low: 2.9	12.53
	High: 1200	High: 50	High: 17	High: 1.25	High: 5.5	
1.4	Low: 1500	Low: 15	Low: 5.7	Low: 2.00	Low: 4.1	8.82
	High: 1800	High: 25	High: 9.5	High: 3.33	High: 8.2	
1.7	Low: 2000	Low: 8	Low: 2.4	Low: 4.55	Low: 12	3.89
	High: 2200	High: 11	High: 3.3	High: 6.25	High: 18	

To increase the laser spot size, the peak power need to be increased and the PRF and traverse speed need to be reduced. These parameters can produce high energy to ensure the surface have sufficient heat to melt the surface. The desired degree of heating and phase transition can be achieved when the irradiance is high and traverse speed is low (Kusinski *et al.*, 2012).

Optimization analysis was conducted to design an experiment within the given range of peak power, pulse repetition rate and traverse speed, with a view to minimize surface roughness and maximize hardness. Laser parameter that yield highest hardness and lowest in surface roughness is used to produced laser cladding samples. Therefore, laser surface melting parameter were used on laser cladding. To develop a new structure and phase to increase the surface strength, chromium and molybdenum powder were placed on the surface.

3.4 Experiment for Laser Surface Cladding

In design of experiment for laser surface cladding, the laser processing parameters setting are taken from laser surface melting optimization. The different in this laser process is the surface was preplaced with dark powder of chromium and molybdenum. The usage of the dark powder is to ensure the powder and the substrate are melted

together and to increase the absorbance. According to Chen et al. (2015b) coating with dark powder on the surface will increase the depth of melting zone when performed in laser cladding because the absorbance increases up to 90 % (Chen *et al.*, 2015b).

3.4.1 Sample Preparation for Laser Cladding

The alloying powder is 99.9 % pure powder which consists of chromium and molybdenum. The size of the powder (diameter of the particle) were measured by ImageJ software. The particle size of Cr and Mo in range of 71.9 to 130 μm and 0.969 to 9.62 μm respectively were used for preplacing on the surface. The Cr particles size is bigger than the Mo where the difference of the size is at 92.6 %. The powder were produced from powder metallurgy process (solid-state reduction). Figure 3.4 show the SEM image of chromium and molybdenum powder.

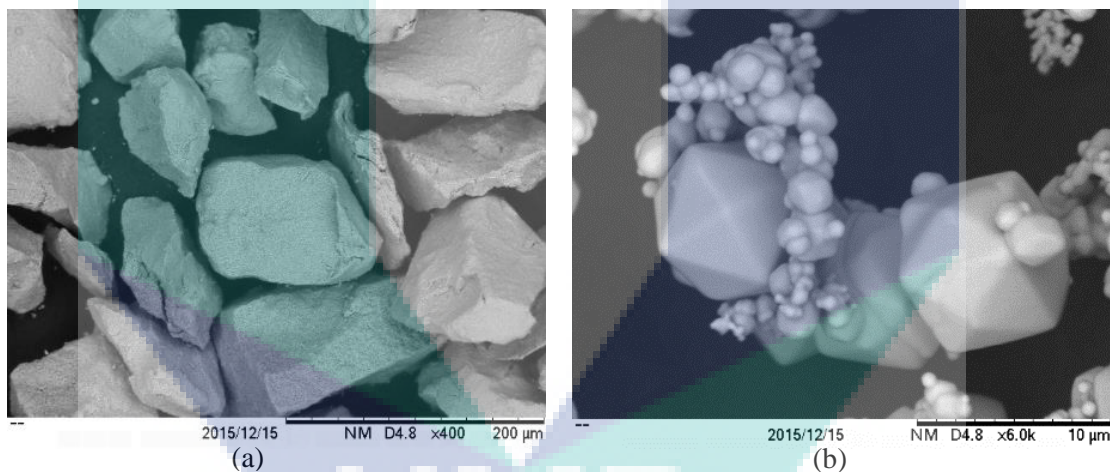


Figure 3.4 SEM image for (a) chromium powder and (b) molybdenum powder.

The substrates surfaces were ground with 250 grit silica sand paper and cleaned with ethanol to ensure appropriate roughness, which enhance the adhesive strength between the coating and substrate. The substrates were placed into the ring models with 40.2 mm inner diameter and 15.7 mm in height. Small amount of sodium silicate (3 %) was added to the powder as an adhesive and was filled into the empty space above the substrates surfaces in the ring models. Mixture of sodium silicate was used to prevent alloying powder from being splashed during laser processing. The initial preplaced layer with precise thickness of 0.7 mm were prepared and then compacted using a pressing machine at 30 Mpa at 3 minute.

Figure 3.5 shows the schematic drawing of the preparation process of the preplaced layers on grey cast iron surface. The result revealed that the preplaced layer thickness became less after compacting due to the force exerted and some air gaps existed in the preplaced layer had been demolished. So, the thickness obtained from this technique were approximately at 0.7 mm. The preplaced surface layer was then dried in a furnace at temperature of 200 °C for 2 h.

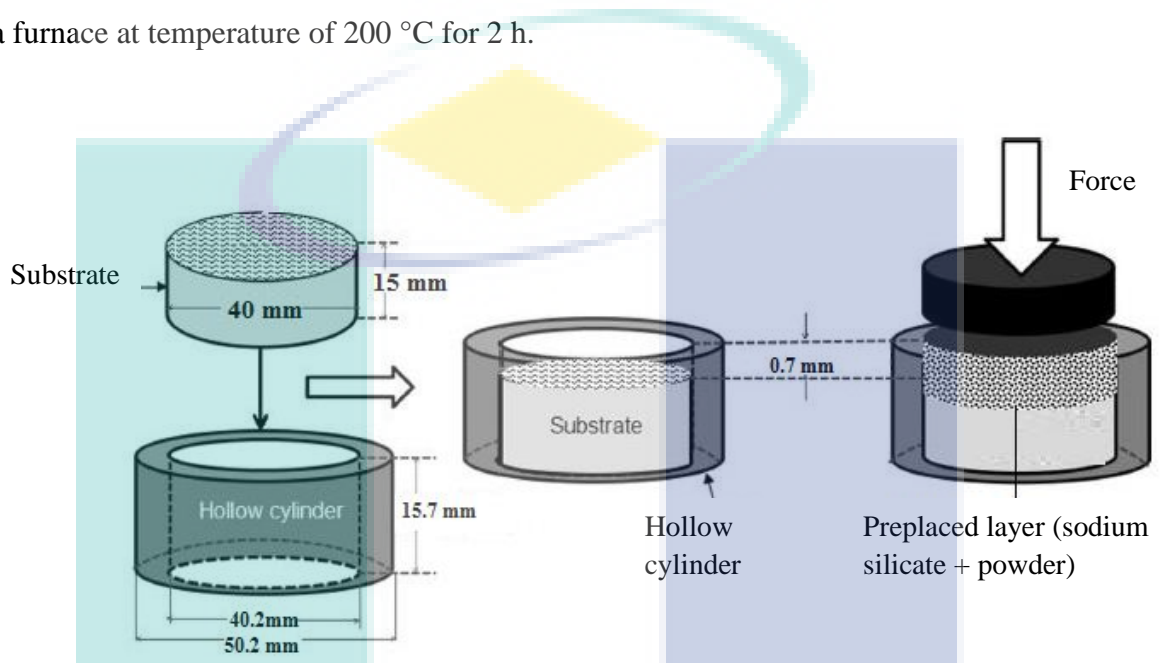


Figure 3.5 The schematic drawing of the preparation process of the preplaced layers.

3.4.2 Mixture Design of Experiment

A comprehensive experiment that combines mixture components of Cr and Mo with process factor of Pp and PRF were used to optimize the laser clad processes to minimize the surface roughness and increases the surface hardness. The model type simplex lattice were chosen as it correlates with the factor and components used. Laser parameter was developed using design expert software where the setting of Cr and Mo components are in range of 0 % to 100 %, Pp and PRF in range of 800 to 1200 W and 80 to 90 Hz respectively. This experiment is to design the relationship between laser parameter and added components of Cr and Mo through statistical analysis in design of experiment.

The combined mixture components design of experiment simplex lattice model was developed and yielded 12 parameters at laser spot size 1.0 mm. Two responses were surface roughness and surface hardness. The parameter setting and calculated parameters

are in Table 3.3. The parameter setting is generated from the design of experiment where it shows the mixture is comprises of 100 % of Cr, 100 % of Mo and mixture of 50 % Cr and 50 % Mo. Design of experiment will provide a direct and comprehensive estimation of the plus and minus prediction errors that laser parameter can achieve and to limit the number of inputs that are included in the response surface model which are identified as the most important response using screening sensitivity analysis. In addition, the calculated parameters from the setting were pulse energy, residence time and irradiance. Setting the parameter at different value will produce significant amount of energy and irradiance to melt and alloy the sample at spot size 1.0 mm. Laser processing was assisted by argon gas in constant flow at 10 Lmin^{-1} to prevent oxidation and to avoid the formation of gas and inter-run porosity inside the coating (Ocelik *et al.*, 2007). Investigations have been carried out on the microstructure cladding zone, surface roughness, surface microhardness and wear.

Table 3.3 Parameter setting for laser surface cladding of grey cast iron at spot size 1.0 mm.

Num.	Input parameter			Calculated parameter					
	A: Cr %	B: Mo %	Pp W	PRF Hz	Pave W	S mms ⁻¹	Ep J	T _R s	I Wmm ⁻²
1	100	0	800	80		19.2	0.63	0.0033	
2	100	0	800	90		21.6	0.56	0.0029	
3	100	0	1200	80		19.2	0.63	0.0022	
4	100	0	1200	90		21.6	0.56	0.0019	
5	0	100	800	80	50	19.2	0.63	0.0033	15.28
6	0	100	800	90		21.6	0.56	0.0029	
7	0	100	1200	80		19.2	0.63	0.0022	
8	0	100	1200	90		21.6	0.56	0.0019	
9	50	50	800	80		19.2	0.63	0.0033	
10	50	50	800	90		21.6	0.56	0.0029	
11	50	50	1200	80		19.2	0.63	0.0022	
12	50	50	1200	90		21.6	0.56	0.0019	

Optimization analysis was conducted to design an experiment within the given range of peak power at 800 to 1200 W, pulse repetition frequency at 80 to 90 Hz and percentage of chromium and molybdenum in range of 0 % to 100 % to minimize surface roughness and maximize hardness of the samples. Laser parameter highest on hardness and lowest surface roughness is used to produce samples for sliding wear experiment.

3.5 Laser Nd:YAG System

Laser surface on grey cast iron surface were carried out using a laser Nd:YAG system 300HPS as shown in Figure 3.6. The operation is divided into two parts of setup. First is to setup the laser processing parameter and the second one is to setup the traverse speed at movable table using CNC controller.



Figure 3.6 Laser Nd:YAG machine.

Laser processing parameter as input parameter are peak power (P_p), average power (P_{avg}) and pulse width (τ). Average power is constant at 50 W while pulse width is from Eq. (3.5).

$$\tau = \frac{1}{PRF} \times \text{Duty cycle} \quad (3.5)$$

where τ is pulse width in ms, PRF is pulse repetition frequency in Hz and duty cycle in percentage. Duty cycle is from power average over peak power. Traverse speed depends on the laser spot size and time of the laser processing to finish. Peak power, pulse repetition frequency (PRF) and traverse speed are the parameters obtained from design of experiment. During the operation, pure argon gas was used to prevent oxidation on the melting surface. The laser processing was assisted by argon gas at 10 Lmin^{-1} . Table 3.4 show the specification of the laser machine used in the experiment.

Table 3.4 Laser Nd:YAG system 300HPS specification.

Specification	
Traverse speed	900 mmmin ⁻¹
Pulse repetition frequency (PRF)	100 Hz
Maximum power	300 kW
Maximum pulse energy	57 J
Maximum Peak power	9 kW
Pulse width range	0.2 – 20 ms

3.6 Laser Spot Size

Laser Nd:YAG system process used a Gaussian laser beam to produced laser spot size by TEM₀₀ laser system. Different laser spot size can be determine by adjust the focal position above or below the material surface (Aqida, 2011). To obtain a high absorption heat on the surface, the focal position z was moved downward into the material surface. Laser spot size 1.0 mm, focal distance is 150 mm and for spot size 1.2 mm, 1.4 mm and 1.7 mm focal distance offset of -5 mm, -7.5 mm and -10 mm to produce these spot sizes respectively. According Eriksson (2005), one way to examine the beam profile with high power laser is to allow the laser to burn a hole in a paper. The shape of the hole represent the shape of the laser beam. The result is dependent on the length of time for which the paper is burnt and only a few power levels can be observed within the beam (Eriksson, 2005). The advantages of the method are its simplicity and the possibility to save and compare laser beam profiles. Paper black colour were used to obtain laser mark at laser setting peak power 1 W. Optical microscope was used to measure the size of laser mark on the paper surface. The surface with laser mark at different spot size as show in Figure 3.7.

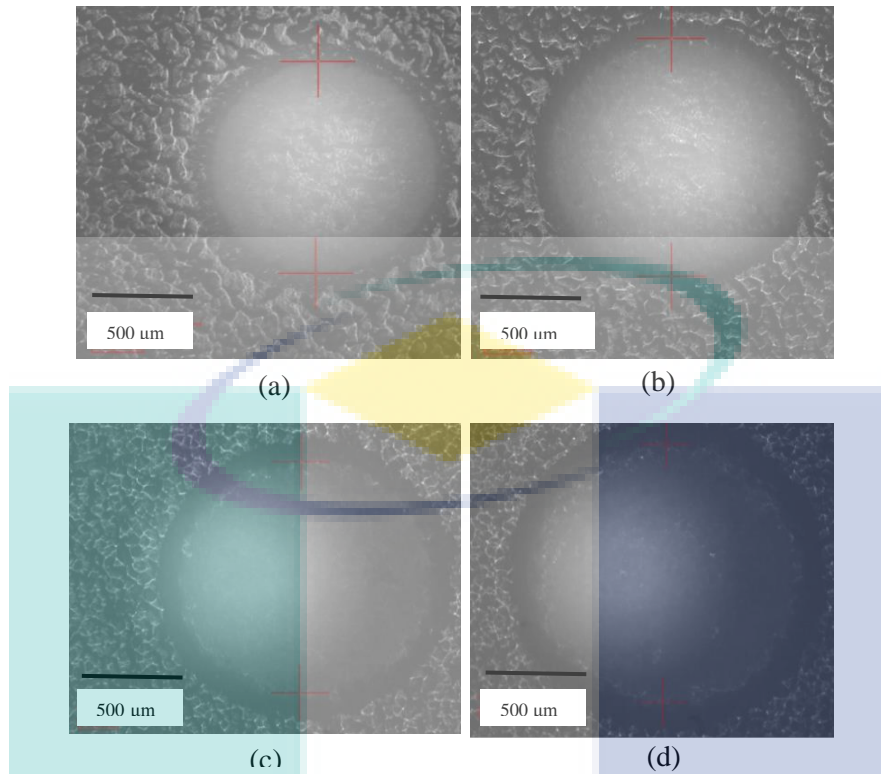


Figure 3.7 Laser spot size at peak power 1 W on black paper, (a) 1 mm, (b) 1.2 mm, (c) 1.4 mm and (d) 1.7 mm.

3.7 Characterizations Techniques

After laser processed, sample were prepared for analysis. Sample preparation consist of sample cutting using abrasive cutter, mounting, grinding, polishing and etching. After sample preparation, sample were used for characterization comprised of metallography study, microhardness testing, surface profilometry, energy dispersive X-ray spectrometer (EDS) and X-ray diffraction (XRD) analysis. Table 3.5 shows the techniques used to characterize the laser processed samples.

Table 3.5 Technique used to characterise the laser processed samples.

Characterization Technique	Analysis involved	Apparatus
Metallographic study	Modified layer dimension Grain size Worn surface	Microscope optics, SEM, Image analyser (imageJ)
Microhardness test	Modified layer hardness Substrate hardness	MMT Matsuzawa Vickers Hardness tester with 100 gf load.
EDS analysis	Chemical composition	SEM with EDS analyser
Surface profilometry	Two-dimensional surface profile Average surface roughness	Mitutoyo SJ-410 2D stylus profilometer.
XRD analysis	Phase identification	X-ray diffractometer with Cu K α generated at 30 KV and a current of 15 mA and a scanning range of 3 to 80 deg.

3.7.1 Sample Preparation

For hardness test and EDS analysis samples were conducted on the samples cross section. Samples were sectioned using Leco MSX200M abrasive cutter with diamond blade 254mm diameter, 0.6 mm thickness and were jet with water to prevent tempering. The size of sample is 1 mm \times 1 mm in square shape. The usage of the abrasive cutter is to obtain a good surface cutting compared to hacksaw machine. The top of the surface modification layer were used on surface profilometry and XRD analysis.

After sectioned, samples were then mounting in Epomet-F moulding compound using Buehler Simpliment 1000 automatic mounting hot press machine. The purpose of this mounting procedure is to make sure that the samples can be handled easily when grinding, polishing and etching. The machine were setup at 3 minutes heating and 5 minute cooling to have better mounting on the sample. Samples were ground based on the silicon carbide (SiC) papers grade started from 240, 600, 800 and 1200 grit size for 5 minutes at 250 rpm grinding wheel speed. Grinding is a step to remove deformation and surface irregularities during sectioning and produced a smooth and perfectly flat for surface finished. Ground samples were polished using Textment 1000 cloth with 3 μ m

and 1 μm size Leco diamond suspension for 3 minutes each, at polishing speed of 200 rpm. Both grinding and polishing were done using Metkon FORCIPOL 2V grinder-polishing machine. Polished samples were washed with continuously running tap water and dry with iMEC hand dryer GSX-2000 to prevent water stain. Samples were chemically etching with carbon steel etching solution in 2% nital for approximately 3 seconds. Samples were rinsed using water and dried before microstructural observation.

3.7.2 Metallographic Study

Metallography study for modified layer dimension and worn surface were performed using IM7000 Series Inverted Optical microscopes with Progress Capture 28.8 Jenoptik Optical System image analyzer software at 500 \times magnification. Worn surface from sliding wear test also taken from this microscope. The figure obtained from worn surface is used to investigate the defect on the surface after the wear test were carried at different load. Detailed microstructure observation and particles size was done using a Hitachi TM3030Plus scanning electron microscope (SEM) integrated with image and EDS analyzer software. EDS detector were build-in scanning electron microscope to collect composition data from the sample. Cross section of the laser samples were used to observe the structure and to analyse the composition in laser melting zone and laser cladding zone.

After the micrograph obtained from microscope, ImageJ software version 1.49v were used to measure particle size. These measurement were determined by statistical area. Area statistical were calculated for the complete image if there is no selection or for a selected subregion defined by the area selection. This measurement calculating was performed with analyze particles menu. The measurement of the particles size started with scale setting on the micrograph, thresholding and background subtraction. The number of particles were measured from high contrast micrograph which was adjust using the image threshold menu. The result from analysis is shown in 'result table', where the table shows the result of the size area of particles.

3.7.3 Microhardness Test

The microhardness properties on the laser modified cross section surface were measured using a MMT Matsuzawa Vickers Hardness tester with 100 gf load and Vickers diamond indenter. Samples cross section surface were polished with 1 μm diamond suspension to ensure measurement accuracy. Measurement were recorded from six indentations at different locations within the modified surface cross section. The cross section of laser modified surface exhibits the modified zone, heat affected zone and the substrate. Each zone will be indent vertically starting from the substrate to the modified zone. Referring to ISO 14577 standard, the distance between indentation were placed at least five diameter of the largest indent to avoid interference (Aqida, 2011). The Vickers hardness test using diamond indenter and the top angle of 136° between opposite faces subjected to a 100 gf load. The load is applied for 10-15 seconds. Slanted surface area of the indentation is measured by using microscope and averaged. The microhardness value is obtained from dividing the load with the squared area of the indentation. Figure 3.8 shows the Vickers hardness test schematic indentation on the surface.

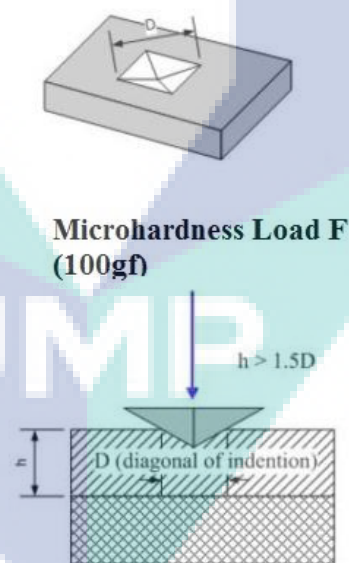


Figure 3.8 Schematic indentation of Vickers hardness test.

3.7.4 Surface Profilometry

Two dimensional surface profilometry was done using Mitutoyo SJ-410 measuring system. The measurement was compliance with the DIN EN ISO 4287 standard. The stylus were placed on top of the surface by adjusting the knob height. Then, the results was calculated after the stylus moving horizontal along 10mm on the surface. The significant surface roughness measurement that were recorded for comparison purposes was the arithmetic average, Ra. This average roughness is the area between the roughness profile and its mean line, or the integral of the absolute value of the roughness profile height over the evaluation length as show in Eq. (3.6).

$$R_a = \frac{1}{L} \int_0^L |r(x)| dx \quad (3.6)$$

As shown in Figure 3.9, the average roughness is the area between the roughness profile and its center line divided by the evaluation length. The measurement were taken three times to obtain the average value.

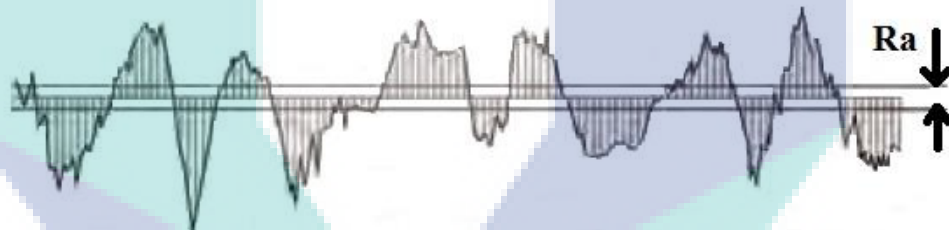


Figure 3.9 Arithmetic average roughness value Ra.

3.7.5 X-ray Diffraction Analysis (XRD)

X-ray diffraction pattern were recorded using XRD machine with Cu K α radiation generated at 30 KV and a current of 15 mA and a scanning range of 3 to 80 deg. The scanning area on the surface was cleaned with alcohol before mounting on the scanning stage. The scanning stage position was between the x-ray source and the detector. The scanning stage position was between the x-ray source and the detector. A fixed detector slit size of 0.2 mm wide and 12 mm long was used throughout the experiments. A z scan was used to position a sample at the correct height on the z drive, and was performed for each sample before the XRD measurement. Using the height value from the z-scan, the

diffraction pattern were recorded in the 2 theta range of 3 ° to 80 ° using locked coupled scan type. The locked coupled scan is a standard XRD scan of any 2 theta values. The scan rate was set at 1 seconds/step with 0.002 steps increment. The diffraction pattern produced was plotted on a graph with intensity plotted against the 2 theta axis.

Conversion of the diffraction peaks to d-spacings allows identification of the mineral because each mineral has a set of unique d-spacings. Typically, this is achieved by comparing the d-spacings with standard reference patterns. The diffraction pattern produced was plotted on a graph with intensity plotted against the 2 theta axis. To identify phase identification, COD powder diffraction database is used from Match software.

The XRD analysis was done to measure the crystallinity of the laser modified surface and to identify the formation of graphite, martensite and metastable phase in the modified layer during processing. The phase formation after laser cladding on grey cast iron surface at spot size 1.0 mm were investigated.

3.7.6 Energy Dispersive Spectrometer (EDS)

The chemical composition of laser modified grey cast iron was measured quantitatively using Hitachi TM3030Plus EDS analyzer software. The samples were observed using the scanning electron microscope while EDS detector was used to collect composition data from the sample. The focusing distance was set less than 14 mm to allow the EDS detector to collect the information from the sample surface. Identification of elements on the samples cross-sectional surface was carried out using the integrated software.

3.8 Sliding Wear Experiment

Sliding wear test was carried out on a inhouse build linear reciprocating wear testing machine that follows ASTM G133-05 standard to analyze the wear rate during dry sliding at load 17.5 N and 24.5 N. The mechanism of wear testing machine is such as the direction of the relative motion between sliding surface reverses where the load is located at the top of the moving part. The speed of the wear test was controlled by the frequency converter, which was linked to the electromotor. To determine the mass loss

and coefficient of friction, laser surface cladding sample with Cr-Mo mixture were used. The test were repeated at least three times to get an average measurement for each samples. Arduino software were used to monitor and record the revolution per minutes (RPM) and coefficient of friction (CoF) during the operation. Figure 3.10 shows schematic diagram reciprocating test.

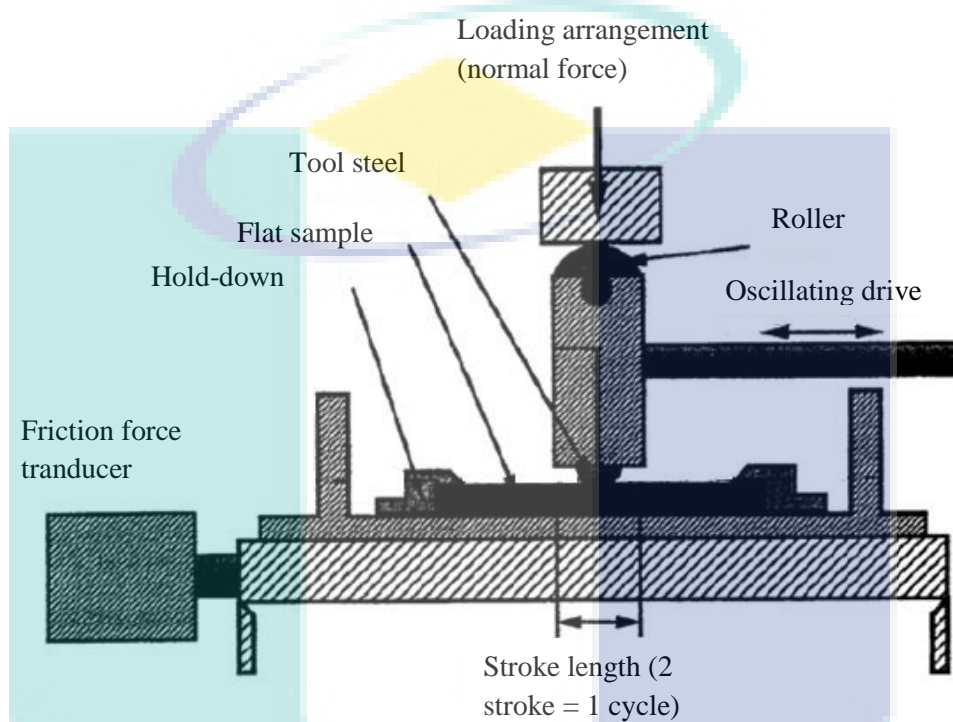


Figure 3.10 Schematic diagram sliding wear test.

In this experiment, speed was set to 0.52 ms^{-1} in 300 s, sliding distance is 47.9 m in 1260 cycle. The analysis consists of the mass loss and coefficient of friction. The balance electronic of GR200 type with precision of $1 \times 10^{-4} \text{ g}$ was used to measure the weight of the sample before and after wear test. Referring to the standard ASTM G133-05, the number of cycles is refer to Eq. (3.7);

$$N = t \times f \quad (3.7)$$

where N is the number of cycle, t is the time and f is the frequency. For this experiment the frequency is 4.2 Hz. To compute the sliding distance Eq. (3.8) is refers;

$$x = 0.002 \times t \times f \times L \quad (3.8)$$

where x is total sliding distance and L is length of stroke. In this experiment the length of stroke is 19 mm. The setting wear test parameter are as shown in Table 3.6.

Table 3.6 Sliding wear test parameter setting.

Num.	Sample	Speed (ms ⁻¹)	Load, N	Time, t (s)	Sliding distance, x (m)	Num. of cycle, N	Frequency, f (Hz)
1	GCI 1		17.5				
2	GCI 2	0.52	24.5	300	47.9	1260	4.2
3	Clad 1		17.5				
4	Clad 2		24.5				

Micrograph for worn surface were taken on samples surface cladding with Cr-Mo mixture. The micrograph of worn surface is to investigate any furrow, scuffing, plastic deformation and tearing damage during sliding wear test. The worn surface were clean with alcohol, dried and then weighed using an electronic balance. From the weight measurement, the wear rate was calculated according to the Eq. (3.9) (Adel, Dhia, & Ghazali, 2008).

$$\text{Wear rate} = \frac{\text{Weight loss (mg)}}{\text{Sliding distance (mm)}} \quad (3.9)$$

Coefficient of friction (CoF) is obtained from data log Arduino software during the sliding wear test. The software were programmed to control the speed in revolution per minute (RPM) and to generate the data of coefficient of friction. The coefficient of friction is calculated as friction force divided by normal load as shown in Eq. (3.10). The data log is generated in the Microsoft Excel for analysis and the coefficient of friction were presented in average. Appendix C shows the programmed use in Arduino.

$$\text{Coefficient of friction, } \mu = \frac{\text{Normal load, N}}{\text{Friction force, F}} \quad (3.10)$$

3.9 Statistical Analysis

Design of experiment parameter setting were developed based on the Box-Behnken design Response Surface Methodology (RSM) design using Design Expert 7.0.0 software for results analysis. RSM is normally used to find these improved or

optimized process setting and helps to determine the setting of the input factors that are needed to obtain a desired output. Experiments were conducted and characterization results were analyzed using regression analysis to obtain a significant model for the response to the independent input variables. The hardness and surface roughness response models were performed with a step-wise regression method which automatically eliminates the insignificant model terms. The sequential F-test and lack of fit test were carried out using the software to evaluate the model. The range of each parameter for laser surface melting and laser cladding was determined from the previous section presented.

Effects of each laser parameter from analysis of the characterization results from laser surface melting were established to determine suitable parameter setting for design of experiment laser cladding. For design of experiment laser cladding, mixture design of experiment simplex lattice model used mixture component of chromium and molybdenum and process factor were Pp and PRF. These parameters were varied at three level different mixture which resulted in a total of 12 parameter setting as given in previous section.

Analysis of variance (ANOVA) and data optimization were conducted with significant term in the model. Model reduction can be performed when non-significant terms exist. Non-significant terms were eliminated using an algorithmic technique which was the step-wise regression method. In this method, a mixture component and factor was added, eliminated or exchanged at each step. Alpha in and out values, associated with each model term, were used in the model reduction to indicate the terms that were allowed into the model. Each term must have a p-value smaller than or equal to alpha values in order to be kept in the model at each iteration step. The model reduction started with the algorithm adding the single new factor that exhibited the highest correlation with the response. Then, factors were added, eliminated, exchanged or the procedure stopped. This step was also used in mixture components of Cr and Mo. With two or more terms in the model, terms having a p-value less than the specified alpha in requirement was added to the model. The terms having probability values greater than the specified alpha out were then removed by the algorithm one at a time. The procedure stops when no

further improvement. Data distribution was assured by regression findings, which were predicted R^2 , actual R^2 and adjusted R^2 .

At the end of experiments and characterization, the design settings for laser surface melting were optimized for the three significant factors which were Pp, PRF and S. Whereas design setting for laser cladding were mixture of Cr and Mo, Pp and PRF. This optimization process involved combining the factors with set desired goals, for each response, into an overall desirability function. In this design the numerical optimization was conducted to minimize surface roughness and maximize hardness. Minimized surface roughness can reduce the wear rate on the surface. If the surface is rough, shear stress could happen and it could cause plastic deformation. Grey cast iron surface which have high hardness are suitable to be used as the engine's components (Jensen *et al.*, 2002). The optimization criteria for laser surface melting and laser cladding was set as 'in range' To maximize or minimize the response, a lower and upper limit was set at values achieved from experimental findings and overall desirability were selected. Design of experiment will screen and generates the predicted solution parameter with minimum surface roughness and maximum hardness in term of desirability.

The logo for UMP (Universiti Malaysia Perlis) is a large, stylized letter 'U' shape. The top part of the 'U' is a light blue horizontal bar. The two vertical sides of the 'U' are composed of two overlapping, semi-transparent shapes: a light blue one on the left and a light purple one on the right. The bottom part of the 'U' is a light blue triangle pointing downwards. The letters 'UMP' are written in a bold, white, sans-serif font across the center of the bottom part of the 'U' shape.

UMP

CHAPTER 4

RESULT AND DISCUSSION

4.1 Introduction

This chapter discusses the result obtained from the experiments conducted in chapter 3. The discussion of the results begin with the result laser surface melting as-received grey cast iron microstructure and properties and then result on laser surface cladding. The final discussion is on the sliding wear experiment on laser cladding samples at different load. The characterization results of laser surface modified of grey cast iron are discussed according to the characterization methods. The discussion covers the effects of spot size and laser parameter on the surface roughness and microhardness are based on the design of experiment factorial model. In laser cladding, discussion were elaborated from design of experiment mixture model which is to establish relationship between laser parameter and mixture components of Cr and Mo. In addition, discussion on sliding wear experiment is to prove the improvement of surface properties after laser cladding with Cr-Mo mixture. The results presentation outline is shown in Figure 4.1. The formation of new structure and phase change of surface roughness, hardness and wear properties in the as-received grey cast iron and laser cladding samples were presented in this section. The analysis include investigation of dendrite and particle structure and metastable phase in the modified layer surface.

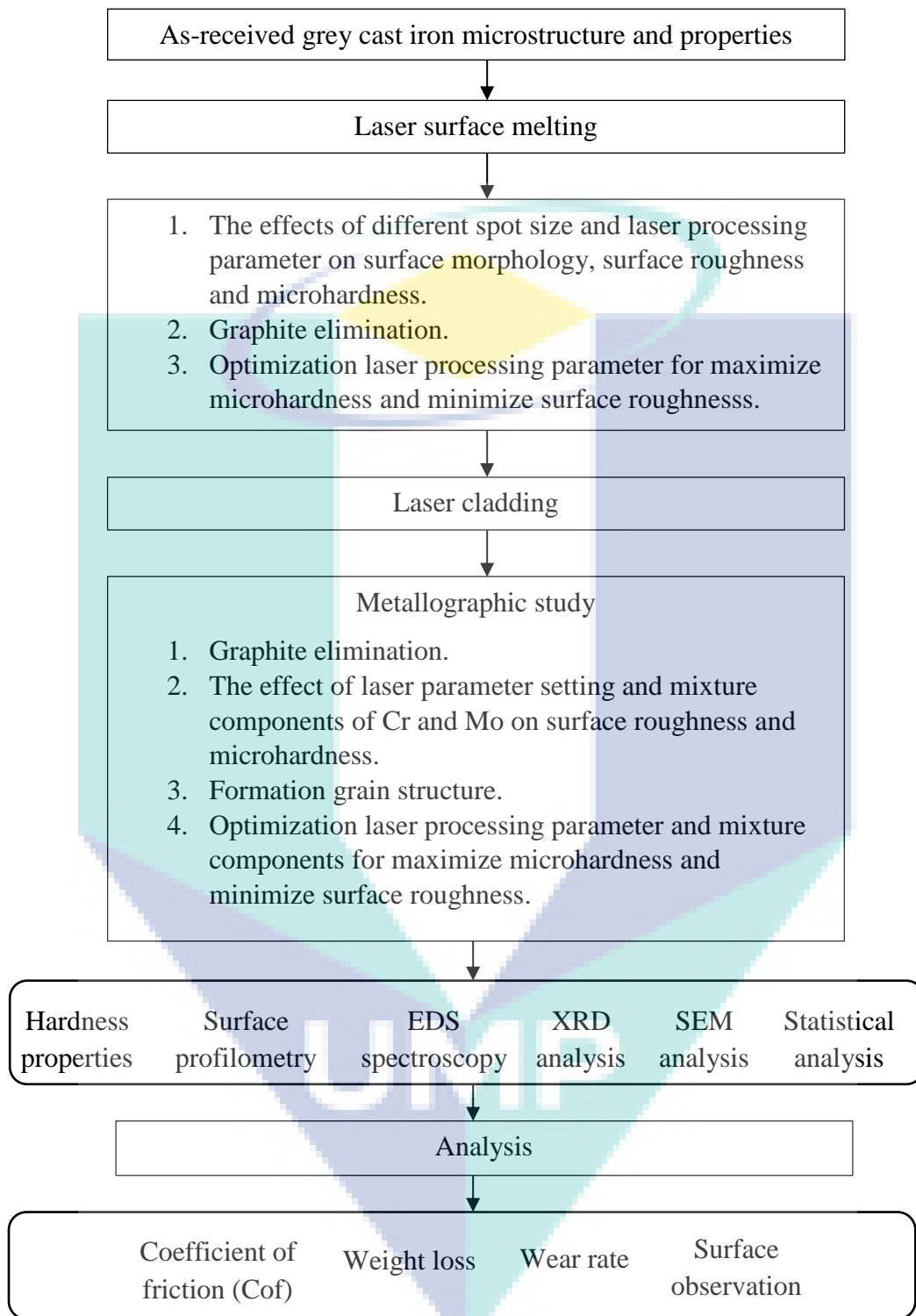


Figure 4.1 Outline of order of results presented in this chapter.

4.2 Preliminary Findings of Laser Surface Melting on Grey Cast Iron

Laser surface melting have been done according to the design of experiment 2-level factorial model at different spot size, to obtain optimized laser parameter to gain the surface roughness and surface microhardness. Using different laser spot sizes and peak power, pulse repetition frequency and traverse speed shown that the surface morphology has formed different sizes of laser mark. The parameter setting was different for each spot size to ensure the surface achieved the melting point. Besides that, calculated parameter such as pulse energy, laser irradiance and residence time have the same effect on the surface roughness and microhardness.

The result of this study indicate that, at a constant irradiance range of 3.89 to 15.28 Wmm^{-2} , the increment of laser spot size and peak power of laser setting will directly increase the pulse energy and residence time from 0.56 to 6.25 J and 1.9 to 18 ms respectively as shown in Figure 4.2. The combined effect from the 3 parameters established temperatures field in the area which in contact with laser beam varies the surface roughness of the samples. High traverse speed from 3.3 to 19.2 mms^{-1} and laser irradiance from 3.89 to 15.28 Wmm^{-2} affected the cooling rate of surface layer. From observations, the higher parameter setting of peak power and PRF tend to evaporate the surface and cause the surface of grey cast iron to be in irregular shape.

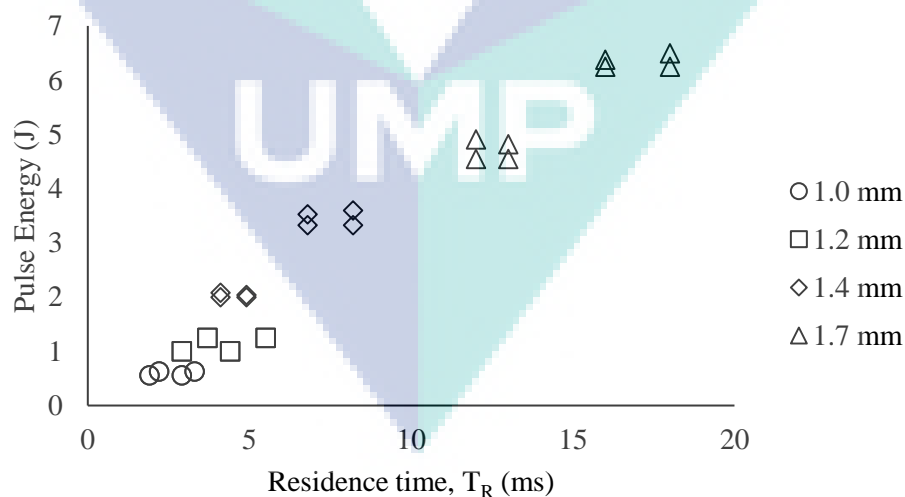


Figure 4.2 Pulse energy as a function of residence time for laser surface melting of grey cast iron at different laser spot sizes.

Laser spot size used in this research shows pulse energy is increased when laser spot size increased. This phenomena supported by previous research on laser modified grey cast iron where the smaller laser spot size produced lower pulse energy (Pang *et al.*, 2015a). Increasing laser spot size will increasing pulse energy to ensure the grey cast iron surface reached the required melting temperature. Determination pulse energy used in this research appropriate with the previous research as shown in Figure 4.3.

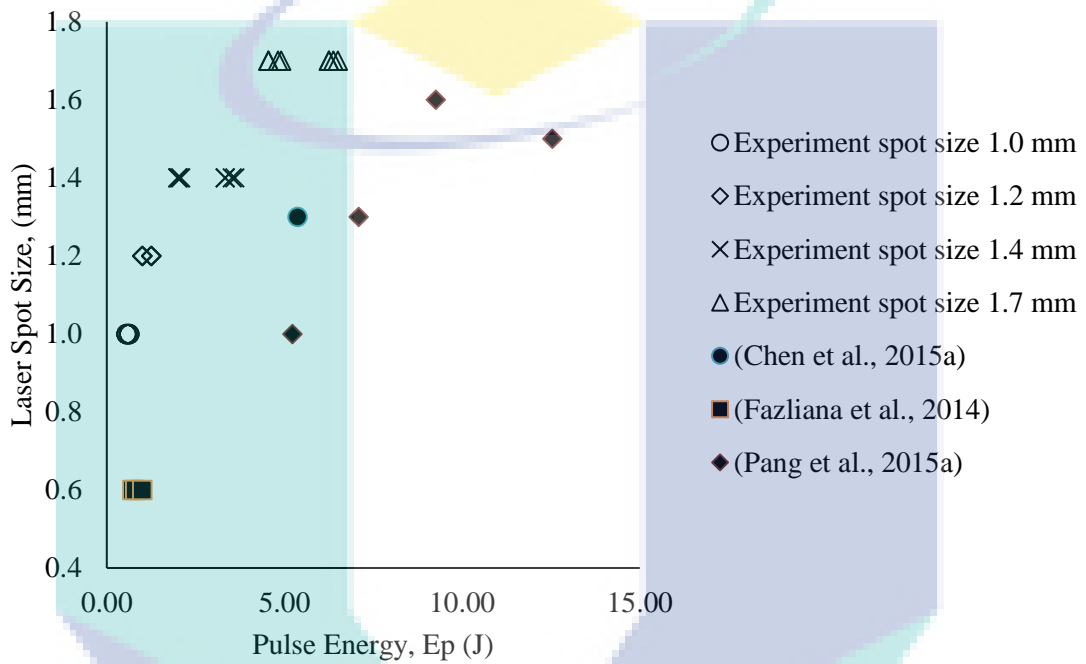


Figure 4.3 Comparison of previous work's in pulse energy versus laser spot size with this research.

4.2.1 Metallography Study

The SEM micrograph in Figure 4.4 depicts the graphite lamella is surrounded with α -ferrite and pearlite. The average hardness of the as-received grey cast iron measured was 278.5 HV_{0.1}. The volume of fraction of graphite and pearlite were in the range of 6 - 10% and 35-95% respectively. The sizes of lamella graphite show no preferred orientation and are mainly collected in interdendritic spaces. According to the standards of ASTM A247, distribution of the graphite is very close to the type D. Type D graphite is found in hypoeutectic or eutectic irons solidified at rather high cooling rate. Based on metallography etching, it shown that graphite is distributed in the ferritic matrix and

several isolated cementite (Fe_3C) where the amount of α -ferrite and cementite has been found.

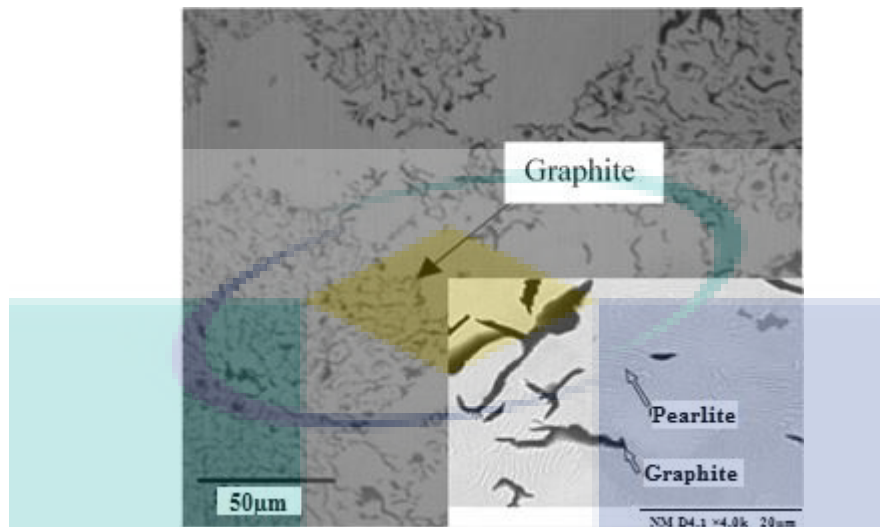


Figure 4.4 Micrograph of grey cast iron with graphite and pearlite microstructure.

Surface morphology with corresponding cross sections of laser surface melting samples is shown in micrographs of Figure 4.5. The laser modified grey cast iron surface resulted in a graphite-free layer and formation of molten zone and substrate layer shown in Figure 4.5 (a). Increasing interaction time between laser beam and grey cast iron surface influenced the structure of the modified surface as shown in Figure 4.5 (b). From microstructure of melting zone in Figure 4.5 (b) the equiaxed crystal grains were presented at the top of melting layers. This formation has contributed to the high hardness of the melting zone (Oloyede, Cochrane, & Mullis, 2016).

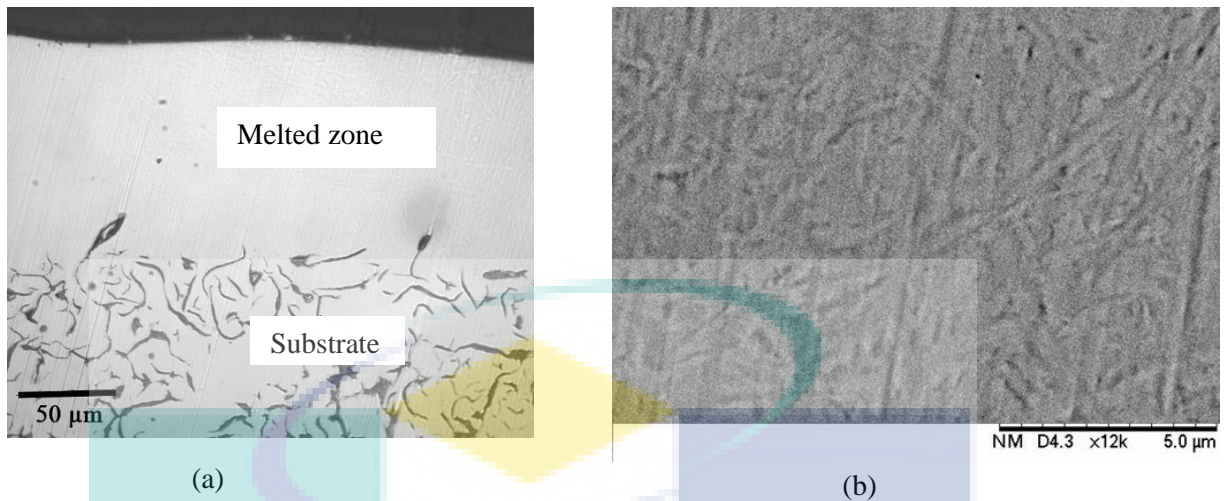


Figure 4.5 Micrograph of cross section (a) laser surface melting layer and (b) microstructure of grey cast iron surface melting zone.

Interestingly, this research has shown that graphite lamella in grey cast iron surface had fully eliminated and formed a new hard phase of crystal grain with new metallurgical properties. The fully dissolution of graphite at melting zone was due to high cooling rate during solidification (Yang *et al.*, 2015). Furthermore, the result in laser surface melting shows a good bonding between melting zone and the substrate.

4.2.2 Surface Geometry

Generally, increasing the laser spot size will increase the laser mark on the surface and the surface roughness. Increasing laser spot size from 1.0 mm to 1.7 mm had increased the laser mark on the surface of the grey cast iron. The lowest laser mark was obtained at spot size 1.0 mm at radius 84 μm at low energy range of 0.56 to 3.33 J and irradiance at 15.28 W/mm^2 . The laser marks were 84 to 87.5 % of the laser spot size. The highest laser mark was obtained at spot size 1.7 mm at radius 207 μm due to the high energy range setting of 4.55 to 6.25 J which have melted 21 % more area of the laser spot size though the irradiance was 3.89 W/mm^2 . Besides that, defocused spot sizes have shorter distance between material and nozzle, thus increased the laser mark size on sample surface. This was due to Gaussian beam effect where 86 % of the energy is in the beam diameter that affect the surface (Allemann & Kaufman, 2011).

Surface geometry of laser surface melted grey cast iron samples at different spot sizes are shown in micrographs of Figure 4.6. Each spot size shows differences in pulse energy, residence time and irradiance as shown in Table 4.1. Comparing Figure 4.6 (a), (b), (c) and (d) increasing laser spot size had influenced the sample surface morphology. The distance of molten pool radius measured on the surface is shown in this micrograph. Based on the micrographs, the radius of the laser marks was 84, 105 and 122 μm for respective spot size of 1 mm, 1.2 mm and 1.4 mm. Whereas the radius of laser pulse mark for spot size 1.7 mm was approximately 207 μm which overlapping at high percentage due to high energy range setting at 4.55 J.

The structure of grey cast iron changed when the graphite flake was eliminated while the melting zone turned into white layer. This finding is consistent with findings from the past studies by other researchers where the graphite is eliminated, which is due to the localized rapid heating and cooling of the melted zone (Benyounis *et al.*, 2005; Chen *et al.*, 2016). The 1.7 mm spot size formed a larger area on the surface of the grey cast iron, absorbed the heat and penetrated into the sample surface. Besides that, higher residence time at 13 ms and lower laser irradiance at 3.89 Wmm^{-2} contribute to the deeper penetration. These results was found in laser melting of H13 steel, whereby the decreasing of irradiance and increasing of residence time produced bulging surface morphology (Aqida *et al.*, 2011).

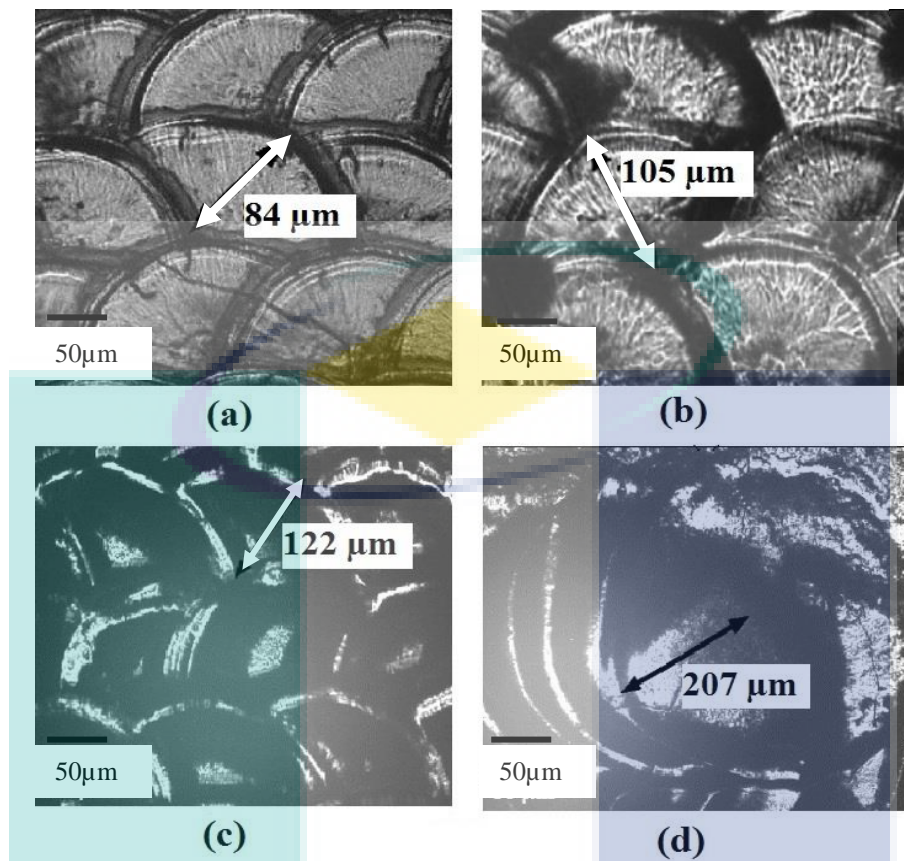


Figure 4.6 Surface geometry of samples processes at spot size (a) 1.0 mm; (b) 1.2 mm; (c) 1.4 mm and (d) 1.7 mm.

Table 4.1 Molten pool radius on grey cast iron surface resulted from different laser.

Laser spot size (mm)	Pp (W)	PRF (Hz)	S (mms ⁻¹)	Ep (J)	T _R (ms)	I (Wmm ⁻²)	Average molten pool radius (μm)
1.0	800	80	19.2	0.63	3.3	15.28	84
1.2	800	40	13.6	1.25	5.5	12.53	105
1.4	1500	15	5.7	3.33	8.2	8.82	122
1.7	2000	11	3.3	4.55	13	3.89	207

4.2.3 Surface Properties of Laser Melted Grey Cast Iron

Laser surface modification with laser melting at different laser spot size will produce different surface properties because of the changes in laser parameter. If the laser parameter was not changed, the surface will exhibit high temperature or not even melting the surface (low temperature state). Surface roughness and hardness are the mechanical properties used to compare the effect of laser parameter.

4.2.3.1 Surface roughness

The surface roughness would increase to the maximum roughness, at $8.3 \mu\text{m}$ when the laser spot size was increased to 1.7 mm. The larger area of laser energy with longer laser beam-surface interaction time had caused the melted materials to reach higher temperature, which in turn leads to the further spreading of heat and deepening of the modified layer (Chen *et al.*). Besides that, high energy input distorted the surface morphology due to low viscosity of molten metal at high surface temperature. Lower surface roughness in sample processed at 1.0 mm spot size was due to low energy and high traverse speed which reduced the energy input to distort the surface morphology.

Figure 4.7 indicates the increment of laser spot size from 1.0 mm to 1.7 mm resulted in increasing of surface roughness. The maximum surface roughness increased from $3.9 \mu\text{m}$ to $8.3 \mu\text{m}$ because to the increasing of residence time from 1.9 ms to 18 ms and the decreasing of irradiance from 15.28 W/mm^2 to 3.89 W/mm^2 at high energy setting. These findings are in agreement of previous work of Hwang *et al.* (2002) where surface roughness of the melt zone increased with the decreasing of traverse speed of a specified laser power in melting of grey cast iron surface (Hwang *et al.*, 2002). The change of surface roughness is due to the high energy setting at laser processing had increased the surface temperature and penetrated into the grey cast iron surface. High thermal conductivity of grey cast iron allows high energy of 6.25 J to penetrate deeper on it. The surface of the grey cast iron would melt when the energy is set to high level and the traverse speed is decreased to the setting in range of 2.40 to 3.30 mms^{-1} and this would

increase the residence time from 1.9 to 18 ms. Figure 4.7 shows the effect high energy setting at different spot size on surface roughness of melting zone.

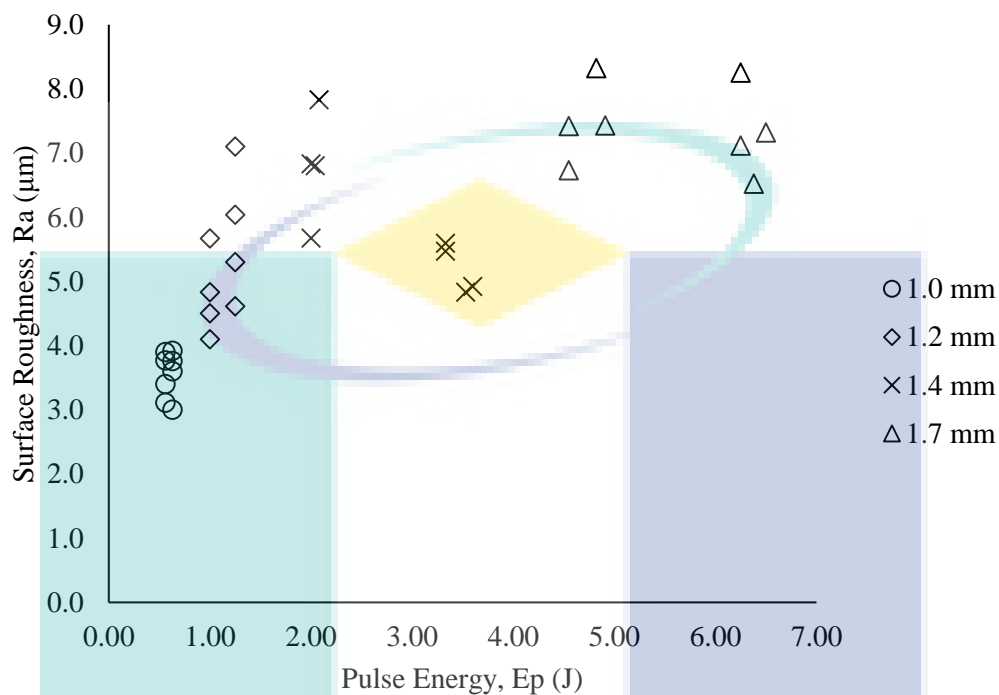


Figure 4.7 High energy setting in laser surface melting effect at different spot size on surface roughness of melting zone.

This finding highlights the increment of laser spot size increased the laser beam area due to high energy range setting in laser processing. It is proven on the increment of laser mark's measurement on the surface. However, high energy setting also increase the surface roughness due to the increasing of residence time and the decreasing of irradiance.

4.2.3.2 Hardness

From the data in Figure 4.8, it is apparent that the microhardness on the surface of grey cast iron increased from the substrate to the surface. Samples surface processed at laser parameter setting of peak power range of 800 W to 1200 W, pulse repetition frequency range of 80 to 90 Hz and traverse speed of 19.2 to 21.6 mms^{-1} exhibited hardness properties of 990 $\text{HV}_{0.1}$, 900.2 $\text{HV}_{0.1}$, 948.3 $\text{HV}_{0.1}$ and 932.0 $\text{HV}_{0.1}$ at respective laser spot size of 1.0 mm, 1.2 mm, 1.4 mm and 1.7 mm. This finding is consistent with the finding from past study by Sohi et al. (2012), when the hardness of the as-received

grey cast iron was 242 HV increased to 816 HV, it is three times higher than the substrate (Sohi *et al.*, 2012). This result also supported by Hussein *et al.* (2014) in laser surface modified when the highest value is obtained at the modified surface and decreasing it to the substrate due to the loss of hardening during solidification (Hussein *et al.*, 2014).

In addition, the hardness properties decreased from the melting zone to the substrate due to the relatively slow cooling rate across the material. Below the melting zone or heat affected zone, the structure is in the form of pearlite instead of martensite at the melting zone (Gadag *et al.*, 1995). The finding is consistent with the finding by Chen *et al.* (2015) where the hardness properties at the surface is 620 HV was higher than at the bottom (260 HV) of the melting zone (Chen *et al.*, 2015a).

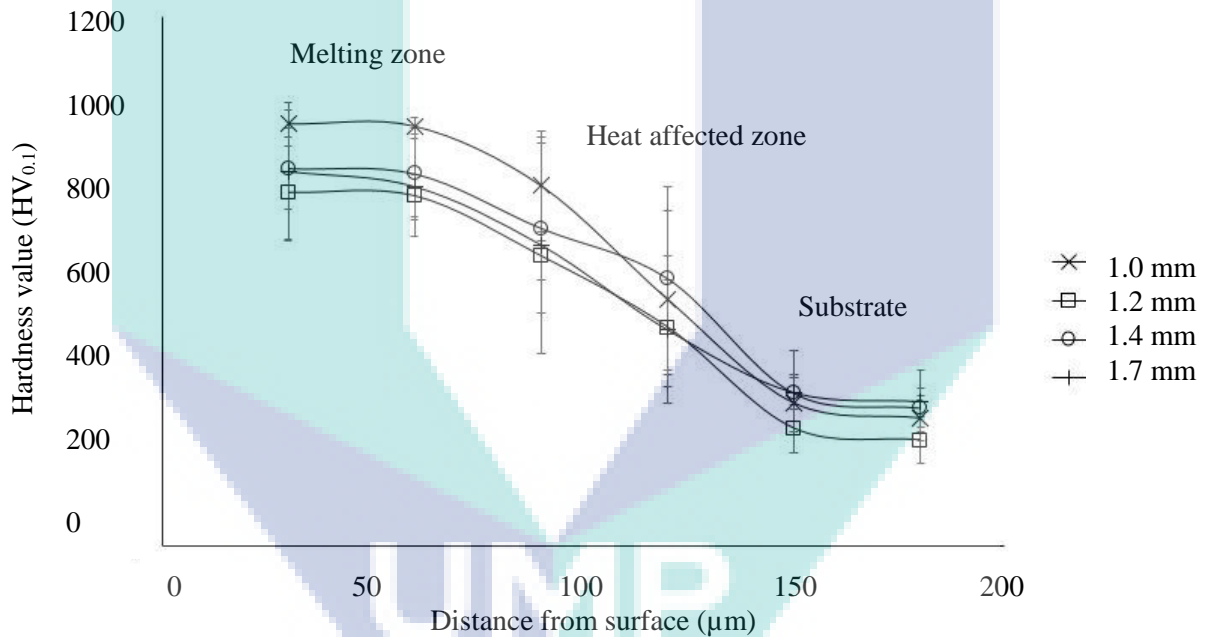


Figure 4.8 Average hardness properties as a function of distance from surface for samples processed using spot size of 1.0 mm, 1.2 mm, 1.4 mm and 1.7 mm.

However, laser spot size at 1.0 mm had shown the highest hardness compared to three other spot sizes. As shown in Figure 4.9, the lowest residence time at spot size 1.0 mm produced the highest hardness properties when the cooling rate increased and form microstructure of martensite, retain austenite and cementite as show in XRD results in the next section. In contrast, laser spot size 1.7 mm had shown the lowest hardness properties at higher residence time.

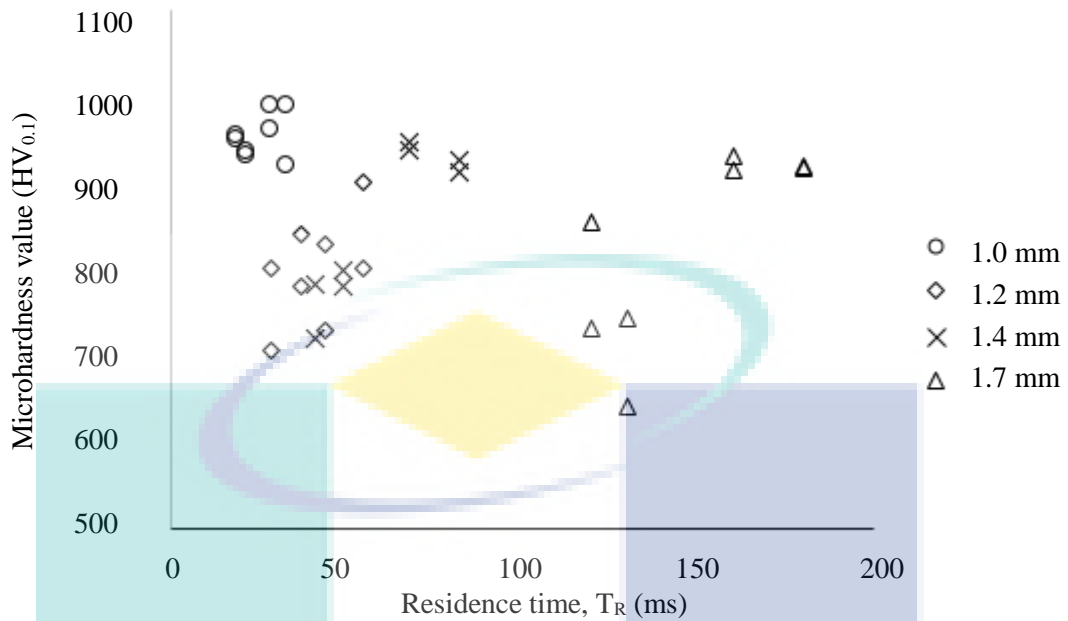


Figure 4.9 Residence time effect on hardness of laser surface melting grey cast iron at different laser spot sizes.

The increment of hardness was partly because of more carbon being dissolved in molten zone and changed the structure of austenite to martensite. The austenite formation mechanism happened when the grey cast iron surface was placed under high energy laser beam. The surface was rapidly heated and cause melting reaction due to the temperature that is higher than the melt point. As a result, when the temperature attained to transform ferrite to austenite temperature, the whole solid was melted into liquid form. The carbon was detached out and diffuse into ferrite during the rapid procedure and the temperature quickly decreased to room temperature as the focal point was moved away. Furthermore, high cooling rate causes austenite to crystallize as primary dendrites and comprising retained austenite as well as some martensite and cementite (Fe_3C) (Benyounis *et al.*, 2005). In addition, microhardness at heat affected zone is decrease due to the relatively slow cooling rate across material and formed fine pearlite instead of martensite (Gadag *et al.*, 1995).

Table 4.2 shows that, laser processing at smaller spot sizes has higher average hardness at 967.2 $HV_{0.1}$ compared to bigger spot size have lower average hardness at 832.0 $HV_{0.1}$. The finding proved that, high cooling rate from laser spot size of 1.0 mm contributes to the increment of microhardness, where the cooling rate (C_R) at laser spot

size 1.0 mm up to $1.80 \times 10^5 \text{ Ks}^{-1}$ compared to the laser spot size of 1.7 mm at $0.19 \times 10^5 \text{ Ks}^{-1}$.

Table 4.2 Microhardness and cooling rate of the melting zone laser surface melting range at four different spot sizes.

Spot size (mm)	1.0	1.2	1.4	1.7
Hardness, HV _{0.1}	936.6 – 990.0	706.8 – 900.2	719.2 – 948.3	642.0 – 932.0
C _R × 10 ⁵ (Ks ⁻¹)	1.43 – 1.80	0.70 – 0.95	0.25 – 0.42	0.14 – 0.19

These findings enhance our understanding of high cooling rate affect the microstructure and mechanical properties of grey cast iron surface. Increasing the hardness surface of grey cast iron in laser melting relative to the formation of secondary dendrite arm spacing and grain, which affected the ultimate tensile strength and fracture toughness of the final product. This is supported by Oloyede et al. 2016 study which reveal formation of martensite, retained austenite, and cementite (Fe₃C) which is improved the mechanical properties of grey cast iron (Oloyede *et al.*, 2016).

4.2.4 X-ray diffraction for laser surface melting

The diffraction peak of as-received grey cast iron is characterized by distinct reflection of α -ferrite (110) and (220), graphite (002) and cementite phase at 45.05°, 65.69°, 26.47° and 23.65° Bragg's angles (2 theta) respectively as shown in Figure 4.10 (a). In the as-received grey cast iron, the amount of cementite is 56.2 % and α -ferrite is 22.4 % whereas graphite phase has a total number of 13 peaks in crystal system of rhombohedral structure. This study indicates that lamellar graphite in grey cast iron produced an intrinsic brittleness which is easy to fracture due to the high temperature, pressure and mechanical friction, which contribute to multifaceted, high-stress condition (Ghasemi & Elmquist, 2014). Furthermore, the graphite may cause graphitic corrosion if exposed to the atmosphere.

The result of this study also indicates that as-received grey cast iron has high chemical composition of carbon and silicon to obtain a graphitic microstructure. Besides that, high cooling rate during casting produces more ferritic matrix. Formation of hard phase cementite (Fe₃C) has proven that this material can completely suppresses

graphitization. The finding provides evidence that as-received grey cast iron has no appreciable strength since the graphite formation can be treated as voids.

In Figure 4.10 (b), most of the austenite phase peaks transformed into martensite phase. Based on the x-ray diffraction on laser melting surface grey cast iron, the peaks detected from the figure were martensite (110), α -ferrite (110), γ -Fe (111) and (220) and cementite phase at 43.88°, 44.59°, 50.94°, 74.36°, 43.88° and 45.74° Bragg's angles (2 theta) respectively. In modified surface of as-received grey cast iron, the amount of martensite is at 54.8 %, α -ferrite in 0.3 %, γ -Fe in 31.2 % and cementite was at 13.6 %. From EDS, carbon content decrease slightly to 28.3 %. Therefore, the cementite (Fe_3C), martensite and retained austenite were found in the molten zone which contributed to the improvement of microhardness

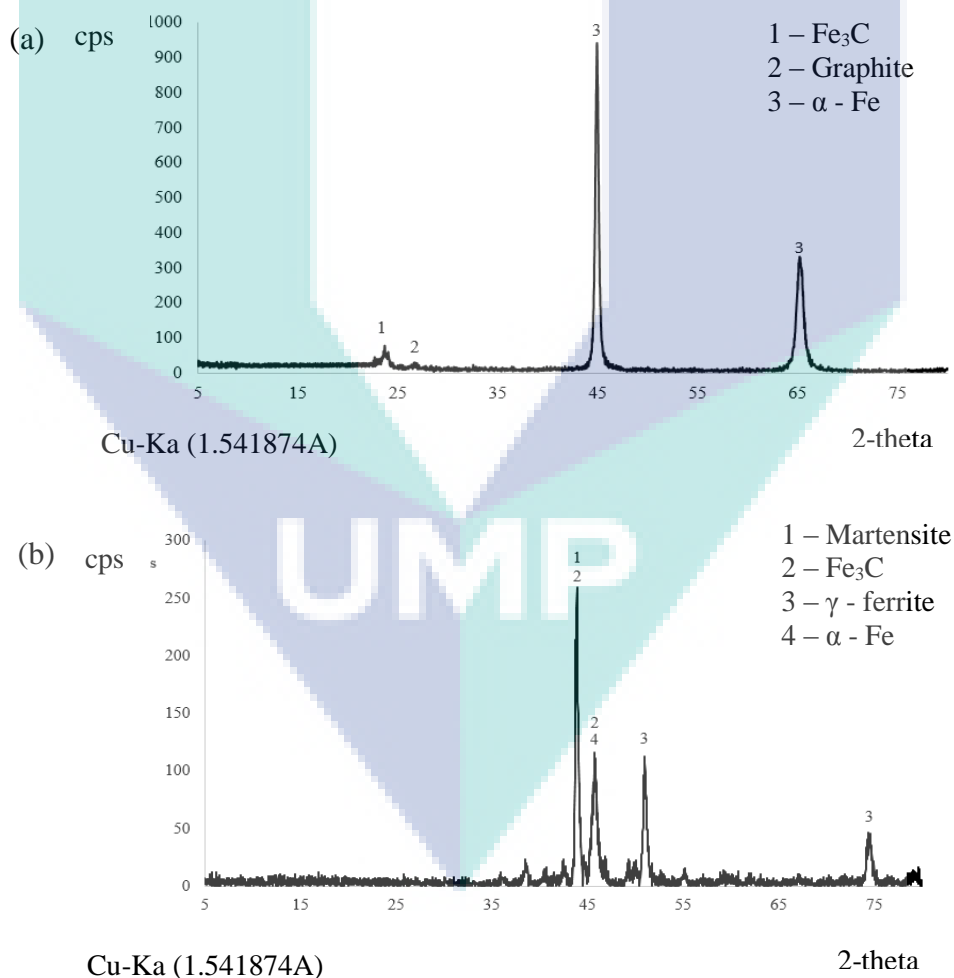


Figure 4.10 (a) X-ray diffraction as-received grey cast iron and (b) surface melting of grey cast iron.

It has been proven from XRD, new phase martensite, Fe₃C and retain austenite contributed to the high hardness on the melting zone. In addition, high cooling rate with lowest residence time set parameter is the cause for the formation of the new phase during laser processing.

4.2.5 ANOVA for Laser Surface Melting of Grey Cast Iron

4.2.5.1 Surface roughness

Analysis of variance (ANOVA) carried out for the modified surface roughness response is given in Table 4.3. However, several terms in the models were insignificant for modified surface roughness which were identified by p-values greater than 0.1000. The insignificant terms were removed using stepwise elimination process. The reduced model is shown in Table 4.3. In the reduced model, though the model is significant, however R² and adjusted R² value were 99 % which indicated a good relationship between the factor and the modified surface roughness response from the regression model. F-value is a measure of how different the means are relative to the variability within each samples. The F-value of 11754.3, 1821.24, 380.05 and 421.95 for spot size 1.0 mm , 1.2 mm, 1.4 mm and 1.7 mm respectively implies that the model is significant with only a 0.71 % , 1.79 % , 3.92 % and 0.24 % chance that an F-value this large could occur due to noise. Terms with values of probability less than 0.05 were taken as significant.

Table 4.3 ANOVA results for modified surface roughness response.

Spot size (mm)	Source	Sum of squares	df	Mean square	F value	p-value Prob>F	
1.0	Model	0.88	6	0.15	11754.3	0.0071	significant
	A-Pp	0.20	1	0.20	15625.0	0.0051	
	B-PRF	0.0015	1	0.0015	121.0	0.0577	
	C-Speed	0.47	1	0.47	37249.0	0.0033	
	AB	0.10	1	0.10	8281.0	0.0070	
	AC	0.095	1	0.095	7569.0	0.0073	
	BC	0.021	1	0.021	1681.0	0.0155	
	Residual	0.000013	1	0.000013			
	Std. Dev.	0.0035		R ²		1.00	
	Mean	3.56		Adjusted R ²		0.99	
C.V. %	0.099		Adequate precision		278.18		
1.2	Model	6.69	6	1.12	1821.24	0.0179	significant
	A-Pp	2.5	1	2.50	4077.73	0.0100	
	B-PRF	1.95	1	1.95	3184.18	0.0113	
	C-Speed	1.67	1	1.67	2718.88	0.0122	
	AB	0.50	1	0.50	808.18	0.0224	
	AC	0.082	1	0.082	133.90	0.0549	
	BC	0.0028	1	0.0028	4.59	0.2780	
	Residual	0.00061	1	0.00061			
	Std. Dev.	0.025		R ²		0.99	
	Mean	5.27		Adjusted R ²		0.99	
C.V. %	0.47		Adequate precision		130.344		
1.4	Model	7.76	6	1.29	380.05	0.0392	significant
	A-Pp	0.48	1	0.48	142.12	0.0533	
	B-PRF	4.99	1	4.99	1467.59	0.0166	
	C-Speed	1.48	1	1.48	433.90	0.0305	
	AB	0.72	1	0.72	212.10	0.0436	
	AC	0.083	1	0.083	24.28	0.1275	
	BC	0.00099	1	0.00099	0.29	0.6851	
	Residual	0.0034	1	0.0034			
	Std. Dev.	0.058		R ²		0.99	
	Mean	5.99		Adjusted R ²		0.99	
C.V. %	0.97		Adequate precision		55.714		
1.7	Model	2.87	5	0.57	421.95	0.0024	significant
	A-Pp	1.54	1	1.54	1130.28	0.0009	
	B-PRF	0.060	1	0.060	43.68	0.0221	
	C-Speed	1.22	1	1.22	898.80	0.0011	
	AB	0.015	1	0.015	11.24	0.0786	
	AC	0.035	1	0.035	25.77	0.0367	
	Residual	0.0027	2	0.0014			
	Std. Dev.	0.037		R ²		0.99	
	Mean	7.39		Adjusted R ²		0.99	
	C.V. %	0.50		Adequate precision		57.325	

4.2.5.2 Hardness

In Table 4.4, the variance analysis for surface hardness response with linear model is presented. The model F-value of 347.96, 38.13, 54.37 and 2349.84 for spot size 1.0 mm, 1.2 mm, 1.4 mm and 1.7 mm respectively with p-value of 0.0410, 0.0258, 0.0182 and 0.0158 imply the model is significant. The predicted R² and adjusted R² were 99 % for spot size 1.0 mm, 98 % and 96 % for spot size 1.2 mm, 99% and 97 % for spot size 1.4 mm and 99 % for spot size 1.7 mm.

Table 4.4 ANOVA results for modified surface hardness response.

Spot size (mm)	Source	Sum of squares	df	Mean square	F value	p-value Prob>F	
1.0	Model	4603.49	6	767.25	347.96	0.0410	significant
	A-Pp	994.58	1	994.58	451.06	0.0300	
	B-PRF	756.60	1	756.60	343.13	0.0343	
	C-Speed	233.28	1	233.28	105.80	0.0617	
	AC	158.42	1	158.42	71.85	0.0748	
	BC	1452.60	1	1452.60	658.78	0.0248	
	ABC	1008.00	1	1008.00	457.15	0.0298	
	Residual	2.20	1	2.20			
	Std. Dev.	1.48		R ²		0.99	
	Mean	953.75		Adjusted R ²		0.99	
C.V. %	141.12		Adequate precision		49.747		
1.2	Model	26266.69	5	5253.34	38.13	0.0258	significant
	A-Pp	2221.11	1	2221.11	16.12	0.0568	
	B-PRF	8058.15	1	8058.15	58.48	0.0167	
	C-Speed	15620.28	1	15620.28	113.36	0.0087	
	AB	94.53	1	94.53	0.69	0.4946	
	AC	272.61	1	272.61	1.98	0.2948	
	Residual	275.58	2	137.79			
	Std. Dev.	11.74		R ²		0.98	
	Mean	798.41		Adjusted R ²		0.96	
	C.V. %	1.47		Adequate precision		18.215	
1.4	Model	55946.15	5	11189.23	54.37	0.0182	significant
	B-PRF	51938.65	1	51938.65	252.36	0.0039	
	C-Speed	1436.48	1	1436.48	6.98	0.1184	
	AB	1971.92	1	1971.92	9.58	0.0904	
	AC	190.13	1	190.13	0.92	0.4379	
	BC	408.98	1	408.98	1.99	0.2940	
	Residual	411.62	2	205.81			
	Std. Dev.	14.35		R ²		0.99	
	Mean	850.73		Adjusted R ²		0.97	
	C.V. %	1.69		Adequate precision		18.440	
1.7	Model	86356.75	6	14392.79	2349.84	0.0158	significant
	A-Pp	5565.12	1	5565.12	908.59	0.0211	
	B-PRF	63546.13	1	63546.13		10374.88	
	C-Speed	7381.12	1	7381.12		1205.08	
	AB	4560.13	1	4560.13		744.51	
	AC	153.13	1	153.13		25.00	
	BC	5151.13	1	5151.13		841.00	
	Residual	6.12	1	6.12			
	Std. Dev.	2.47		R ²		0.99	
	Mean	831.88		Adjusted R ²		0.99	
C.V. %	0.30		Adequate precision		126.024		

4.2.5.3 Design optimization laser surface melting

Optimization analysis was conducted to design an experiment within the given range of peak power, pulse repetition frequency and traverse speed, with a view to minimize surface roughness and maximize microhardness. Laser spot size 1.0 mm, 1.2 mm, 1.4 mm and 1.7 mm within the constraint and range given in Table 4.5. Peak power,

PRF and traverse speed range were as outlined between 800 and 2200 W, 8 and 90 Hz and 2.4 and 21.6 mms^{-1} respectively.

Table 4.5 Constraints in design optimization for laser surface melting.

Name	Spot size (mm)	Goal	Lower limit	Upper limit	Important
Peak Power (W)		is in range	800	1200	3
PRF (Hz)		is in range	80	90	3
Traverse speed (mms^{-1})	1.0	is in range	19.2	21.6	3
Surface roughness, Ra (μm)		minimize	3.0	3.92	3
Microhardness ($\text{HV}_{0.1}$)		maximize	920.1	990.0	3
Peak Power (W)		is in range	800	1200	3
PRF (Hz)	1.2	is in range	40	50	3
Traverse speed (mms^{-1})		is in range	13.6	17	3
Surface roughness, Ra (μm)		minimize	4.1	7.1	3
Microhardness ($\text{HV}_{0.1}$)		maximize	706.8	900.2	3
Peak Power (W)		is in range	1500	1800	3
PRF (Hz)	1.4	is in range	15	25	3
Traverse speed (mms^{-1})		is in range	5.7	9.5	3
Surface roughness, Ra (μm)		minimize	4.831	7.83	3
Microhardness ($\text{HV}_{0.1}$)		maximize	719.2	948.3	3
Peak Power (W)		is in range	2000	2200	3
PRF (Hz)	1.7	is in range	8	11	3
Traverse speed (mms^{-1})		is in range	2.4	3.3	3
Surface roughness, Ra (μm)		minimize	6.52	8.32	3
Microhardness ($\text{HV}_{0.1}$)		maximize	642	932	3

The design solution calculated from optimized parameter are within the range of experimentally achieved hardness and minimized surface roughness as shown in Appendix D, Appendix E and Appendix F for all spot sizes. The selected parameter setting from design solution which high have hardness and low surface roughness from each spot size are presented in Table 4.6. Increasing the spot size diameter will affect the laser parameter setting when the peak power is increased and pulse repetition frequency

and traverse speed is reduced. Peak power, PRF and traverse speed are significant factors to optimize the surface of grey cast iron through laser processes.

Table 4.6 Processing parameter setting based on high desirability for spot size 1.0 mm, 1.2 mm, 1.4 mm and 1.7 mm.

Spot size	Peak power (W)	Pulse repetition frequency (Hz)	Traverse speed (mms ⁻¹)	Surface roughness (μm)	Hardness (HV _{0.1})
1.0	800	90	19.2	3.10	989
1.2	800	50	13.6	4.09	829
1.4	1800	15	5.7	5.49	935
1.7	2021	8	3.30	7.23	920

The results revealed that the highest hardness and the lowest surface roughness are 989 HV_{0.1} and 3.10 μm which were produced at laser spot size 1.0 mm. Based on the results, laser spot size 1.0 mm at range peak power of 800 to 1200 W and pulse repetition frequency in range of 80 to 90 Hz is the most suitable laser parameter for laser cladding with addition of Cr and Mo powder. In this experiment, Cr and Mo powder are dark that would give advantage for deeper penetration. According to Chen et al. (2015) penetration laser beam on grey cast iron surface can be increased using dark powder because of high absorbance on the surface (Chen *et al.*, 2015b).

The findings from this study make several contributions to the current literature. First, to obtain high hardness and minimum surface roughness, smallest spot size is better than the biggest spot size. Secondly, setting the parameter at higher pulse repetition frequency and travers speed will increase the hardness and decrease the surface roughness. However, high energy and low traverse speed can decrease the hardness and increase the surface roughness.

4.3 Laser Surface Cladding of Grey Cast Iron

Laser cladding with addition of Cr and Mo powder were produced according design of experiment mixture model, which is a combination of laser parameter peak power and pulse repetition frequency as a factor and components of Cr and Mo as a mixture. The correlation between laser parameter and mixture of Cr and Mo are

interesting as the peak power and pulse repetition frequency from laser processing has different effect on powder elements. Cr and Mo powder have different properties such as Mo have higher melting point compared to the Cr. Furthermore, particle size of Cr powder is larger than Mo powder at difference of 92.6 %. The development of design of experiment in laser cladding is to obtain relationship between laser parameter and mixture of Cr and Mo which is still no reliable evidence has been reported.

4.3.1 Metallographic Study

A new structure of dendritic and particles formation has been developed and also a new phase of carbide is detected on the surface. Interestingly, graphite lamella in grey cast iron surface also has fully eliminated as in laser surface melting. The fully dissolution of graphite at clad zone due to the high alloy element in clad zone also being observed by other researchers in laser alloying processes (Tong *et al.*, 2008; Yang *et al.*, 2015; Zhong *et al.*, 2006).

This study has shown that, the graphite is eliminated from the surface because of the carbon migration from the graphite to the liquid phase at high cooling rate during solidification that occurred in cladding zone and lead to its complete dissolution. Moreover dendritic refinement in cladding zone was attributable to the high cooling rate of localized molten pool heating. As the structure of cladding zone has finer grain, new phases were generated in the cladding layer that mainly consisted of M-C carbide (M = Cr, Mo, Fe) and retained austenite (Amirsadeghi & Sohi, 2008; Yang *et al.*, 2015).

The microstructure clad zone for Cr, Mo and Cr-Mo mixture shown in micrograph in Figure 4.11. Based on the micrograph, the clad zone with chromium and molybdenum powder shows the formation of bright particle randomly dispersed at or near the boundaries of the dendrite, while the black particles occasionally interspersed in the matrix were observed. The particle of chromium powder formed bigger size of particles structure compared to the small particle powder of molybdenum. The combination of chromium and molybdenum powder shows that the formation of small dendrite structure with fine particles.

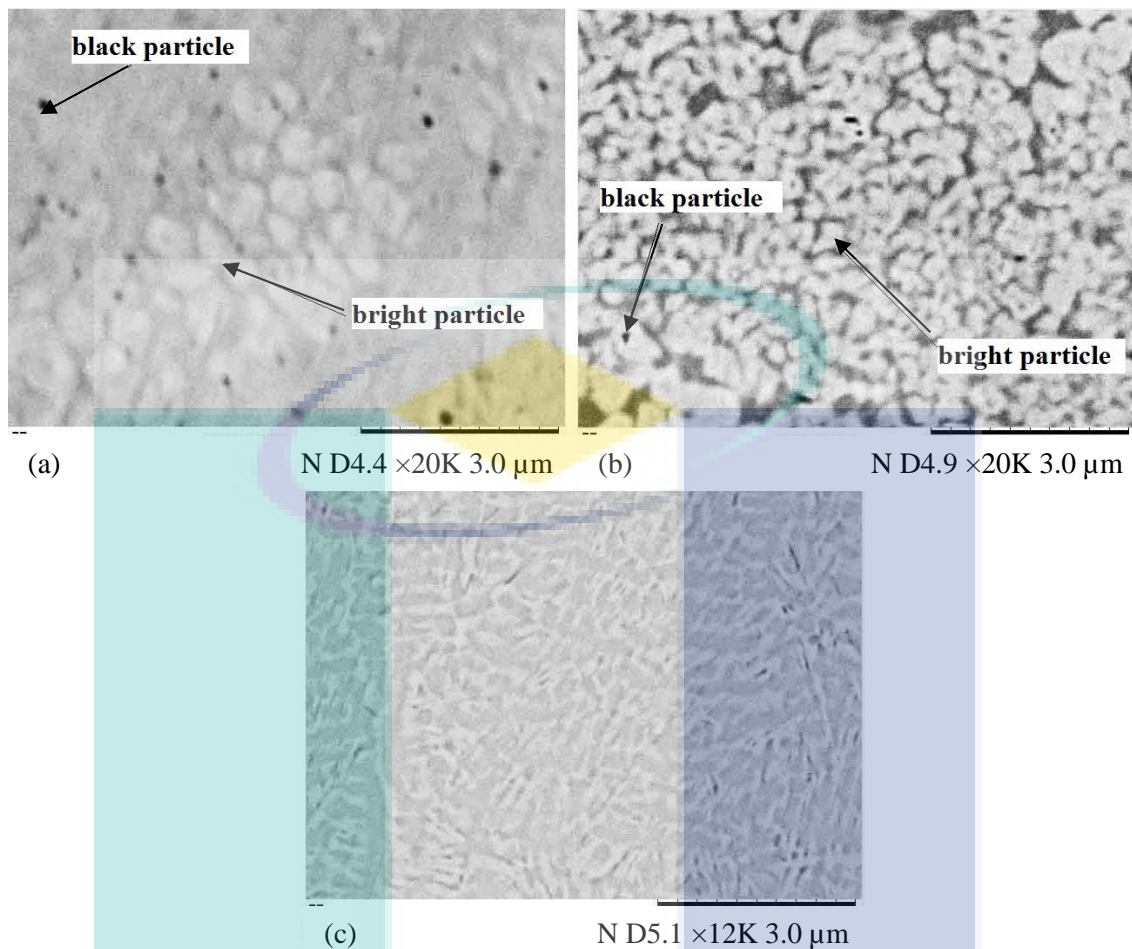


Figure 4.11 Micrograph of laser cladding grey cast iron microstructure with addition of (a) Cr powder, (b) Mo powder and (c) Cr-Mo mixture powder.

These results indicate that the melted Cr and Mo might enter the metastable miscibility gap and liquid phase separation that had taken place due to rapid solidification. Moreover, uniform deposition can be observed in Cr-Mo added after etching, while the element of substrate had diffused to the modified layer. Hence, it is proven on carbon diffusion where the graphite is eliminated. At a moderate cooling rate if $< 5000 \text{ K s}^{-1}$, the main microstructure structure is that of an interconnected network of primary dendritic with interdendritic eutectic (Oloyede *et al.*, 2016). However, laser cladding with Cr and Mo at the high cooling rates in the range of $3.52 \times 10^5 \text{ K s}^{-1}$ to $21.2 \times 10^5 \text{ K s}^{-1}$ caused the microstructure to develop a lath type morphology with a refinement of the structure scale of the laths, together with bright spheroidal particles which were evident at the highest cooling rate. According to the solidification theory, the dendritic characteristic length is inversely proportional to the cooling rate, and hence, laser cladding with added Cr-Mo

has shown smaller than addition of others. The bigger particle of chromium powder formed bigger sizes of bright particles compared to the small particle powder of molybdenum. The combination of chromium and molybdenum powder showed the formation of small dendrite structure with fine particles. The different sizes of the particles in the clad zone are due to the change of laser power varied surface heating and cooling rate (Fazliana, Aqida, & Saidin, 2013).

Figure 4.12 shows particle analysis of clad zone, in modified samples with Cr, Mo and Cr-Mo mixture powder addition at peak power 800 W, pulse repetition frequency 80 Hz and pulse energy 0.63 J. It shows particles structure with the average size of 123 nm formed in the clad zone of chromium. However, the clad surface with Mo powder produced much smaller particles size, which is about in average of 57 nm. Clad zone with mixture of 50 % Cr and 50 % Mo powder shows the particles structure is finer and homogenous in the size of 32 nm.



UMP

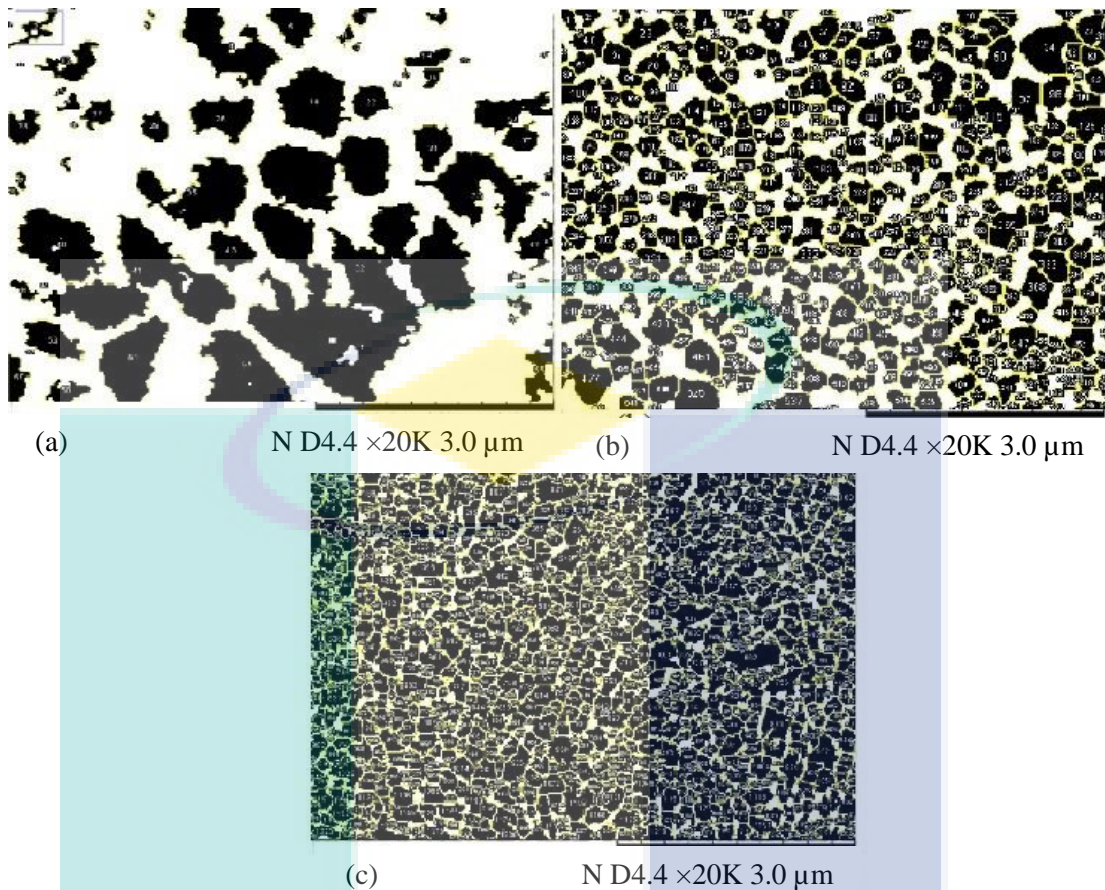


Figure 4.12 Particle analysis in clad zone of grey cast iron with addition of (a) Cr, (b) Mo and (c) Cr-Mo mixture.

The result from the experiment shown that, laser clad with Mo added and Cr-Mo mixture added had particles size at 53.7 % and 74.0 % smaller than Cr added respectively. It has been known that smaller particle powder sizes tend to be heated and accelerated more quickly at a higher temperature and velocity (Chivavibul *et al.*, 2010). Moreover, surface layers and substrate were bonded through the interface zone which exhibited excellent metallurgical bonding generation. The smaller size of particles obtained in Cr-Mo mixture added are finer and homogenous. These sizes produced different results because of the particle size used for cladding.

4.3.2 X- ray diffraction for laser surface cladding

The X-ray diffraction analysis of the laser cladding samples conducted between 5° to 80° Bragg's angle was sufficient to investigate the phase crystallinity and effect of the graphite and α -Fe phase. A comparison of phase formation between as-received grey

cast iron surface and clad layer with addition of Cr, Mo and Cr-Mo mixture powders is shown by x-ray diffraction pattern in Figure 4.13. In Figure 4.13 (a), the as-received grey cast iron sample consists of ferrite (α -Fe), cementite (Fe_3C) and graphite phases at 45.05° , 65.69° , 26.47° and 23.65° Bragg's angles (2 theta) respectively. Maximum intensity of α -Fe phase is 634 cps whereas, Fe_3C and graphite phase is at 24 and 103 cps. The α -Fe phase intensity reduced to 34.2 %, 64.3 % and 60.5 % in clad samples with respective powder addition of Cr, Mo and Cr-Mo. The decrement of α -Fe phase intensity in cladding sample was resulted from phase transformation at high cooling rate. The graphite phase was absent in all the cladding layers patterns shown in Figure 4.13 (b)-(d). Peak graphite was eliminated in all laser cladding due to the high alloying elements of Cr and Mo. In cladding zone, no graphite is observed because at high temperature of molten pool the graphite is burned down or dissolved completely during the remelting processing (Chen *et al.*, 2015b). Furthermore, Cr and Mo elements can hinder graphite precipitation and increase the inclination to form iron carbide in grey cast iron (Atmadja *et al.*, 2013).

Meanwhile, the M_2C , M_{23}C_6 and M_3C_2 carbide phases were detected in Mo and Cr-Mo added cladding layer. In Figure 4.13 (c), apart from the carbide phases, the cladding layer also comprised retained austenite. In Cr added clad layer sample of Figure 4.13 (b) the diffraction peaks were α -Fe and $\text{Cr}_{0.1}\text{Fe}_{0.63}\text{Si}_{0.27}$ phase at 45.30° and 65.42° Bragg's angles (2 theta). The α -Fe phase has a higher composition of 84.6 % while $\text{Cr}_{0.1}\text{Fe}_{0.63}\text{Si}_{0.27}$ phase is at 15.5 %. Carbide phase is absent from Cr-added grey cast iron clad surface.

Laser cladding layer with Mo powder in Figure 4.13 (c) shows that the peaks are α -Fe and MoFe at 45.04° , 40.52° , 58.71° and 73.77° Bragg's angles (2 theta). Mo added clad have shown formation of carbide M_2C and M_{23}C_6 phase at 42.34° and 43.05° Bragg's angles (2 theta). Apart from the carbide phases, the cladding layer comprise of retained austenite at 50.11° Bragg's angle (2 theta). According to Vadiraj *et al.* (2011) higher alloying element in the matrix iron leads to larger amount of retained austenite (Vadiraj, Balachandran, Kamaraj, & Kazuya, 2011). Besides that, higher carbon content in 18.6 % in Mo added promoted formation of retained austenite.

Formation of carbide phase were also detected in laser cladding Cr-Mo mixture added as show in Figure 4.13 (d). Cr-Mo mixture added phase formation consists of carbide $M_{23}C_6$ and M_3C_2 at 50.74° and 42.74° , 43.72° , 50.32° Bragg's angles (2 theta). Another's phase of Cr-Mo mixture added were α -Fe and MoFe detected at 45.04° and 73.77° Bragg's angles (2 theta) respectively.

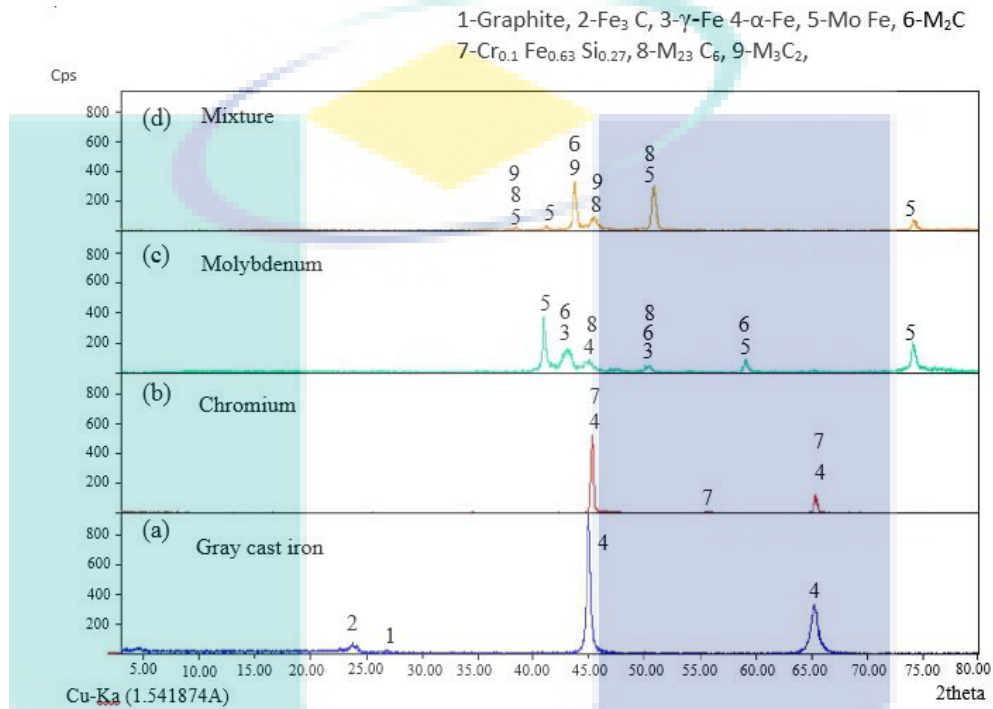


Figure 4.13 X-ray diffraction pattern for (a) grey cast iron substrate, (b) Cr-added clad, (c) Mo-added clad and (d) Cr-Mo mixture clad zone.

It was found that the α -Fe phase intensity reduced to 34.2 %, 64.3 % and 60.5 % in Cr, Mo and Cr-Mo cladding sample. This finding also highlights the graphite phases was absent in all cladding layers pattern. Meanwhile, carbide phases were only detected in Mo and Cr-Mo added cladding layer which are M_2C , $M_{23}C_6$ and M_3C_2 . The $M_{23}C_6$ carbide can be observed at both added particles, which is associated with slower growth rates and longer times available for redistribution of carbon and carbide forming elements both in the liquid and solid phases (Wieczorzak, Bala, Stepień, Cios, & Koziel, 2016). This type of carbide can be found in all high speed steels which has the highest hardness and wear resistance (Krauss, 2005).

Laser cladding on grey cast iron surface were done to strengthen the surface properties by increasing the surface hardness, wear resistance and also corrosion and thermal fatigue resistance. Cr and Mo elements can form carbide phase in the structure which is significant to increase the wear resistance. Moreover, by adding Cr elements in cast iron can resist the oxidation and have wetting capability in iron matrix (Shang-ping *et al.*, 2009). Meanwhile, adding Mo in grey cast iron can improve heat resistance and can withstand at extreme temperature without significantly expanding or softening, makes it useful in application that involves intense heat (Branco *et al.*, 2002; Maluf *et al.*, 2009; Moonesan *et al.*, 2012). This study has found that generally, adding Cr and Mo powder on the surface the composition of grey cast iron will change the structure and properties of the surface.

4.3.3 Energy Dispersive Spectrometer Analysis

Energy dispersive spectrometer (EDS) analysis were carried out onto the samples of as-received grey cast iron and samples obtained from laser cladding. The purpose of this analysis is to determine the percentage of the modified surface composition and to compare between these two samples.

4.3.3.1 Energy Dispersive Spectrometer As-received Grey Cast Iron

The chemical composition of grey cast iron substrate analysis using EDS is given in Table 4.7. In this table, six elements were detected from the grey cast iron substrate; carbon (C), silicon (Si), phosphorus (P), sulfur (S), Manganese (Mn) and Iron (Fe). Figure 4.14 shows the selected area in the grey cast iron substrate used for composition area analysis. The EDS qualitative analysis spectrums of phase detected in the selected area given in Figure 4.15.

Table 4.7 Chemical composition of the gary cast iron substrate analysed from selected area.

Material	Elements (wt. %)					
	C	Si	Mn	S	P	Fe
Grey cast iron	3.4	2.11	0.71	0.10	0.08	93.6

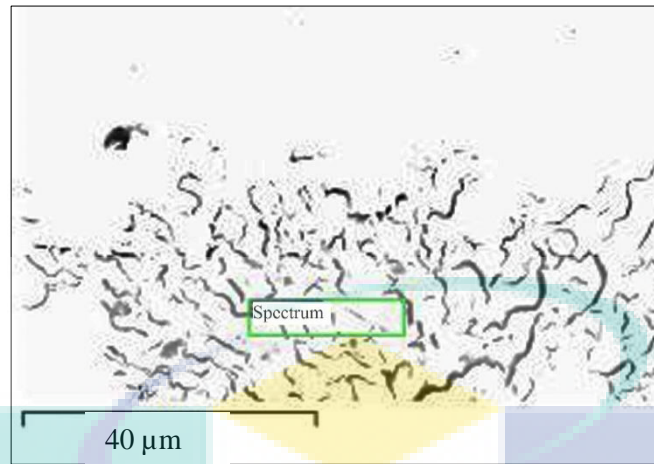


Figure 4.14 Selected area in grey cast iron substrate.

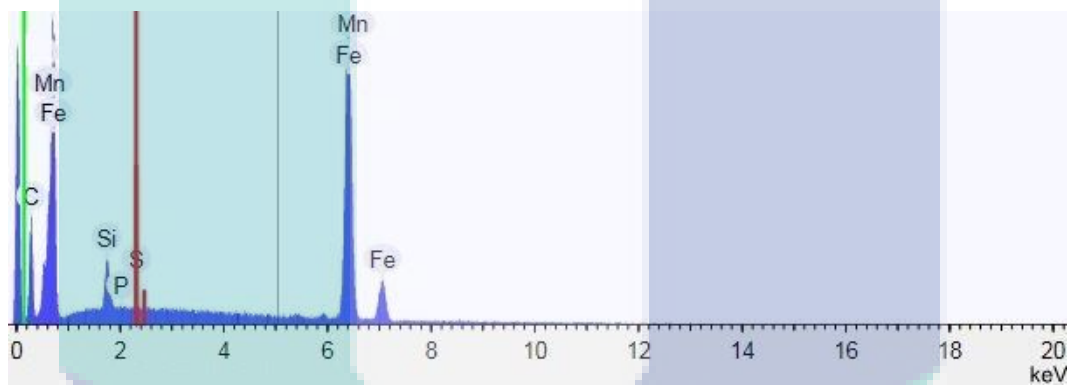


Figure 4.15 EDS qualitative analysis spectrum of phase for grey cast iron substrate.

4.3.3.2 Energy Dispersive Spectrometer Laser Cladding

The chemical composition for laser cladding with Cr, Mo and Cr-Mo added was compared and shows in Table 4.8. The analysis for laser cladding samples was conducted using a single spectrum where the chemical composition was measured from area selected as shown in Figure 4.16. In all clad samples, the content of C was higher, while Mn and P was absent or the content was too low. In Cr clad, S was detected but it was lower when compared with Mo and Cr-Mo mixture. Based on the data, carbide formation phase in Cr-Mo mixture cladding layer was due to low concentration of Cr and Mo particles at weight percent of 1.7 % and 1.3 % respectively along with high carbon composition of grey cast iron substrate at 18.3 %. Laser cladding layer with Mo added has shown the weight percent of Mo is 32 % at high carbon content of 21 %.

Table 4.8 Composition analysis for laser clad samples.

Material	Elements (wt. %)							
	C	Si	Mn	S	P	Cr	Mo	Fe
Cr clad	14.8	1.9	0	0	0	67.3	0.0	16.0
Mo clad	21.0	1.0	0	0.02	0	0.0	32.0	45.7
Cr-Mo mixture clad	18.3	1.2	0	0.05	0	1.7	1.3	77.4

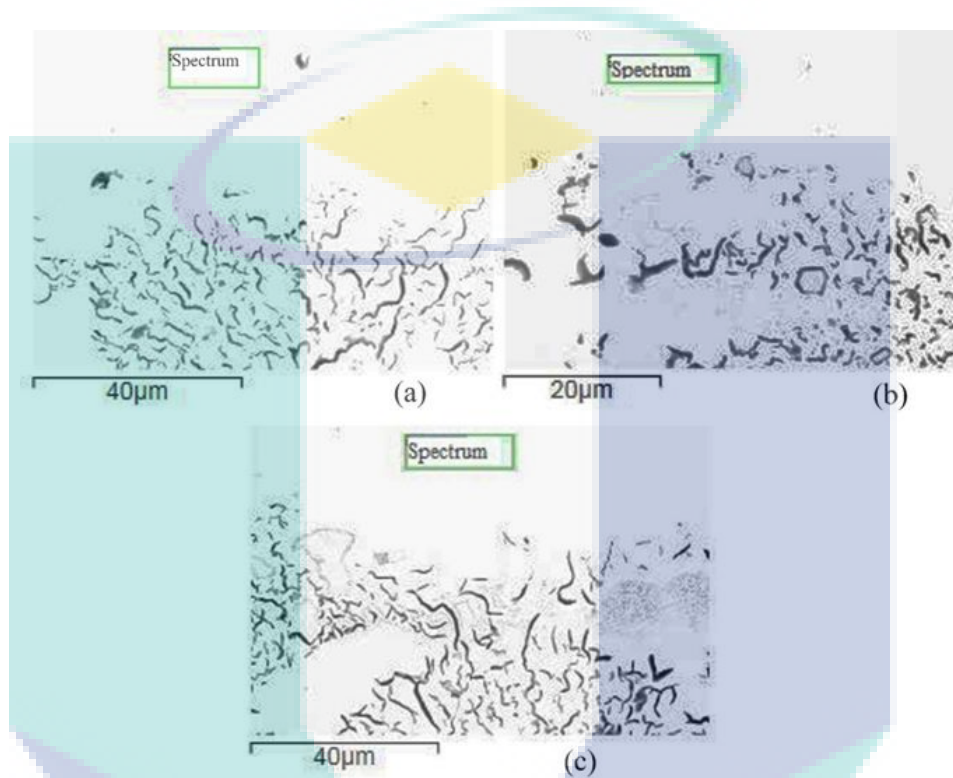


Figure 4.16 Selected area in laser clad zone of (a) Cr, (b) Mo and (c) Cr-Mo mixture.

Cr and Mo atom can be dissolved in α -Fe and subsequently detached out during solidification which had formed the carbide phase. Besides that, high cooling rate during rapid quenching of clad zone had caused incomplete carbon diffusion, nucleation and growth of carbide in iron matrix (Aqida, 2011). According to the Fe-C phase diagram, pearlite in substrate began to decompose into ferrite and cementite as temperature exceeded the eutectoid point, whereas pearlite transformed into austenite. As temperature continuously increased, the primitive ferrite was converted into austenite with some carbon element decomposing into austenite. However, some austenite cannot be converted completely and turned into residual austenite because of the rapid cooling rate, which is had been detected in Mo added (Yi *et al.*, 2014).

In contrast, high concentration of Cr particles at weight percentage of 67.3 % and low carbon at 14.8 % in laser clad Cr added have obstructed the carbide formation in clad zone. Meanwhile, high silicon content at 1.9 % has formed CrSi phase as shown in XRD resulted. In the cladding layer with Cr particles addition, the rapid cooling during cladding was inadequate to allow carbide precipitation in the cladding zone. Consequently, there is no carbide detected in laser cladding with Cr added except with high amount of α -Fe at 84.6 %. This is supported by Hirota et al. (2005) study which reveals that formation of Cr carbides (Cr_3C_2 , Cr_7C_3 and Cr_{23}C_6) depending on the Cr/C ratios (Hirota, Mitani, Yoshinaka, & Yamaguchi, 2005). The EDS qualitative analysis spectrums of phase detected in the selected area given in Figure 4.17.

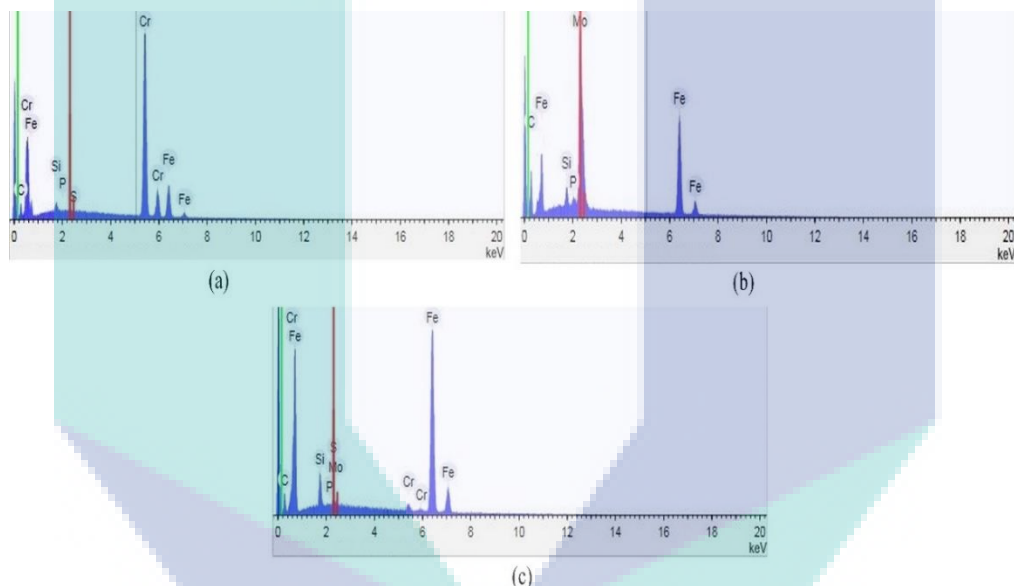


Figure 4.17 EDS qualitative analysis spectrum of phases for modified layer (a) Cr clad, (b) Mo clad and (c) Cr-Mo mixture clad.

4.3.4 Hardness Properties

One of the most significant findings to emerge from this study is the modified surface of grey cast iron with Cr and Mo added. The elimination of graphite and the formation of dendritic and particles structure had increased the hardness properties of the grey cast iron. The highest hardness of grey cast iron is obtained laser clad because of the formation of finer grain particle and secondary carbide (Aqida, 2011).

Figure 4.18 shows the comparison of microhardness for Cr, Mo and Cr-Mo mixture added samples at laser processing of peak power in range of 800 to 1200 W, pulse repetition frequency in range of 80 to 90 Hz, irradiance at 15.28 W/mm^2 and pulse energy in range of 0.56 to 0.63 J. From this figure, it is obvious that the microhardness at the surface of grey cast iron increased from the substrate to the surface, which is similar with laser surface melting. However, with increasing the distance from the treated surface and reduced heat input will result in remaining graphite at interface zone where the hardness is lower than the clad zone.

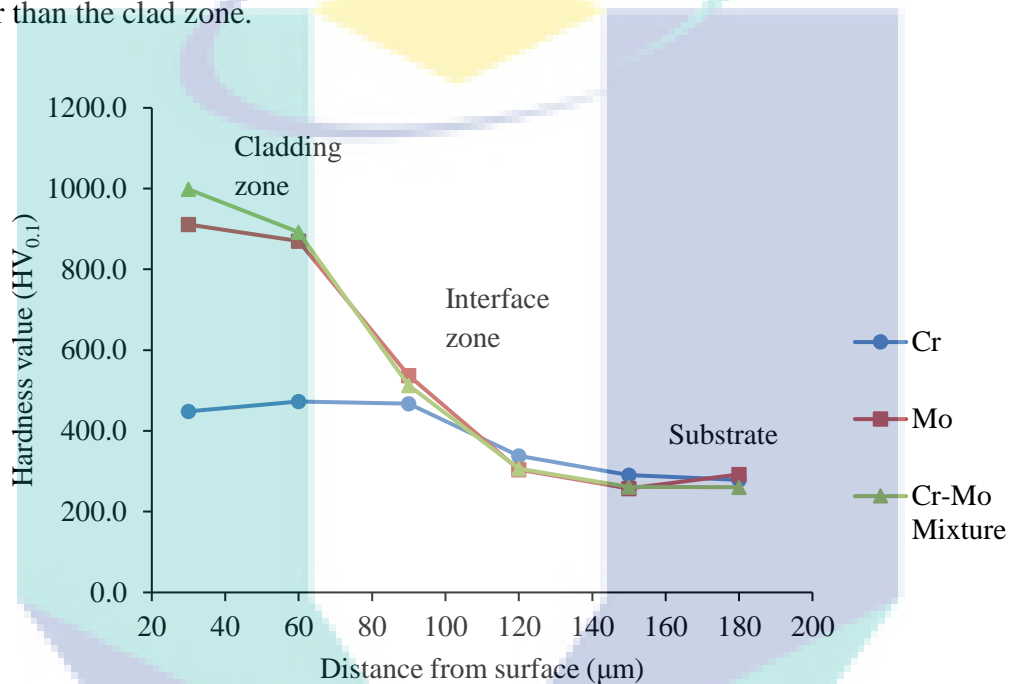


Figure 4.18 Hardness properties of laser cladding surface with addition of Cr, Mo and Cr-Mo mixture as a function of distance from surface all cladding samples were processed at spot size 1.0 mm.

By comparing the data microhardness at cladding zone in Table 4.9 with Cr, Mo and Cr-Mo added, mixture added samples exhibited high hardness properties of 998.3 $\text{HV}_{0.1}$ at Cr-Mo mixture samples and lower hardness of 566.0 $\text{HV}_{0.1}$ and this was measured in Cr added sample. Parallel with XRD results, carbides formation in Mo and Cr-Mo mixture added clad surface increased the hardness properties, while Cr added samples did not show any carbide formation.

Table 4.9 Microhardness of cladding zone at spot sizes 1.0 mm.

Clad layer	Hardness HV_{0.1}
Chromium	460.3 – 566.0
Molybdenum	911.1 – 995.5
Cr-Mo mixture	875.1 – 998.3

Strengthened by the Cr and Mo elements, the hardness of the clad layer had increased significantly up to 998.3 HV_{0.1} compared to the substrate hardness of as-received grey cast iron at 278.5 HV_{0.1}. This result is supported by Sun et al. (2011), that hardness in laser surface modification by adding transition metal had increased the hardness from substrate to the surface (Sun *et al.*, 2011). Laser cladding with Cr-Mo mixture added had exhibited slightly higher hardness compared to the Mo and Cr added. The lowest hardness was obtained at laser clad with Cr added at 566.0 HV_{0.1}. One of the plausible explanation for these findings is that particle size of Cr powder was larger than Mo powder at difference of 92.6 % μm , which affected the hardness and structure of the cladding zone. Correspond with previous findings, alloying with smaller particle size was significant to increase the hardness properties and reduce pores inside the structure, while larger size particles resulted in a lower hardness with porosity presence (Chivavibul *et al.*, 2010; Kong, Carroll, Brown, & Scudamore, 2007). The results of the laser clad on grey cast iron indicate that hardness at the surface of grey cast iron had improved up to 68.3 %. The finding is consistent with the findings of past studied by Amirsadeghi and Sohi (2008), where the hardness modified layer of cast iron with Cr and Mo had increased at 66.7 % and 66.2 % respectively (Amirsadeghi & Sohi, 2008).

The microhardness properties of laser cladding on grey cast iron correspond to different hardening mechanisms. Four major strengthen mechanism identified from the metallographic were carbide formation, dendritic, particles formation and elimination of graphite. This is supported by Amirsadeghi and Sohi (2008) study which revealed that formation of carbide phase and retain austenite had improved the hardness of cast iron's surface (Amirsadeghi & Sohi, 2008). In agreement with previous work, carbide formation in clad zone contributed to the increment of hardness (Chung *et al.*, 2013). The double increment of hardness properties in Cr-added clad from its substrate was relatively caused by the dendrite structure with formation of particle.

However, the most surprising in this study is the development of dendritic and particles structure on grey cast iron's surface which have not been mention in other report. Rapid quenching and the presence of particles during solidification obstructed atom settlement, thus resulted in dendritic and particles formation in cast iron. Formation of metal carbides and elimination of graphite had been reported in other processing such as in laser melting (Benyounis *et al.*, 2005; Karamış & Yıldızlı, 2010). Elimination of graphite was also observed by other researchers when surface of cast iron is modified by laser alloying processes (Tong *et al.*, 2008; Yang *et al.*, 2015; Zhong *et al.*, 2006).

Based on the statistical analysis in measuring particles size using Image J, the particles size in clad zone had shown different size on each different clad added. In this study, the particles size of clad zone depends on the particle powder and laser power setting which can form smaller or bigger size of particles. The smallest particle size is in range of 0.969 to 9.62 μm and the biggest particle size is in range of 71.9 to 130 μm . These formation have resulted the hardness of Cr-Mo mixture added is 43.3 % higher than Cr added. This finding suggests that using smaller particle size powder can form smaller particles structure which have high hardness. A possible explanation for this behavior is attributed to the reduction of porosity and due to the improvement of splat-splat bonding. The finding is consistent with findings of past studies by Chivavibul *et al.* (2010), which coating integrity can be improved with smaller powder for hardness increment (Chivavibul *et al.*, 2010). According to the Fazliana *et al.* (2013), laser power setting can cause varied surface heating and cooling which will form different size of grain particles in clad zone (Fazliana *et al.*, 2013). Smaller particles structure contributes to the higher hardness of the clad layer (Norhafzan *et al.*, 2016). This has been proven in clad zone which shows that Cr-Mo mixture samples exhibit the high hardness compared to other clad zone.

4.3.5 Surface Profile

The metallographic study reveals a clad layer formation on grey cast iron substrate as shown in Figure 4.19. Micrographs of modified sample cross section in Figure 4.19 indicate the presence of clad zone, interface zone and substrate material. The result also show that the clad zone with chromium, molybdenum and mixture particle addition formed a graphite-free layer. Elimination of graphite was also observed by other

researcher when surface of cast iron is modified by laser alloying processes (Tong *et al.*, 2008; Yang *et al.*, 2015; Zhong *et al.*, 2006). It was found that the highest clad zone depth for Cr, Mo and Cr-Mo mixture is 127 μm , 131 μm and 96 μm .

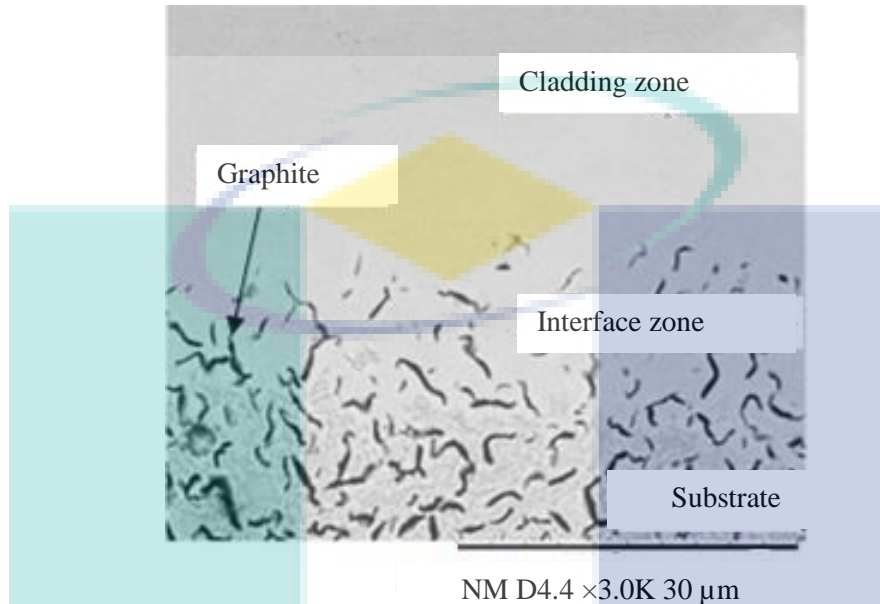


Figure 4.19 Micrograph of formation clad layer on grey cast iron substrate.

Table 4.10 shows the range of layer's depth of the clad zone and surface roughness of samples at 1.0 mm laser spot size. The result shows that, the highest clad layer thickness and surface roughness obtain at Mo added samples at 131 μm and 18.96 μm respectively. The lowest clad layer and surface roughness obtain at Cr-Mo mixture samples at 96 μm and 8.38 μm . The samples with Cr added samples produced depth of clad layer thickness in 127 μm and surface roughness in 13.10 μm which is between the value of highest and lowest depth of clad layer and surface roughness.

Table 4.10 Surface roughness of clad zone at spot sizes 1.0 mm.

Clad layer	R_a (μm)	Depth (μm)
Chromium	10.60 – 13.10	98 – 127
Molybdenum	11.20 – 18.96	53 – 131
Mixture 50% Cr 50% Mo	7.00 – 8.38	54 – 96

The result of this study indicated that, cladding with chromium and molybdenum powder will increase the surface roughness and the depth of clad layers compared to laser melting. Meanwhile, the microhardness on clad zone shows similar result with melting zone where the microhardness increased from the substrate to the surface. The highest hardness was 998.3 HV in laser surface cladding, compared to the laser surface melting which is at 990 HV. In surface roughness, it was shown that the highest surface roughness was 18.96 μm for laser surface cladding which is higher than the laser surface melting at 8.3 μm . The finding indicates that a new dendrite and particle structure formed on the clad zone and new phase formation of carbide contributed to the high hardness in clad zone. However, clad with chromium shows the lowest hardness compared to the clad molybdenum and Cr-Mo mixture.

4.4 Statistical Analysis

In design of experiment of mixture model, the metallographic study was performed to statistical analyze the surface roughness and microhardness. These analysis were performed as a respond to laser parameter and mixture components in laser processing. In addition, the effect of clad layer components and laser parameter were determined from this work. The findings from design of experiment show the ANOVA analysis is a linear model with F-value less than 0.05. The surface roughness and microhardness show that the model is significant.

4.4.1 ANOVA for Laser Cladding

Analysis of variance (ANOVA) method in statistical analysis was used to determine the significant model for two responses, which are surface roughness and hardness in laser surface cladding.

4.4.1.1 Surface roughness

In Table 4.11, the variance analysis for surface roughness response with linear model is presented. The model F-value of 22.36, 16.47, 114.72, 33.60 and p-value of 0.0135, 0.027, 0.0017 and 0.0102 imply the model is significant with related terms of AB and BD. The predicted R^2 and adjusted R^2 were 98 % and 94 % respectively. The final response surface equation for the linear model of surface roughness is given by Eq. (4.1).

Table 4.11 ANOVA results for modified surface roughness response laser cladding.

Source	Sum of squares	df	Mean square	F value	p-value Prob>F	
Model	137.63	8	17.20	22.36	0.0135	significant
Linear Mixture	12.68	1	12.68	16.47	0.0270	
AB	88.28	1	88.28	114.72	0.0017	
AC	0.82	1	0.82	1.06	0.3791	
AD	3.57	1	3.57	4.64	0.1202	
BC	0.43	1	0.43	0.56	0.5076	
BD	25.86	1	25.86	33.60	0.0102	
ABD	4.82	1	4.82	6.26	0.0876	
BCD	5.55	1	5.55	7.22	0.0746	
Residual	2.31	3	0.77			
Cor Total	139.94	11				
Std. Dev.	0.88		R ²		0.98	
Mean	11.49		Adjusted R ²		0.94	
C.V. %	7.64		Adequate precision		15.65	

$$\text{Surface roughness of clad zone: } 12.15A + 14.66B - 23.01AB + 0.41AC - 0.95AD - 0.30BC - 2.54BD + 5.38ABD + 1.05BCD \quad (4.1)$$

Where A and B are mixture components of Cr and Mo, while C and D are laser factor of peak power and pulse repetition frequency. Investigation on peak power in range 800 W to 1200 W and mixture component effect on surface roughness of clad layer at lower pulse repetition frequency of 80 Hz and 90 Hz is presented in Figure 4.20. It is apparent on this Figure 4.20, that surface roughness of clad zone is higher at region 16.72 at 80 Hz, while 90 Hz it show the surface roughness are not too high. This finding highlights that the increment of peak power at 100 % Mo added increase the surface roughness of clad zone at lower PRF. At higher PRF at 100 % Mo and Cr, the peak power are not affect the surface roughness. However, at 50% of Cr and Mo the surface roughness are lower for both PRF setting.

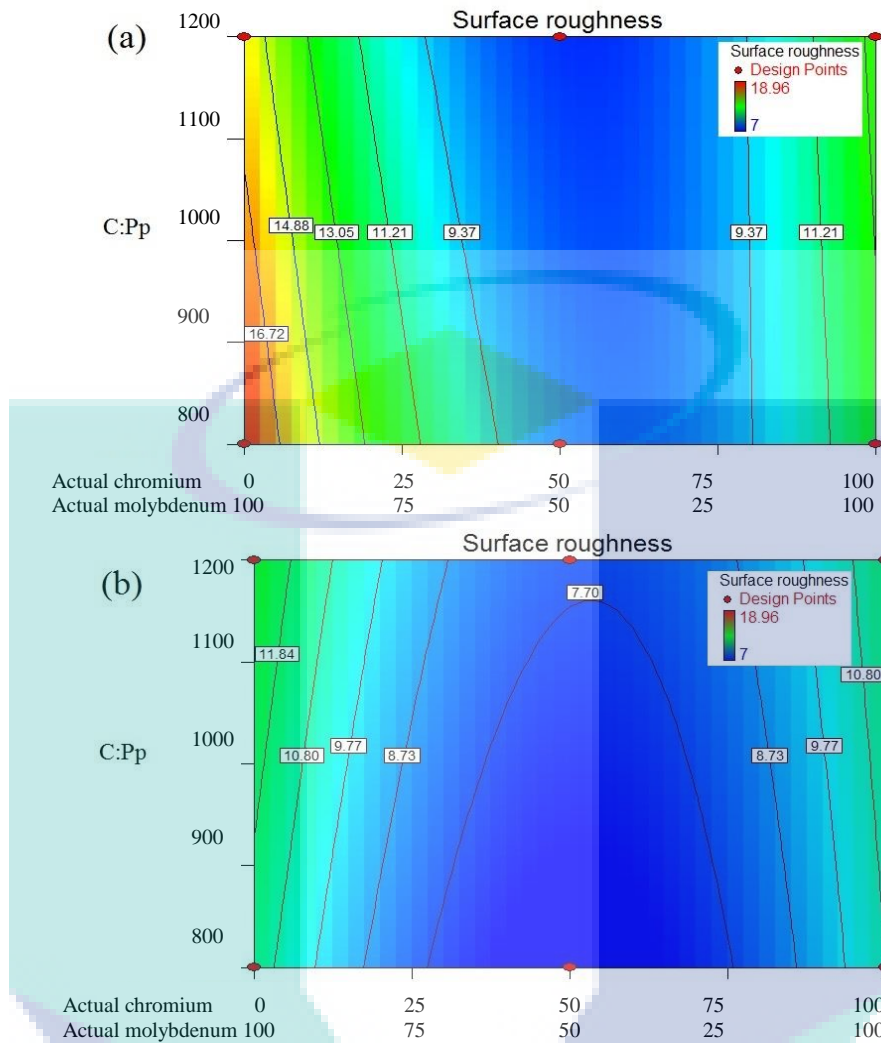


Figure 4.20 Contour plot of peak power and mixture component on surface roughness of clad zone at constant (a) 80 Hz and (b) 90 Hz.

4.4.1.2 Hardness

For the hardness response variance analysis where a linear model fit was used is shown in Table 4.12. The model F-value of 41849.17, 0.000031, 91093.74, 885.42, 3630.96, 180.07, 1127.21, 1110.44 and 4054.07 with p-value less than 0.05, indicates the model is significant. The predicted R^2 and adjusted R^2 were 100 %. The final response surface equation for the linear model of clad zone surface hardness is shown in Eq. (4.2).

Table 4.12 ANOVA results for modified surface hardness response laser cladding.

Source	Sum of squares	df	Mean square	F value	p-value Prob>F	
Model	0.000058	10	57651.59	41849.17	0.0038	significant
Linear Mixture	0.000043	1	0.000043	0.000031	0.0011	
AB	0.000013	1	0.000013	91093.74	0.0021	
AC	1219.76	1	1219.76	885.42	0.0214	
AD	5002.03	1	5002.03	3630.96	0.0106	
BC	127.69	1	127.69	92.69	0.0659	
BD	248.06	1	248.06	180.07	0.0474	
ABC	49.74	1	49.74	36.10	0.1050	
ABD	1552.85	1	1552.85	1127.21	0.0190	
ACD	1529.75	1	1529.75	1110.44	0.0191	
BCD	5584.90	1	5584.90	4054.07	0.0100	
Residual	1.38	1	1.38			
Cor Total	0.000058	11				
Std. Dev.	1.17		R ²		1.00	
Mean	799.70		Adjusted R ²		1.00	
C.V. %	0.15		Adequate precision		478.498	

$$\begin{aligned}
 \text{Surface hardness of clad zone: } & 495.86A + 958.92B + 867.73AB - 17.46AC \\
 & - 35.36AD - 5.65BC - 7.88BD - 17.27ABC - 96.53ABD + 17.85ACD \\
 & - 34.11BCD
 \end{aligned} \tag{4.2}$$

The effect of peak power and powder elements on microhardness properties investigated at constant 80 Hz and 90 Hz pulse repetition frequency setting is shown in contour mix process plot in Figure 4.21. The finding indicates that the maximum hardness of region 956.015 HV_{0.1} and 919.63 HV_{0.1} was measured at high peak power and components of Mo and Cr-Mo mixture added. The finding provides evidence that laser cladding hardness had increased because of the mixture of elements between Cr and Mo at highest peak power at 80 Hz and lowest peak power at 90 Hz.

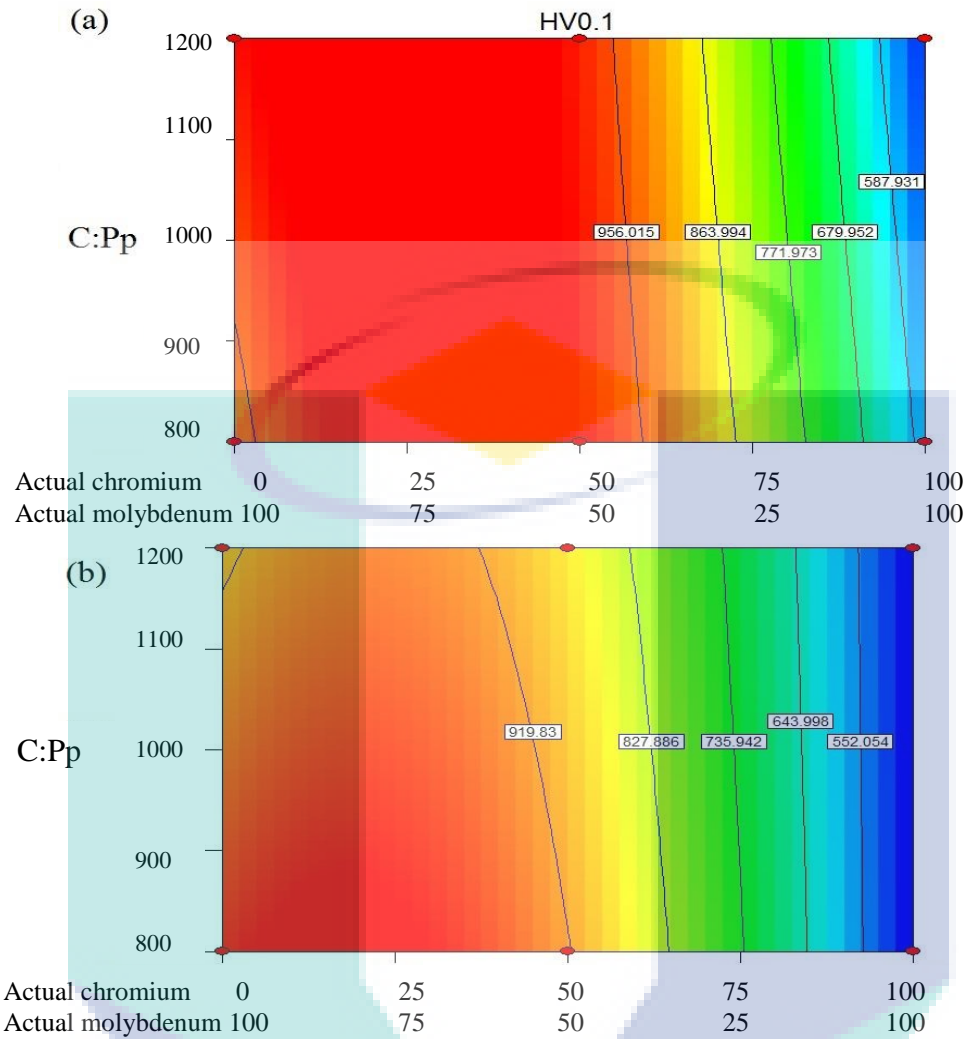


Figure 4.21 Contour plot of peak power and mixture component on microhardness at constant (a) 80 Hz and (b) 90 Hz PRF.

4.4.2 Optimization Laser Cladding

Optimizations analysis was conducted for laser spot size 1.0 mm, within the given range of peak power of 800 W to 1200 W, pulse repetition frequency 80 Hz to 90 Hz and Cr-Mo mixture from 0 % to 100% in order to minimize surface roughness and maximize microhardness as shown in Table 4.13. The highest and lowest desirability are represented by 1 and 0 value. The desirability value and parameter setting solution are listed in Table 4.14 and Figure 4.22 shows the contour plot of predicted desirability at 0.882 in region 0.765. From a set of design solution found, the highest and lowest desirability factors obtained were 0.882 and 0.862 respectively, see Table 4.14. The highest desirability exhibit hardness in 1003.8 HV_{0.1} and surface roughness in 7.75 μm obtain at peak power

1200 W, pulse repetition frequency at 80 Hz and mixture Cr at 45.3 % and Mo at 54.7 %. The important properties for grey cast iron surface is hardness properties which are exhibit in solution 8 at highest hardness of 1039.7 HV_{0.1}. However, surface roughness for this solution shown the higher in 8.88 µm. Although, the roughness of the surface can be reduce by grinding the surface as suggested by previous authors (Brytan, Bonek, & Dobrzański, 2010). Therefore, solution 8 which is at 32.3 % Cr, 67.7 % Mo, 1200 W peak power and 80 Hz were used in laser cladding samples in sliding wear experiment to investigate the coefficient of friction (CoF), weight loss and wear rate.

Table 4.13 Constraints in design optimization with microhardness were maximized and surface roughness was minimized.

Name	Goal	Lower limit	Upper limit	Important
Peak Power (W)	is in range	800	1200	3
PRF (Hz)	is in range	80	90	3
Cr added (%)	is in range	0	100	3
Mo added (%)	is in range	0	100	3
Surface roughness, Ra (µm)	minimize	7.0	18.9	3
Microhardness (HV _{0.1})	maximize	460.4	998.3	3

Table 4.14 Predicted parameters for laser cladding of grey cast iron.

Solution	Cr (w.t %)	Mo (w.t %)	Peak power (W)	Pulse repetition frequency (Hz)	Surface roughness (µm)	Hardness (HV _{0.1})	Desirability
1	45.3	54.7	1200	80	7.75	1003.8	0.882
2	44.5	55.5	1197	80	7.80	1006.9	0.881
3	42.3	57.7	1199	80	7.93	1015.2	0.880
4	45.0	55.0	1200	80	7.77	1002.7	0.880
5	46.3	53.8	1182	80	7.76	1000.2	0.880
6	44.7	55.3	1200	81	7.79	998.3	0.876
7	44.6	55.4	1200	81	7.80	998.3	0.874
8	32.3	67.7	1200	80	8.88	1039.7	0.874
9	41.5	58.5	1200	82	8.00	998.3	0.862

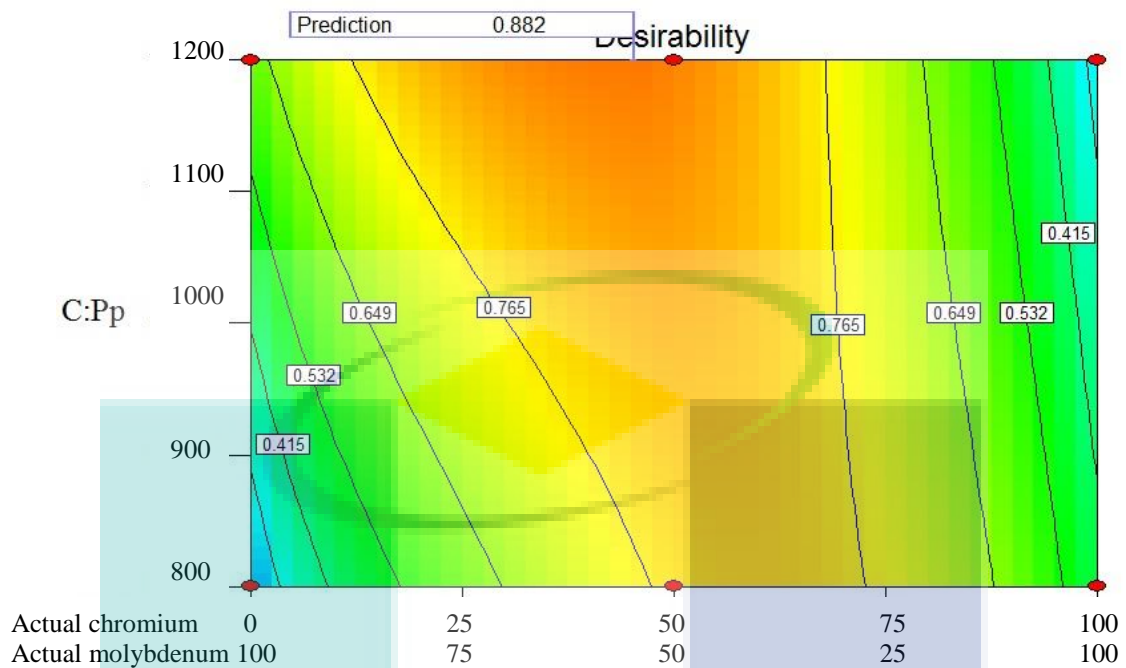


Figure 4.22 Counter plot of design for laser surface cladding process optimization of grey cast iron at 1.0 mm laser spot size.

The selection priority of higher hardness in laser cladding is due to the problem encountered in automotive components which exposed to the high pressure and mechanical friction during the operational (Ghasemi & Elmquist, 2014; Jensen *et al.*, 2002). The modified surface hardness with various alloying elements in previous report had shown that the microhardness can increase up to 1000 HV depending on type of carbide (Nagai *et al.*, 2002; Sohi *et al.*, 2012; Sun *et al.*, 2011; Zhong *et al.*, 2006). However, the modified surface roughness range in this study were less found in the previous works. According to Sun *et al.* (2011), the factor that influenced the wear resistance depends on the hardness (Sun *et al.*, 2011). Moreover, the relationship between the laser parameter and mixture elements in laser cladding are also have not been reported.

The required specification for diesel engine cylinder liner and piston ring made from grey cast iron are the hardness above 450 HV and surface roughness below 6.3 μm (Hwang *et al.*, 2002). The result of this optimization shows that the hardness of laser clad surface extremely increase to 56.7 % from the required specification. However, surface roughness are not achieved according to the required specification. Higher surface roughness in this study can be improved by adjusting the laser power and the traverse

speed. According to the Hwang et al. (2002), the surface roughness can be reduced by increasing the traverse speed (Hwang *et al.*, 2002).

4.5 Laser Surface Cladding from Optimisation Parameter

Samples laser cladding were develop with 32.3 % Cr, 67.7 % Mo, 1200 W peak power and 80 Hz. From the result, the surface roughness and hardness is 8.30 μm and 1002.5 HV_{0.1}. Compare to the data obtain from DOE the surface roughness and hardness at clad zone is reduce to 6.53 % and 3.6 %. In cast iron, formation of carbide phase attains a very high hardness and thus contributes to significant in wear resistance (Krauss, 2005) (Sohi *et al.*, 2012). In laser processing, parameter such as peak power and traverse speed have no significant effect on the hardness value as reported by the previous author (Hwang *et al.*, 2002). Many researchers had agree that grey cast iron with high hardness can increase wear resistance properties which is suitable to use for engine's components. Furthermore, Jensen et al. (2002) showed that high hardness of grey cast iron surface can increase the material's life (Jensen *et al.*, 2002).

4.5.1 Sliding Wear Test

Figure 4.23 shows the results of sliding wear test for coefficient of friction, surface roughness and weight loss for as-received grey cast iron and laser cladding. The coefficient of friction of as-received grey cast iron and laser cladding samples at different loads is shown in Figure 4.23 (a). The range of coefficient of friction of as-received grey cast iron and cladding at load 17.5 N is 0.38 and 0.42 respectively. At load 24.5 N, the coefficient of friction of as-received grey cast iron and cladding is decrease to 0.30 and 0.31 respectively.

Coefficient of friction in the clad zone samples is slightly higher than as-received grey cast iron due to the fact that the clad zone has higher hardness properties which require less energy to get sheared during sliding. This findings also support by the friction force at the surface. It has shown that, the highest friction force as-received grey is 7.35 N at normal load of 24.5 N, while for cladding samples friction force is 7.595 N. Based on the result, the friction force has increase at 24.5 % due to the improvement of hardness properties. In addition, friction force acting on the surface for clad samples is highest than

as-received grey cast iron which is prove that the hardness of clad samples is improved. However, coefficient of friction on as-received grey cast iron is slightly lower than those of laser cladding due to the graphite phase acting as solid lubricant during sliding (Sugishita & Fujjyoshi, 1982; Yan, Wang, Xiong, Xu, & Huang, 2010).

The increment of the load also increase the surface roughness in both as-received grey cast iron and laser clad samples as shown in Figure 4.23 (b). Increase pressure at the surface by increase the load have generated heat at contact surface which decrease the strength of surface material. (Chowdhury, Khalil, Nuruzzaman, & Rahaman, 2011). This action caused the surface's roughness increased. The result also show large amount of wear debris as black powder was generated in as-received grey cast iron, which could possibly a mixture of iron debris, graphite and oxidized. In contrast, the clad samples produced less quantity of wear debris which has higher average coefficient of friction and formation of hard phase in clad zone.

Figure 4.23 (c) shows the weight loss in sliding wear of laser cladding and the as-received grey cast iron sample at different loads. At load of 17.5 N the weight loss of as-received grey cast iron is 89.1 mg and for clad samples the weight loss is 1.7 mg. By increasing the load to 24.5 N, the weight loss increased slightly in both samples. The most striking result to emerge from the data is that the weight loss reduced more than 96 % compared to the as-received grey cast iron when tested using both loads. This was due to absence of graphite layer from the surface and formation of fine dendrite structures in clad layer.

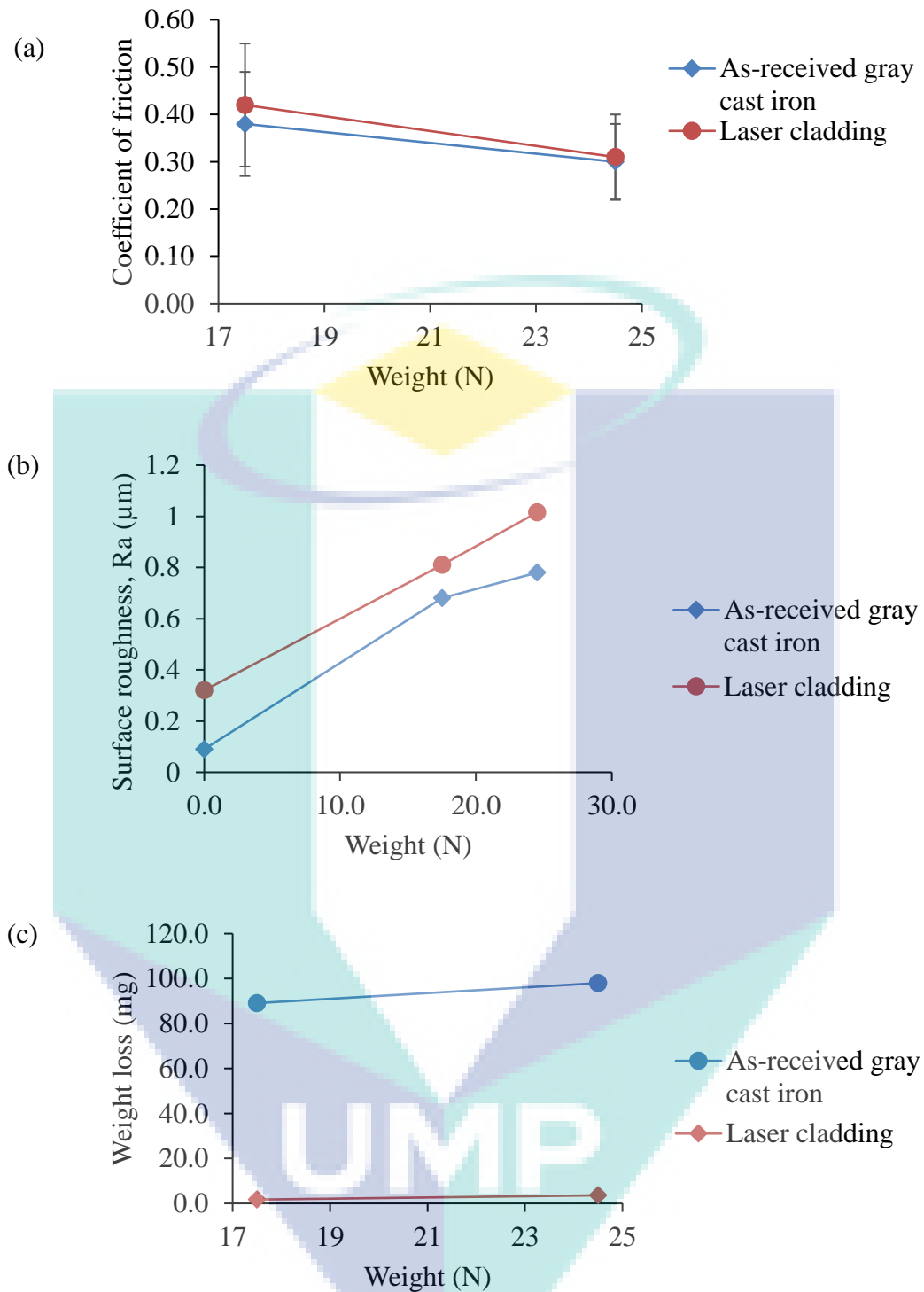


Figure 4.23 As-received grey cast iron and laser surface cladding layers result in (a) coefficient of friction (b) surface roughness and (c) weight loss.

This result is supported by the surface wear micrograph showing that the worn surface are relatively smooth with light scratches. Consistent with findings by Yan et al. (2010), that weight loss of cast iron can be significantly improved by introducing carbide on the surface by laser processing which have reduced up to 85 % compared to the

substrate (Yan *et al.*, 2010). As a result, formation of carbide phase made the surface hard to be plastically deformed or furrowed during the wear sliding process, which imparts excellent abrasive wear resistance to the laser surface cladding layers (Yan *et al.*, 2010). This result is also supported by previous authors that wear weight loss of the substrate was reduced after the laser surface modified (Sun *et al.*, 2011; Zhou *et al.*, 2014).

The wear mechanism was investigated via surface wear morphology on the as-received grey cast iron and laser cladding samples as shown in Figure 4.24. Micrograph from this figure can be compared with the hardness and XRD results which shows the carbide phase contribute to the high hardness on clad zone. The surface of as-received grey cast iron showed both ways of metallic wear formed which is by the material transfer phenomena and the adhesive wear features, for example tearing damage, which are created by the impact of extreme contact wear. These affect has cause some crack and furrows on the surface. In laser cladding samples, the worn surface are relatively smooth with light scratches with adhesive characteristics.

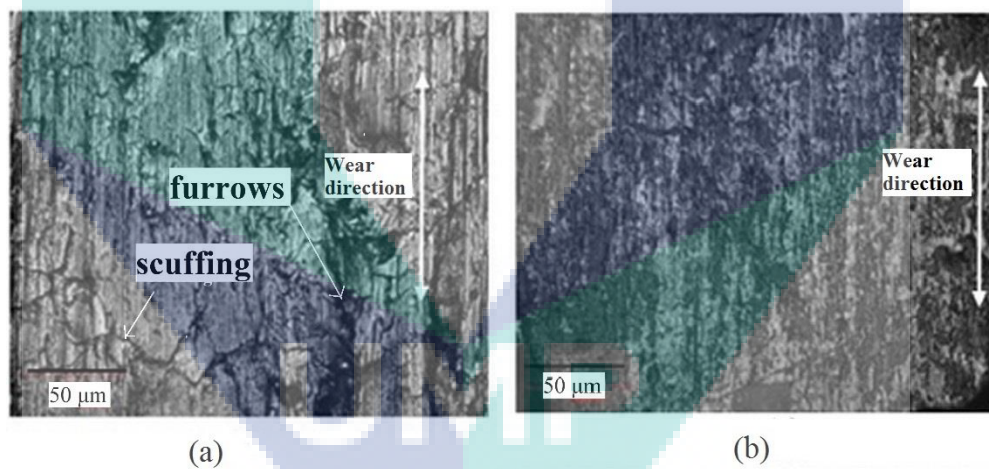


Figure 4.24 Micrograph of the worn surface after the wear sliding test at 17.5 N. (a) as-received grey cast iron and (b) Cr-Mo mixture clad zone.

The phenomena occurred in this study explained that localized heating on substrate surface caused high cooling rate, thus a fully dissolution of graphite occurred in the clad layer. Rapid solidification in laser surface cladding produced finer dendritic and particles which increased the hardness of the properties and directly reduced the weight loss. It is proven that, by increasing the peak power along with PRF 80 Hz in Cr-Mo

mixture will produced higher hardness of clad layer which can increase life of grey cast iron surface. This is due to the high energy from the laser beam has formed hard phase of carbide with small dendrite structure in grey cast iron surface.

As shown in Figure 4.25, the wear rate in as-received grey cast iron at load 17.5 N and 24.5 N is 2.05×10^{-6} mgmm⁻¹ and 1.86×10^{-6} mgmm⁻¹. In this study, the wear rate in laser clad sample at load 17.5 N and 24.5 N has reduced to 7.60×10^{-8} mgmm⁻¹ and 3.50×10^{-8} mgmm⁻¹ which is lower than as-received grey cast iron. The obvious different in wear rate is because of the different hardness in 70.2 % for grey cast iron and laser cladding samples.

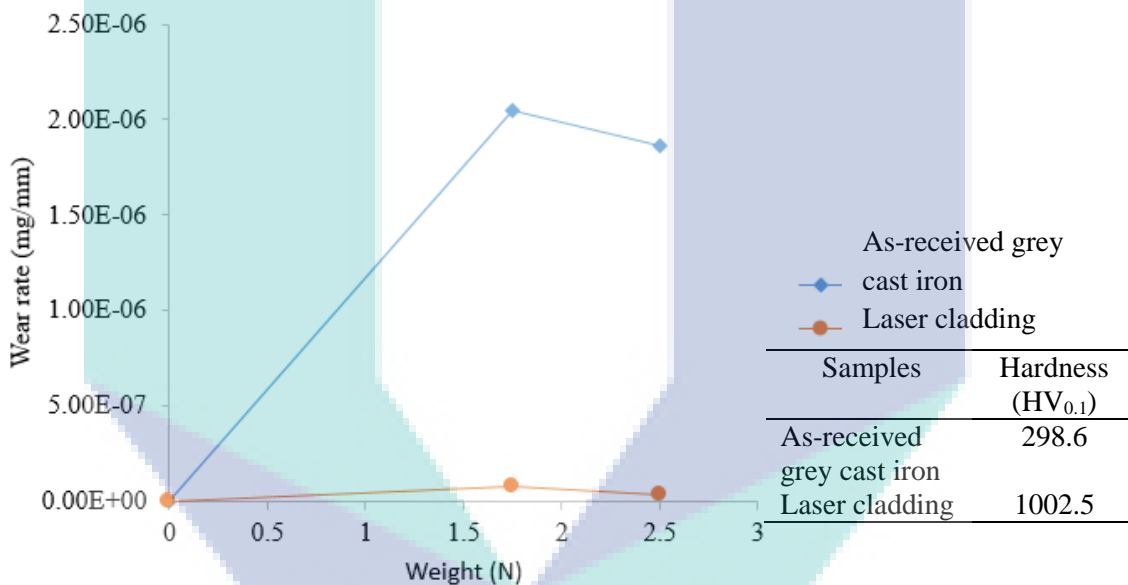


Figure 4.25 Wear rate at different load on as-received grey cast iron and laser clad sample.

According to Amirsadeghi and Sohi (2008), surface modification with chromium and molybdenum had reduced the wear rate of cast iron about 66% and 62% respectively (Amirsadeghi & Sohi, 2008). This study had revealed that Cr-Mo mixture added in surface modification had reduced the wear rate at 96.3 % and 98.1 % in load 17.5 N and 24.5 N respectively. The evidence from this study suggested that, wear rate on grey cast iron surface can be improved by mixing the Cr and Mo in proper composition compared to single elements. Mixture between Cr and Mo elements in grey cast iron promotes high hardness and introduce fine carbide and refinement microstructure. Besides that, these

elements can hinder graphite precipitation and increased the inclination to form carbide in grey cast iron (Atmadja *et al.*, 2013).

The finding provides evidence that the grey cast iron wear resistance was significantly improved by laser cladding with formation of new hard phase, which was mainly benefit from the high hardness and free-defect microstructure of the clad layers (Yan *et al.*, 2010). Strengthened by both of the alloying elements and the formation of small dendrite and bright particles, the hardness of the clad layer has increased significantly up to 998.3 HV_{0.1} compared to the substrate hardness of as-received grey cast iron at 278.5 HV_{0.1}.

4.6 Summary Result and Findings

The purpose of laser surface cladding on grey cast iron is to strengthen the surface properties by adding chromium and molybdenum powder on it. Laser processing parameter were used based on the findings in previous section. The results presented here may facilitate improvements in grey cast iron surface properties through the laser surface modification. There were two laser surface processing used in this study. Firstly is the laser surface melting for preliminary experiment at different laser spot size to optimize the laser parameter in order to minimize the surface roughness and maximize microhardness of melting zone. Secondly, the optimized parameters from this preliminary experiment will be used for laser cladding by adding Cr and Mo powder on the surface to enhance the surface properties.

In this study, each laser parameter at different spot size shows different surface morphology where the laser mark and surface roughness is higher at spot size 1.7 mm due to the high energy range of 0.56 to 3.33 J, residence time in range of 3.3 to 18 ms and irradiance from 15.28 to 3.89 W/mm². Laser mark and surface roughness of melting zone will increase according from small to bigger spot size when energy at laser beam and residence time are increased and irradiance is decreased. The findings from preliminary experiment suggest that laser spot size at 1.0 mm at range peak power of 800 to 1200 W, pulse repetition frequency in range of 80 to 90 Hz and pulse energy 0.56 to 0.63 J is the parameter used for laser cladding. The result also shows that the higher hardness melting zone were presented at laser spot size 1.0 mm which is high interaction time and high

cooling rate that contribute to the high hardness. It is proven based on the formation of martensite, cementite and retain austenite. Interestingly, the microhardness were improved more than three times than the substrate.

In laser cladding, microhardness in the clad zone is higher than in the substrate where small dendrite and particles structure and carbide phase observed here. Compared to the melting zone, clad zone shows slightly higher than melting zone. Clad with Cr-Mo mixture shows the highest hardness due to smaller dendrite and particles structure and high peak power laser setting. From cross-section micrograph, graphite flakes was eliminated and the equiaxed crystal grains were presented at the melting zone. Elimination of graphite flakes also found in clad zone in laser cladding with Cr and Mo powder. This finding highlights that the higher surface roughness is obtained in Mo powder and the lowest surface roughness is obtain in Cr-Mo mixture powder. The overall results from each DOE are presented in Table 4.15.

In sliding wear test shows the weight loss clad samples reduced more than 96 % compared to the as-received grey cast iron when tested using load 17.5 N and 24.5 N. Increasing the load from 17.5 N to 24.5 N resulted in decrement of coefficient of friction and the increment of the surface roughness and weight loss in clad samples. The formation of the carbide phase, small dendrite and particles structure in the clad zone attributed to the high hardness and reduced weight loss in sliding wear test. The result also show the wear rate have reduced from 2.05×10^{-6} mg/mm to 7.60×10^{-6} mg/mm at load 17.5 N and from 1.86×10^{-8} mg/mm to 3.50×10^{-8} mg/mm at load 24.5 N. The modified surface of grey cast iron shows that the surface is hard to be plastically deformed or furrowed during the wear sliding process, which imparts excellent abrasive wear resistance to the laser surface cladding layers.

In conclusion, it is proven that laser cladding on grey cast iron can increase the microhardness and wear resistance. This finding had shown that new formation of carbide phase, dendritic and particles structure had contribute for enhanced surface properties. Laser parameter at peak power 1200 W, pulse repetition frequency at 80 Hz and mixture Cr at 32.3 % and Mo at 67.7 % will produce higher desirability with high hardness of clad zone and minimum surface roughness.

Table 4.15 Summary of laser parameters setting ranges and characterization results for factorial model and mixture model.

DOE	Set parameters						Calculated				Result	
	Spot size (mm)	Pp (W)	PRF (Hz)	S (mms ⁻¹)	Cr (%)	Mo (%)	Ep (J)	TR (ms)	I (W/m ²)	CR×10 ⁵ (Ks ⁻¹)	Ra (µm)	HV _{0.1}
Factorial model	1.0	800-1200	80-90	19.2-21.6	-	-	0.56-0.63	1.9-3.3	15.28	1.43-1.80	3.0-3.9	936.6-990.0
	1.2	800-1200	40-50	13.6-17.0	-	-	1.00-1.25	2.9-5.5	12.53	0.70-0.95	4.1-6.0	706.8-900.2
	1.4	1500-1800	15-25	5.7-9.5	-	-	2.00- 3.33	4.1-8.2	8.82	0.25-0.42	4.8-6.8	719.2-948.3
	1.7	2000-2200	8-11	2.4-3.3	-	-	4.55-6.25	12.0-18.0	3.89	0.14-0.19	6.5-8.3	642.0-932.0
Mixture model	1.0	800-1200	80-90	19.2-21.6	100	0	0.56-0.63	1.9-3.3	15.28	2.1-2.6	10.0-13.1	460.3-566.0
					0	100				2.8-3.5	10.5-19.0	911.1-995.5
					50	50				2.8-3.5	7.7-10.0	875.1-998.3

UMP

CHAPTER 5

CONCLUSION

5.1 Introduction

This chapter concludes the results and discussion obtained from the experiments conducted in chapter 3. Future work on laser surface modification on grey cast iron to enhance surface properties is presented in the last section.

5.2 Conclusion

Based on the results of the experimental works conducted, the following conclusions are drawn.

In laser surface melting, a new metallurgical properties and phase has been developed at laser processing setting in high energy in range of 4.55 to 6.25 J, lower irradiance in 3.89 W/mm^2 and higher residence time in range of 13 to 18 ms. These parameters had distorted the surface morphology due to the low viscosity of molten metal at high surface temperature, whereas the highest microhardness on surface melting was obtained at smaller laser spot size. Elimination of graphite and formation of new metallurgical properties and phase of martensite, retained austenite and cementite had contributed to enhancing the surface hardness. Furthermore, low residence time in range of 1.9 to 3.3 ms and high irradiance in 15.28 Wmm^{-2} increased the hardness due to the higher cooling rate in range of 1.4×10^5 to $1.8 \times 10^5 \text{ Ks}^{-1}$.

In Laser cladding, it also have made a new metallurgical properties and phase on grey cast iron surface. At the end of the parameter and mixture components investigation, the result shown that Cr-Mo mixture added had produced the lowest surface roughness which is the combination of different size particles. The finding of this study suggest that, the lower surface roughness can be obtained by mixing small and big particle size. The evidence from this study suggests that the formation of carbide, dendritic, particles formation and elimination of graphite can enhance the hardness of grey cast iron surface. The most obvious finding from this study is the formation of grain particles structure which is not mentioned in other report.

To strengthen the surface properties of grey cast iron through laser cladding is by adding Cr and Mo powder. It has been known that Cr and Mo can withstand extreme temperature without significantly expanding or softening which makes it useful in application that involves intense heat. Furthermore, this mixture also had increased the microhardness compared to the single powder of Cr and Mo which has finer grain particles size. Laser cladding with Cr-Mo mixture had enhanced the microhardness up to 68.3 % compared to the substrate.

Sliding wear experiment was conducted at different load to investigate the coefficient of friction, weight loss and wear rate. Average coefficient of friction in as-received grey cast iron is slightly lower than laser cladding in 9.5 % and 3.2 % at load 17.5 N and 24.5 N. This is due to the embedded graphite in grey cast iron moved out during friction and act as solid lubricant. However, the increment of load decreased the coefficient of friction in both materials because of the pressure during sliding. This increased the frictional heat which decreased the strength of material surface. The surface roughness for both material increased when the load increases. Besides that, increasing the load increased the weight loss for both material. Amazingly, the weight loss of laser clad had decreased more than 96 % with light scratches compared to the as-received grey cast iron which has some crack, scuffing and furrows on the surfaces. The study also indicates that the strengthen surface of grey cast iron by laser clad with Cr-Mo mixture added had achieved as the result shown that the wear rate had reduced to 96.3 % and 98.1 % in load 17.5 N and 24.5 N respectively. This is due to the formation of new hard phase and structure in clad layers. Many researches had argued that grey cast iron with high

hardness can increase wear resistance properties which is suitable to use for engine's components.

The statistical analysis in design of experiments has been used to analyze relationship between laser parameter and mixture elements of Cr and Mo. The results from this study suggests that, laser processing with Cr and Mo addition at spot size 1.0 mm, peak power in range of 800 to 1200 W, pulse repetition frequency in range of 80 to 90 Hz and traverse speed in range of 19.2 to 21.6 mm s^{-1} produced the high hardness and the lowest surface roughness. A set of optimized processing parameters and percent mixture of Cr-Mo added were found at 1200 W peak power, 80 Hz pulse repetition frequency and percent of Cr and Mo in 32.3 % and 67.7 % respectively which produced a hardened surface of 1039.7 $\text{HV}_{0.1}$ with surface roughness of 8.88 μm . Laser cladding with Cr-Mo mixture added had improved the hardness to 56.7 % compared to the required specification of cylinder liner and piston ring in engine diesel. High hardness on the surface can prolong cylinder liner and piston ring life. In addition, minimum surface roughness can be achieved by increasing the traverse speed. Nevertheless, the surface roughness requires grinding finishing and polishing at high precision within depth range referring to the required specification. The current finding provides thorough understanding about the relationship between the laser parameter and added elements of Cr and Mo in laser cladding. Finally, the laser cladding of Cr-Mo mixture powders on grey cast iron substrate represent a promising way for a substantial improvement of local wear, thermal fatigue and corrosion resistance of industrial parts traditionally made from grey cast iron.

5.3 Future Work

More work considerably need to be done to determine the mechanical surface properties of grey cast iron. Laser cladding with Cr-Mo mixture are predicted to increase corrosion resistance, thermal fatigue and changes from brittle to ductile properties. Because of that, more experiment on evaluating the mechanical properties such as tensile test, thermal fatigue test and corrosion test need to be done.

The formation of new hard phase and new metallographic are related to heating rate and cooling rate. Further analysis such as thermal analysis using high magnification and thermal camera can be used for detail explanation. The advantages of combination between scanning electron microscopy (SEM) observation with the information about crystal or grain orientation typical for transmission electron microscopy (TEM) observation may be the most efficient method to study complicated microstructure that formed during the laser cladding and fast solidification associated to it.

Focusing in laser parameter setting in laser cladding processes, different process parameter including duty cycles, overlapped percentage (η) and pulse width or pulse duration (τ) need further discussion in order to control the dimension, mechanical properties and final deformation.



UMP

REFERENCES

- Abbas, A. A. (2014). *Optimization of parameters of laser non-linear inclined cutting on stainless steel metal*. (Master Engineering), Universiti Tun Hussein Onn Malaysia.
- Abbouda, J. H., Benyounisb, K. Y., Olabic, A. G., & Hashmic, M. S. J. (2007). Laser surface treatments of iron-based substrates for automotive application. *Journal of Materials Processing Technology*, 182(427–431). doi:doi:10.1016/j.jmatprotec.2006.08.026
- Adel, k. M., Dhia, A. S., & Ghazali, M. J. (2008). The Effect Of Laser Surface Hardening On The Wear And Friction Characteristics Of Acicular Bainitic Ductile Iron. *Diyala Journal of Engineering Sciences*, 1(1), 110-121.
- Agunsoye, J. O., Bello, S. A., Talabi, S. I., Hassan, S. B., & Moumoh, K. I. (2014). The Effect of Molybdenum on the Tribological Behavior of Nfgrey (8) Cast Iron. *Journal of Metallurgical Engineering*, 3(3). doi:10.14355/me.2014.0303.05
- Al-Samarai, A. R., Haftirman, Ahmad, K. R., & Al-Douri, Y. (2012). Evaluate the Effects of Various Surface Roughness on the Tribological Characteristics under Dry and Lubricated Conditions for Al-Si Alloy. *Journal of Surface Engineered Materials and Advanced Technology*, 2(167-173). doi:http://dx.doi.org/10.4236/jseamat.2012.23027
- Alabeedi, K. F., Abboud, J. H., & Benyounis, K. Y. (2009). Microstructure and erosion resistance enhancement of nodular cast iron by laser melting. *Wear*, 266, 925-933.
- Allemann, I. B., & Kaufman, J. (2011). Laser Principles. *Basics in Dermatological laser Applications*, 42, 7-23.
- Alp, T., Wazzan, A. A., & Yilmaz, F. (2005). Microstructure property relationships in cast irons. *The Arabian Journal for Science and Engineering*, 30(28).
- Amirsadeghi, A., & Sohi, M. H. (2008). Comparison of the influence of molybdenum and chromium TIG surface alloying on the microstructure, hardness and wear resistance of ADI. *Journal of Materials Processing Technology*, 201, 673-677. doi:10.1016/j.jmatprotec.2007.11.157

- Amirsadeghi, A., Sohi, M. H., & Bozorg, S. F. K. (2008). Effects Of Tig Surface Melting And Chromium Surface Alloying On Microstructure Hardness And Wear Resistance Of ADI. *Journal of Iron and Steel Research International*, 15(4), 85-94.
- Aqida, S. N. (2011). *Laser surface modification of steel*. Dublin City University.
- Aqida, S. N., Naher, S., & Brabazon, D. (2011). *Laser Surface Modification of H13 Die Steel using Different Laser Spot Sizes*. Paper presented at the 14th International ESAFORM Conference on Material Forming, Queen's University Belfast, Northern Ireland, United Kingdom.
- Aqida, S. N., Naher, S., Maurel, M., & Brabazon, D. (2008). *An Overview of Laser Surface Modification of Die Steels*. Paper presented at the International Manufacturing Conference Proceedings, Dublin.
- Atmadja, S. T., Sulardjaka, Nugroho, S., Adnan, F., & Cahyono, A. D. (2013). The Effect Of Alloy Elements On Fatigue Strength Of Gray Cast Iron At Room And High Temperature. *Jurnal Teknik Mesin*, 15(1), 23-28.
- Balachandran, G., Vadiraj, A., Kamaraj, M., & Kazuya, E. (2011). Mechanical and wear behavior of alloyed gray cast iron in the quenched and tempered and austempered conditions. *Materials & Design*, 32(7), 4042-4049. doi:10.1016/j.matdes.2011.03.054
- Benyounis, K. Y., Fakron, O. M. A., Abboud, J. H., Olabi, A. G., & Hashmi, M. J. S. (2005). Surface melting of nodular cast iron by Nd-YAG laser and TIG. *Journal of Materials Processing Technology*, 170(1-2), 127-132. doi:10.1016/j.jmatprotec.2005.04.108
- Blarasin, A., Corcoruto, S., Belmonto, A., & Bacci, D. (1983). Development of a laser surface melting for improvement of the wear resistance of gray cast iron. *Wear*, 86, 315-325.
- Branco, C. M., Infante, V., Sousa e Brito, A., & Martins, R. F. (2002). A failure analysis study of wet liners in maritime diesel engines. *Engineering Failure Analysis*, 9(4), 403-421. doi:http://dx.doi.org/10.1016/S1350-6307(01)00027-9
- Brytan, Z., Bonek, M., & Dobrzański, L. A. (2010). Microstructure and properties of laser surface alloyed PM austenitic stainless steel. *Journal of Achievement in Materials and Manufacturing Engineering*, 40(1).

- Chen, Z.-k., Meng, C., Dong, J.-x., Zhou, T., Tong, X., & Zhou, H. (2016). The comparative study of W/Cr addition in Fe-base by laser surface alloying on fatigue wear resistance of GCI. *Surface and Coating Technology*, 286(25-35).
- Chen, Z.-K., Zhou, T., Zhang, H.-f., Yang, W.-s., & Zhou, H. (2015a). Influence of Orientations of Bionic Unit Fabricated by Laser Remelting on Fatigue Wear Resistance of Gray Cast Iron. *Journal of Materials Engineering and Performance*, 24(6), 2511-2520. doi:10.1007/s11665-015-1499-9
- Chen, Z.-k., Zhou, T., Zhao, R.-y., Zhang, H.-f., Lu, S.-c., Yang, W.-s., & Zhou, H. (2015b). Improved fatigue wear resistance of gray cast iron by localized laser carburizing. *Materials Science and Engineering A*, 644, 1-9. doi:http://dx.doi.org/10.1016/j.msea.2015.07.046
- Cheng, X., Hu, S., Song, W., & Xiong, X. (2014). A comparative study on gray and nodular cast irons surface melted by plasma beam. *Vacuum*, 101, 177-183. doi:10.1016/j.vacuum.2013.08.012
- Chivavibul, P., Watanabe, M., Kuroda, S., Kawakita, J., Komatsu, M., Sato, K., & Kitamura, J. (2010). *Effect of Powder Characteristics on Properties of Warm-Sprayed WC-Co Coatings*. Paper presented at the International Thermal Spray Conference, Las Vegas.
- Chowdhury, M. A., Khalil, M. K., Nuruzzaman, D. M., & Rahaman, M. L. (2011). The effect of sliding speed and normal load on friction and wear property of aluminum. *International Journal of Mechanical & Mechatronics Engineering*, 11(1).
- Chung, R. J., Tang, X., Li, D. Y., Hinckley, B., & Dolman, K. (2013). Microstructure refinement of hypereutectic high Cr cast irons using hard carbide-forming elements for improved wear resistance. *Wear*, 301(1-2), 695-706. doi:10.1016/j.wear.2013.01.079
- Collini, L., Nicoletto, G., & Konečná, R. (2008). Microstructure and mechanical properties of pearlitic gray cast iron. *Materials Science and Engineering: A*, 488(1-2), 529-539. doi:10.1016/j.msea.2007.11.070
- Eriksson, I. (2005). *The monitoring of a laser beam*. Retrieved from Department of Information Technology and Media (ITM):
- Eroglu, M., & zdemir, N. O. (2002). Tungsten-inert gas surface alloying of a low carbon steel. *Surface and Coating Technology*, 154, 209-217.

- Espadafor, F. J., Villanueva, J. B., García, M. T., & Trujillo, E. C. (2010). Analysis of a diesel generator cylinder failure. *Engineering Failure Analysis, 17*(4), 913-925. doi:<http://dx.doi.org/10.1016/j.engfailanal.2009.11.003>
- Fan, K. L., He, G. Q., She, M., Liu, X. S., Lu, Q., Yang, Y., . . . Shen, Y. (2014). High-temperature low cycle fatigue behavior of a gray cast iron. *Materials Characterization, 98*, 37-46. doi:[10.1016/j.matchar.2014.10.005](http://dx.doi.org/10.1016/j.matchar.2014.10.005)
- Farnia, A., Ghaini, F. M., & Sabbaghzadeh, J. (2013). Effects of pulse duration and overlapping factor on melting ratio in replaced pulsed Nd:YAG laser cladding. *Optics and Laser in engineering, 51*, 69-76.
- Fazliana, F., Aqida, S. N., & Saidin, M. (2013). Laser Surface Modification of AISI 1025 Low Carbon Steel using Pulsed Nd:YAG Laser for Enhanced Surface Properties. *Material science and engineering, 554-557*, 596-602. doi:[10.4028/www.scientific.net/KEM.554-557.596](http://dx.doi.org/10.4028/www.scientific.net/KEM.554-557.596)
- Fazliana, F., Aqida, S. N., & Saidin, M. (2014). Optimisation of Pulsed Nd: YAG Laser Processing of Gray Cast Iron for Enhanced Surface Properties. *Advanced Materials Research, 1024*, 215-218. doi:[10.4028/www.scientific.net/AMR.1024.215](http://dx.doi.org/10.4028/www.scientific.net/AMR.1024.215)
- Fouquet, F., & Szmatala, E. (1998). *Laser Surface Melting of a Pearlitic Grey Cast Iron*. Paper presented at the 6th International Conference on Rapidly Quenched Metals, Montreal.
- Gadag, S. P., Srinivasan, M. N., & Mordike, B. L. (1995). Effect of laser processing parameters on the structure of ductile iron. *Materials Science and Engineering: A, 196*(1-2), 145-154. doi:[http://dx.doi.org/10.1016/0921-5093\(94\)09719-4](http://dx.doi.org/10.1016/0921-5093(94)09719-4)
- Ghasemi, R., & Elmquist, L. (2014). The relationship between flake graphite orientation, smearing effect, and closing tendency under abrasive wear conditions. *Wear, 317*(1-2), 153-162. doi:<http://dx.doi.org/10.1016/j.wear.2014.05.015>
- Henry, S. (1958). Experiments with Mixture. *J. R. Statist Soc., 20*, 344-360.
- Hirota, K., Mitani, K., Yoshinaka, M., & Yamaguchi, O. (2005). Simultaneous synthesis and consolidation of chromium carbides (Cr₃C₂, Cr₇C₃ and Cr₂₃C₆) by pulsed electric-current pressure sintering. *Material science and engineering A, 399*(154-160). doi:[doi:10.1016/j.msea.2005.02.062](http://dx.doi.org/10.1016/j.msea.2005.02.062)

- Hussein, N. I. S., Asri, N. F., & Shamsuri, S. R. (2014). The Effect of Cladding Parameters on Microstructure and Microhardness of 308L Stainless Steel Single Bead Clad Deposited on Cast Iron Using Gas Metal Arc Heat Source. *International Journal of The Institute of Materials Malaysia*, 1(2).
- Hussein, N. I. S., Kamarul, S. R., & Ayof, M. N. (2013). Preliminary Study Of On Cladding Process On Gray Cast Iron Substrate. *International Journal of Research in Engineering Technology*, 2(11).
- Hwang, J.-H., Lee, Y.-S., Kim, D.-Y., & Youn, J.-G. (2002). Laser Surface Hardening of Gray Cast Iron Used for Piston Ring. *Journal of Materials Engineering and Performance*, 11(3), 294-300.
- Imurai, S., Thanachayanont, C., Pearce, J. T. H., Tsuda, K., & Chairuangstri, T. (2015). Effects of W on microstructure of as-cast 28wt.%Cr-2.6wt.%C-(0-10)wt.%W irons. *Materials Characterization*, 99, 52-60.
doi:10.1016/j.matchar.2014.11.012
- Jacobs, G. (2006). Understanding spot size for laser scanning. *Professional Surveyor Magazine*.
- Jensen, M. F., Bøttiger, J., Reitz, H. H., & Benzon, M. E. (2002). Simulation of wear characteristics of engine cylinders. *Wear*, 253(9-10), 1044-1056.
doi:http://dx.doi.org/10.1016/S0043-1648(02)00251-X
- Jeong, B.-Y., & Kim, M.-H. (2001). Corrosion characteristics of duplex surface-treated spheroidal graphite cast iron. *Surface and Coatings Technology*, 141(2-3), 262-268. doi:http://dx.doi.org/10.1016/S0257-8972(01)01230-0
- Jhavar, S., Paul, C. P., & Jain, N. K. (2013). Causes of failure and repairing options for dies and molds: A review. *Engineering Failure Analysis*, 34, 519-535.
doi:http://dx.doi.org/10.1016/j.engfailanal.2013.09.006
- Kagawa, A., & Ohta, Y. (1998). Utilization Of Cast Iron Scraps As A Raw Material For Laser Clad Chromium Carbide Hardfacing. *Journal of Materials Science Letters*, 17, 99-101.
- Karamış, M. B., & Yıldızlı, K. (2010). Surface modification of nodular cast iron: A comparative study on graphite elimination. *Materials Science and Engineering: A*, 527(20), 5225-5229. doi:10.1016/j.msea.2010.04.067

- Keller, J., Fridrici, V., Kapsa, P., Vidaller, S., & Huard, J. F. (2007). Influence of chemical composition and microstructure of gray cast iron on wear of heavy duty diesel engines cylinder liners. *Wear*, 263(7-12), 1158-1164. doi:10.1016/j.wear.2007.01.091
- Kong, C. Y., Carroll, P. A., Brown, P., & Scudamore, R. J. (2007). *The effect of average powder particle size on deposition efficiency, deposit height and surface roughness in the direct metal laser deposition process*. Paper presented at the 14th International Conference on Joining of Materials, Helsingor Denmark.
- Krauss, G. (2005). *Steels: Processing, structure and performance*: ASM International.
- Kusinski, J., Kac, S., Kopia, A., Radziszewska, A., Rozmus-Górnikowska, M., Major, B., . . . Lisiecki, A. (2012). Laser modification of the materials surface layer – a review paper. *Bulletin of the Polish Academy of Sciences: Technical Sciences*, 60(4). doi:10.2478/v10175-012-0083-9
- Liu, F., & Zhou, K.-C. (2012). Effect of Molybdenum-Rich Carbides on Wear Behavior of Powder Metallurgy Steel. *Materials Transactions*, 53(6), 1203 - 1205.
- Maluf, O., Angeloni, M., Castro, D. B. V., Filho, W. W. B., Spinelli, D., & Ruckert, C. O. F. T. (2009). Effect of Alloying Elements on Thermal Diffusivity of Gray Cast Iron Used in Automotive Brake Disks. *ASM International*, 18, 980-984. doi:10.1007/s11665-008-9326-1
- Man, H. C., Leong, K. H., & Ho, K. L. (2008). Process monitoring of powder pre-paste laser surface alloying. *Optics and Lasers in Engineering*, 46(10), 739-745. doi:10.1016/j.optlaseng.2008.05.006
- Mezghania, S., Perrin, E., Vrabie, V., Bodnar, J. L., Marthec, J., & Cauwec, B. (2016). Evaluation of paint coating thickness variations based on pulsed Infrared thermography laser technique. *Infrared Physics & Technology*, 76, 393-401.
- Montealegre, M. A., Castro, G., Rey, P., Arias, J. L., Vazquez, P., & Gonzalez, M. (2010). Surface Treatments By Laser Technology. *Contemporary Materials*, 1(1), 19-30. doi:DOI: 10.5767/anurs.cmat.100101.en.019M
- Monteiro, W. A., Silva, E. M. R., & Rossi, W. d. (2009). *Evaluation Of The Laser Superficial Hardening (Lsh) In Gray Cast Iron Used In Automobile Industry*. Paper presented at the 3rd International Conference on Integrity, Reliability and Failure., Porto Portugal.

- Moonesan, M., raouf, A. H., Madah, F., & zadeh, A. H. (2012). Effect of alloying elements on thermal shock resistance of gray cast iron. *Journal of alloy and compounds*, 520(226-231). doi:10.1016/j.jallcom.2012.01.027
- Nadel, J., & Eyre, T. S. (1978). Cylinder liner wear in low speed diesel engines. *Tribology International*, 267-271.
- Nagai, T., Inoue, T., & Utsunomiya, T. (2002). Surface Modification of Cast Iron by Pulsed Laser Deposition. *Bulg. Journal Physic*, 29, 128-141.
- Norhafzan, B., Aqida, S. N., Chikarakara, E., & Brabazon, D. (2016). Surface modification of AISI H13 tool steel by laser cladding with NiTi powder. *Applied physics A*(122:384). doi:10.1007/s00339-016-9937-6
- Ocelik, V., Oliveira, U. d., Boer, M. d., & Hosson, J. T. M. d. (2007). Thick Co-based coating on cast iron by side laser cladding: Analysis of processing conditions and coating properties. *Surface and Coating Technology*, 201, 5875-5883. doi:10.1016/j.surfcoat.2006.10.044
- Ocelík, V., Oliveira, U. d., & Hosson, J. T. M. D. (2009). *Surface effects and contact mechanics*. Paper presented at the 9th International Conference On Surface Effects and Contact Mechanics: Computational Methods and Experiments, Algarve Portugal.
- Oloyede, O., Cochrane, R. F., & Mullis, A. M. (2016). Effect of rapid solidification on the microstructure and microhardness of BS1452 grade 250 hypoeutectic grey cast iron. *Journal of Alloys and Compounds*(1-4).
- Paczkowska, M. (2016). The evaluation of the influence of laser treatment parameters on the type of thermal effects in the surface layer microstructure of gray irons. *Optics & Laser Technology*, 76(143-148).
- Pang, Z., Zhou, H., Chang, F., Zhang, P., Cong, D., & Meng, C. (2015a). Effect of the microhardness difference between base metal and bionic coupling unit on wear resistance of gray cast iron. *Optics & Laser Technology*, 75, 151-156.
- Pevec, M., Oder, G., Potrč, I., & Šraml, M. (2014). Elevated temperature low cycle fatigue of grey cast iron used for automotive brake discs. *Engineering Failure Analysis*, 42, 221-230. doi:http://dx.doi.org/10.1016/j.engfailanal.2014.03.021

- Qu, C. C., Li, J., Bai, L. L., Shao, J. Z., Song, R., & Chen, J. L. (2015). Effects of the thickness of the pre-placed layer on microstructural evolution and mechanical properties of the laser-clad coatings. *Journal of Alloys and Compounds*, 644, 450-463.
- Rao, P. R. (2013). Recent Progress in The Development of Materials. *Material Engineering*(3), 13-17.
- Sands, D. (2011). Pulsed laser heating and melting *Heat transfer-engineering application*. United Kingdom: University of Hull.
- Schneider, M. F. (1998). *Laser cladding with powder*. (Ph.D), University of Twente, University of twente Enshede.
- Seidu, S. O. (2014). Effect of Compositional Changes on the Mechanical Behaviour of Grey Cast Iron. *Journal of Metallurgical Engineering*, 3(2), 92. doi:10.14355/me.2014.0302.05
- Shang-ping, L., He-Li, L., Di, F., Xu, C., & Xi-e, Z. (2009). Abrasive Performance of Chromium Carbide Reinforced Ni₃Al Matrix Composite Cladding. *Journal of Iron and Steel Research International*, 16(5), 87-91.
- Sohi, M. H., Ebrahimi, M., Ghasemi, H. M., & Shahripour, A. (2012). Microstructural study of surface melted and chromium surface alloyed ductile iron. *Applied Surface Science*, 258(19), 7348-7353. doi:10.1016/j.apsusc.2012.04.014
- Sugishita, J., & Fujiyoshi, S. (1982). The effect of cast iron graphite on friction and wear performance III: The lubricating effect of graphite under rolling-sliding contacts. *Wear*, 77(181-193).
- Sun, G., Zhou, R., Li, P., Feng, A., & Zhang, Y. (2011). Laser surface alloying of C-B-W-Cr powders on nodular cast iron rolls. *Surface and Coatings Technology*, 205(8-9), 2747-2754. doi:10.1016/j.surfcoat.2010.10.032
- Tong, X., Zhou, H., Ren, L.-q., Zhang, Z.-h., Cui, R.-d., & Zhang, W. (2008). Thermal fatigue characteristics of gray cast iron with non-smooth surface treated by laser alloying of Cr powder. *Surface and Coatings Technology*, 202(12), 2527-2534. doi:10.1016/j.surfcoat.2007.09.014
- Triefenbach, F. (2008). *Design of Experiments: The D-Optimal Approach and Its Implementation As a Computer Algorithm*. (Degree in Information And Communication Technology), Umea University, Sweden.

- Vadiraj, A., Balachandran, G., Kamaraj, M., & Kazuya, E. (2011). Mechanical and wear behavior of quenched and tempered alloyed hypereutectic gray cast iron. *Materials & Design*, 32(4), 2438-2443. doi:<http://dx.doi.org/10.1016/j.matdes.2010.11.052>
- Wandera, C. (2010). *Performance of High Power Fibre Laser Cutting Of Thick-Section Steel and Medium-Section Aluminium*. (Degree of Doctor of Science), Lappeenranta University of Technology, Acta Universitatis Lappeenrantaensis.
- Wang, P. S., & Fang, J. J. (2010). *The Optimization of Medicine Formulation Using Mixture Experiments*. Paper presented at the Proceedings of the International MultiConference of Engineers and Computer Scientists, IMECS 2010, Hong Kong.
- Wieczerek, K., Bala, P., Stepień, M., Cios, G., & Koziel, T. (2016). Formation of eutectic carbides in Fe–Cr–Mo–C alloy during non-equilibrium crystallization. *Material and Design*, 94(61-68).
- Wiengmoon, A. (2011). Carbides in High Chromium Cast Irons. *Naresuan University Engineering Journal*, 6(1), 64.
- William, H. D., & Leonid, V. Z. (2007). Computational study of cooling rates and recrystallization kinetics in short pulse laser quenching of metal targets. *Journal of Physics: Conference Series*, 59, 413-417. doi:10.1088/1742-6596/59/1/088
- Xu, X., & Yu, Z. (2006). Failure analysis of a diesel engine cylinder head. *Engineering Failure Analysis*, 13(7), 1101-1107. doi:10.1016/j.engfailanal.2005.07.016
- Yan, H., Wang, A., Xiong, Z., Xu, K., & Huang, Z. (2010). Microstructure and wear resistance of composite layers on a ductile iron with multcarbide by laser surface alloying. *Applied Surface Science*, 256(23), 7001-7009. doi:10.1016/j.apsusc.2010.05.015
- Yang, X., Zhang, Z., Wang, J., & Ren, L. (2015). Investigation of nanomechanical properties and thermal fatigue resistance of gray cast iron processed by laser alloying. *Journal of Alloys and Compounds*, 626, 260-263. doi:<http://dx.doi.org/10.1016/j.jallcom.2014.11.169>
- Yao, J., Zhanga, J., Wua, G., Wang, L., Zhang, Q., & Liu, R. (2017). Microstructure and wear resistance of laser clad composite coatings prepared from pre-alloyed WC-NiCrMo powder with different laser spots. *Optics and Laser Technology*. doi:<https://doi.org/10.1016/j.optlastec.2017.12.007>

- Yi, P., Xu, P., Fan, C., Li, C., & Shi, Y. (2015). The Effect of Dynamic Local Self-Preheating in Laser Cladding on Grey Cast Iron. *Journal of Mechanical Engineering*, 61(1), 43-52.
- Yi, P., Xu, P., Fan, C., Yang, G., Liu, D., & Shi, Y. (2014). Microstructure Formation and Fracturing Characteristics of Grey Cast Iron Repaired Using Laser. *The Scientific World Journal*, 2014, 1-10. doi:10.1155/2014/541569
- Yilbas, B. S., Akhtar, S. S., Karatas, C., & Boran, K. (2016). Laser treatment of dual matrix cast iron with presence of WC particles at the surface: Influence of self-annealing on stress fields. *Optics & Laser Technology*, 76, 6-18. doi:http://dx.doi.org/10.1016/j.optlastec.2015.07.003
- Zhong, M., Liu, W., & Zhang, H. (2006). Corrosion and wear resistance characteristics of NiCr coating by laser alloying with powder feeding on grey iron liner. *Wear*, 260(11-12), 1349-1355. doi:10.1016/j.wear.2005.09.033
- Zhou, H., Zhang, P., Zhang, Z., Qiu, W., Liu, Y., & Ren, L. (2014). Thermal Cycling Effect on the Wear Resistance of Bionic Laser Processed Gray Iron. *Journal of Bionic Engineering*, 11(2), 288-295. doi:http://dx.doi.org/10.1016/S1672-6529(14)60031-7

APPENDIX A

LASER SURFACE MELTING PARAMETER AT SPOT SIZE 1.0 MM AND 1.2 MM

Num.	Setting parameter							Calculated parameter								Responded	
	Pp	PRF	Pave	V	η	d	DC	Ep	T _R	F	I	τ	t _{cooling}	C _R	H _R	Ra(μ m)	Average HV _{0.1}
	W	Hz	W	mms ⁻¹	%	mm	%	J	ms	Jmm ⁻²	Wmm ⁻²	ms	ms	$\times 10^5$ Ks ⁻¹	$\times 10^5$ Ks ⁻¹		
1	800	80	50	19.2	70	1	6.25	0.63	3.3	0.80	15.28	0.78	9.2	1.59	4.53	3.00	920.1
2	800	90	50	21.6	70	1	6.25	0.56	2.9	0.71	15.28	0.69	8.2	1.79	5.10	3.90	960.3
3	1200	80	50	19.2	70	1	4.17	0.63	2.2	0.80	15.28	0.52	10.3	1.42	6.80	3.76	930.2
4	1200	90	50	21.6	70	1	4.17	0.56	1.9	0.71	15.28	0.46	9.2	1.60	7.65	3.77	950.5
5	800	90	50	21.6	70	1	6.25	0.56	2.9	0.71	15.28	0.70	8.2	1.79	5.10	3.11	990.0
6	1200	90	50	21.6	70	1	4.17	0.56	1.9	0.71	15.28	0.50	9.2	1.60	7.65	3.40	953.1
7	800	80	50	19.2	70	1	6.25	0.63	3.3	0.80	15.28	0.80	9.2	1.59	4.53	3.60	989.2
8	1200	80	50	19.2	70	1	4.17	0.63	2.2	0.80	15.28	0.50	10.3	1.42	6.80	3.92	936.6
9	800	40	50	13.6	70	1.2	6.25	1.25	5.5	1.11	12.53	1.56	19.5	0.75	2.67	4.61	900.2
10	800	50	50	17.0	70	1.2	6.25	1.00	4.4	0.88	12.53	1.25	15.6	0.94	3.34	4.83	729.8
11	1200	40	50	13.6	70	1.2	4.17	1.25	3.7	1.11	12.53	1.04	21.3	0.69	4.01	6.04	840.1
12	1200	50	50	17.0	70	1.2	4.17	1.00	2.9	0.88	12.53	0.83	17.1	0.86	5.02	5.67	706.8
13	1200	40	50	13.6	70	1.2	4.17	1.25	3.7	1.11	12.53	1.00	21.3	0.69	4.01	7.10	780.0
14	1200	50	50	17.0	70	1.2	4.17	1.00	2.9	0.88	12.53	0.80	17.1	0.86	5.02	4.50	800.1
15	800	40	50	13.6	70	1.2	6.25	1.25	5.5	1.11	12.53	1.60	19.5	0.75	2.67	5.30	800.3
16	800	50	50	17.0	70	1.2	6.25	1.00	4.4	0.88	12.53	1.30	15.6	0.94	3.34	4.10	830.0

APPENDIX B

LASER SURFACE MELTING PARAMETER AT SPOT SIZE 1.4 MM AND 1.7 MM

Num	Setting parameter							Calculated parameter								Responded	
	Pp W	PRF Hz	Pave W	V mms ⁻¹	η %	d m	DC %	Ep J	T _R ms	F Jmm ⁻²	I Wmm ⁻²	τ ms	t _{cooling} ms	C _R ×10 ⁵ Ks ⁻¹	H _R ×10 ⁵ Ks ⁻¹	Ra (μm)	Average HV _{0.1}
17	1500	15	50	5.70	70	1.4	3.33	3.33	8.2	2.17	8.82	2.22	58.5	0.25	1.80	5.59	911.7
18	1500	25	50	9.50	70	1.4	3.33	2.00	4.9	1.30	8.82	1.33	35.1	0.42	3.00	5.67	799.0
19	1800	15	50	5.70	70	1.4	2.78	3.33	6.8	2.17	8.82	1.85	59.8	0.24	2.16	5.46	938.4
20	1800	25	50	9.50	70	1.4	2.78	2.00	4.1	1.30	8.82	1.11	35.9	0.41	3.60	6.83	782.4
21	1500	25	50	9.50	70	1.4	3.40	2.04	4.9	1.33	8.82	1.40	35.1	0.42	3.00	6.80	780.0
22	1800	25	50	9.50	70	1.4	2.90	2.08	4.1	1.35	8.82	1.20	35.9	0.41	3.60	7.83	719.2
23	1800	15	50	5.70	70	1.4	2.90	3.53	6.8	2.30	8.82	2.00	59.8	0.24	2.16	4.83	948.3
24	1500	15	50	5.70	70	1.4	3.60	3.60	8.2	2.34	8.82	2.40	58.5	0.25	1.80	4.92	926.8
25	2000	11	50	3.30	80	1.7	2.50	4.55	13.0	2.00	3.89	2.27	78.0	0.18	1.14	7.41	743.0
26	2000	8	50	2.40	80	1.7	2.50	6.25	18.0	2.75	3.89	3.13	107.3	0.13	0.83	8.25	917.7
27	2200	11	50	3.30	80	1.7	2.27	4.55	12.0	2.00	3.89	2.07	79.2	0.18	1.26	6.73	854.0
28	2200	8	50	2.40	80	1.7	2.27	6.25	16.0	2.75	3.89	2.84	108.9	0.13	0.91	7.11	915.6
29	2200	8	50	2.40	80	1.7	2.30	6.38	16.0	2.81	3.89	2.90	108.9	0.13	0.91	6.52	932.0
30	2000	8	50	2.40	80	1.7	2.60	6.50	18.0	2.86	3.89	3.30	107.3	0.13	0.83	7.32	920.0
31	2000	11	50	3.30	80	1.7	2.70	4.82	13.0	2.12	3.89	2.40	78.0	0.18	1.14	8.32	642.0
32	2200	11	50	3.30	80	1.7	2.50	4.91	12.0	2.16	3.89	2.20	79.2	0.18	1.26	7.43	732.0

APPENDIX C ARDUINO PROGRAMME

```
/*
THIS PROGRAM WORKS WITH PulseSensorAmped_Arduino-xx ARDUINO CODE
THE PULSE DATA WINDOW IS SCALEABLE WITH SCROLLBAR AT BOTTOM
OF SCREEN
PRESS 'S' OR 's' KEY TO SAVE A PICTURE OF THE SCREEN IN SKETCH
FOLDER (.jpg)
*/
import processing.serial.*;
PFont font;
Scrollbar scaleBar;
PrintWriter output;
Serial port;

int Sensor; // HOLDS PULSE SENSOR DATA FROM ARDUINO
int IBI; // HOLDS TIME BETWEEN HEARTBEATS FROM ARDUINO
int RPM; // HOLDS HEART RATE VALUE FROM ARDUINO
int[] RawY; // HOLDS HEARTBEAT WAVEFORM DATA BEFORE SCALING
int[] ScaledY; // USED TO POSITION SCALED HEARTBEAT WAVEFORM
int[] rate; // USED TO POSITION BPM DATA WAVEFORM
float zoom; // USED WHEN SCALING PULSE WAVEFORM TO PULSE WINDOW
float offset; // USED WHEN SCALING PULSE WAVEFORM TO PULSE WINDOW
color eggshell = color(255, 253, 248);
int heart = 0; // This variable times the heart image 'pulse' on screen
// THESE VARIABLES DETERMINE THE SIZE OF THE DATA WINDOWS
int PulseWindowWidth = 490;
int PulseWindowHeight = 512;
int BPMWindowWidth = 180;
int BPMWindowHeight = 300;
boolean beat = false; // set when a heart beat is detected, then cleared when the BPM
graph is advanced

void setup() {
  output = createWriter( "data.txt" );
  size(700, 600); // Stage size
  frameRate(100);
  font = loadFont("Arial-BoldMT-24.vlw");
  textFont(font);
  textAlign(CENTER);
  rectMode(CENTER);
  ellipseMode(CENTER);
  // Scrollbar constructor inputs: x,y,width,height,minVal,maxVal
  scaleBar = new Scrollbar (400, 575, 180, 12, 0.5, 1.0); // set parameters for the scale
bar
  RawY = new int[PulseWindowWidth]; // initialize raw pulse waveform array
  ScaledY = new int[PulseWindowWidth]; // initialize scaled pulse waveform array
  rate = new int [BPMWindowWidth]; // initialize BPM waveform array
}
```

```

zoom = 0.75; // initialize scale of heartbeat window

// set the visualizer lines to 0
for (int i=0; i<rate.length; i++){
  rate[i] = 555; // Place BPM graph line at bottom of BPM Window
}
for (int i=0; i<RawY.length; i++){
  RawY[i] = height/2; // initialize the pulse window data line to V/2
}

// GO FIND THE ARDUINO
println(Serial.list()); // print a list of available serial ports
// choose the number between the [] that is connected to the Arduino
port = new Serial(this, Serial.list()[0], 115200); // make sure Arduino is talking serial
at this baud rate
port.clear(); // flush buffer
port.bufferUntil('\n'); // set buffer full flag on receipt of carriage return
}

void draw() {
  background(0);
  noStroke();
// DRAW OUT THE PULSE WINDOW AND BPM WINDOW RECTANGLES
  fill(eggshell); // color for the window background
  rect(255,height/2,PulseWindowWidth,PulseWindowHeight);
  rect(600,310,BPMWindowWidth,BPMWindowHeight);

// DRAW THE PULSE WAVEFORM
// prepare pulse data points
RawY[RawY.length-1] =Sensor; // place the new raw datapoint at the end of the array
zoom = scaleBar.getPos(); // get current waveform scale value
offset = map(zoom,0,100,150,0); // calculate the offset needed at this scale
for (int i = 0; i < RawY.length-1; i++) { // move the pulse waveform by
RawY[i] = RawY[i+1]; // shifting all raw datapoints one pixel left
float dummy = RawY[i] * zoom + offset; // adjust the raw data to the selected scale
ScaledY[i] = constrain(int(dummy),44,556); // transfer the raw data array to the scaled
array
}
stroke(250,0,0); // red is a good color for the pulse waveform
noFill();
beginShape(); // using beginShape() renders fast
for (int x = 1; x < ScaledY.length-1; x++) {
  vertex(x+10, ScaledY[x]); //draw a line connecting the data points
}
endShape();

// DRAW THE BPM WAVE FORM
// first, shift the BPM waveform over to fit then next data point only when a beat is found
//if (beat == true){ // move the heart rate line over one pixel every time the heart beats
//beat = false; // clear beat flag (beat flag waset in serialEvent tab)

```



```

for (int i=0; i<rate.length-1; i++){
  rate[i] = rate[i+1];          // shift the bpm Y coordinates over one pixel to the left
}
// then limit and scale the BPM value
//BPM = min(BPM,200);          // limit the highest BPM value to 200
float dummy = map(RPM,0,3000,555,215); // map it to the heart rate window Y
rate[rate.length-1] = int(dummy); // set the rightmost pixel to the new data point
value
//}
// GRAPH THE HEART RATE WAVEFORM
stroke(250,0,0);               // color of heart rate graph
strokeWeight(2);               // thicker line is easier to read
noFill();
beginShape();
for (int i=0; i < rate.length-1; i++){ // variable 'i' will take the place of pixel x position
  vertex(i+510, rate[i]-100);        // display history of heart rate datapoints
}
endShape();

// DRAW THE HEART AND MAYBE MAKE IT BEAT
//fill(250,0,0);
//stroke(250,0,0);
// the 'heart' variable is set in serialEvent when arduino sees a beat happen
//heart--;                      // heart is used to time how long the heart graphic swells when
your heart beats
//heart = max(heart,0);        // don't let the heart variable go into negative numbers
//if (heart > 0){              // if a beat happened recently,
// strokeWeight(8);           // make the heart big
//}
//smooth(); // draw the heart with two bezier curves
//bezier(width-100,50, width-20,-20, width,140, width-100,150);
//bezier(width-100,50, width-190,-20, width-200,140, width-100,150);
// strokeWeight(1);          // reset the strokeWeight for next time

// PRINT THE DATA AND VARIABLE VALUES
fill(eggshell);               // get ready to print text
text("RECIPROCATING WEAR TESTER",245,30); // tell them what you are
text("FRICTION "+Sensor,575,585);
text("MOTORSPPEED ",600,110); // print the time between heartbeats in mS
text(RPM + " RPM",600,500);   // print the Beats Per Minute
text(" Window Scale " + nf(zoom,1,2), 150, 585); // show the current scale of Pulse
Window
output.println( Sensor);
output.println( RPM );
// DO THE SCROLLBAR THINGS
scaleBar.update (mouseX, mouseY);
scaleBar.display();
//
} //end of draw loop

```

APPENDIX D
DESIGN SOLUTION IN DOE LASER SURFACE MELTING AT SPOT SIZE 1.0
MM AND 1.2 MM

Spot size 1.0 mm

Solu tion	Pp (W)	PRF (Hz)	S (mms⁻¹)	Surface roughness (μm)	Microhardness (HV_{0.1})	Desir ability	
1	800.00	90.0	19.20	3.10	989.48	0.86	Selected
2	802.22	90.0	19.20	3.10	989.28	0.86	
3	806.54	90.0	19.20	3.10	988.89	0.85	
4	800.05	90.0	19.21	3.10	989.29	0.85	
5	810.34	90.0	19.20	3.11	988.55	0.85	
6	800.20	89.9	19.20	3.10	988.76	0.85	
7	813.43	90.0	19.20	3.11	988.27	0.85	
8	800.00	90.0	19.23	3.11	989.14	0.85	
9	800.00	89.8	19.20	3.10	988.49	0.85	
10	823.32	90.0	19.20	3.12	987.38	0.85	
11	800.00	89.7	19.20	3.10	987.53	0.84	
12	925.89	90.0	19.20	3.19	978.19	0.81	
13	942.31	90.0	19.20	3.21	976.72	0.80	
14	800.00	89.3	19.47	3.18	982.17	0.78	
15	1070.16	90.0	19.20	3.30	965.26	0.73	

Spot size 1.2 mm

Solu tion	Pp (W)	PRF (Hz)	S (mms⁻¹)	Surface roughness (μm)	Microhardness (HV_{0.1})	Desir ability	
1	800.11	50.0	13.60	4.09	829.91	0.69	Selected
2	809.94	50.0	13.60	4.10	828.98	0.68	
3	800.00	50.0	13.63	4.10	829.04	0.68	
4	800.00	49.6	13.60	4.11	832.21	0.68	
5	825.74	50.0	13.60	4.12	827.47	0.68	
6	800.00	49.8	13.68	4.12	828.61	0.68	
7	831.74	50.0	13.60	4.12	826.90	0.68	
8	800.00	50.0	13.73	4.12	826.17	0.68	
9	800.01	48.8	13.60	4.15	838.09	0.68	
10	844.83	49.5	13.60	4.17	828.83	0.67	
11	832.75	47.8	13.60	4.26	841.61	0.66	
12	1076.01	42.4	13.60	5.30	849.73	0.65	
13	1081.17	42.3	13.60	5.32	849.50	0.65	
14	1072.62	42.0	13.60	5.33	852.28	0.65	
15	1079.77	41.9	13.60	5.37	852.08	0.65	
16	1065.23	42.8	13.60	5.22	848.60	0.65	
17	1078.56	41.1	13.60	5.46	856.98	0.65	
18	1034.02	44.3	13.60	4.97	843.09	0.65	
19	1031.06	44.3	13.60	4.95	842.95	0.65	
20	1021.29	44.4	13.60	4.92	843.70	0.65	
21	1007.94	45.1	13.60	4.82	840.85	0.65	
22	987.04	45.7	13.60	4.71	839.33	0.65	
23	985.19	45.8	13.60	4.69	838.63	0.65	

APPENDIX E
DESIGN SOLUTION IN DOE LASER SURFACE MELTING AT SPOT SIZE 1.4

Spot size 1.4 mm.

Solu tion	Pp (W)	PRF (Hz)	S (mms⁻¹)	Surface roughness (μm)	Microhardness (HV_{0.1})	Desir ability	
1	1799.96	15.00	5.70	5.49	935.87	0.90	Selected
2	1800.00	15.00	5.74	5.48	936.12	0.90	
3	1798.65	15.00	5.70	5.49	935.78	0.90	
4	1798.30	15.00	5.73	5.48	935.94	0.90	
5	1800.00	15.00	6.20	5.40	938.82	0.90	
6	1800.00	15.07	5.74	5.50	934.73	0.90	
7	1800.00	15.07	5.70	5.51	934.34	0.90	
8	1800.00	15.00	6.48	5.35	940.45	0.90	
9	1800.00	15.13	5.70	5.52	933.22	0.89	
10	1800.00	15.00	7.61	5.15	947.08	0.88	
11	1799.98	15.00	7.71	5.13	947.64	0.88	
12	1709.28	15.00	5.88	5.48	930.11	0.87	
13	1800.00	15.00	8.03	5.07	949.46	0.87	
14	1691.27	15.00	5.70	5.52	928.03	0.86	
15	1677.92	15.00	5.70	5.52	927.07	0.86	
16	1757.54	15.00	8.00	5.09	944.59	0.86	
17	1704.28	15.00	7.19	5.26	935.23	0.86	
18	1800.00	15.00	8.52	4.98	952.41	0.85	
19	1746.02	15.00	8.89	4.94	947.72	0.83	
20	1591.25	15.00	5.70	5.55	920.81	0.83	
21	1734.90	15.00	9.31	4.87	948.30	0.82	
22	1544.33	15.00	5.70	5.56	917.42	0.81	
23	1541.77	15.00	5.70	5.56	917.24	0.81	
24	1561.68	15.00	9.50	4.91	925.44	0.79	

UMP

APPENDIX F
DESIGN SOLUTION IN DOE LASER SURFACE MELTING AT SPOT SIZE 1.7
MM

Spot size 1.7 mm.

Solu tion	Pp (W)	PRF (Hz)	S (mms⁻¹)	Surface roughness (μm)	Microhardness (HV_{0.1})	Desir ability	
1	2021.32	8.00	3.30	7.24	920.59	0.74	Selected
2	2020.04	8.00	3.30	7.24	920.50	0.74	
3	2017.62	8.00	3.30	7.25	920.34	0.74	
4	2022.61	8.00	3.30	7.23	920.68	0.74	
5	2027.29	8.00	3.30	7.21	921.00	0.74	
6	2030.64	8.00	3.30	7.20	921.23	0.74	
7	2016.21	8.00	3.30	7.26	920.15	0.74	
8	2011.36	8.00	3.30	7.28	919.91	0.74	
9	2024.66	8.00	3.29	7.23	920.79	0.73	
10	2002.70	8.00	3.30	7.32	919.31	0.73	
11	2000.65	8.00	3.30	7.32	919.17	0.73	
12	2024.69	8.02	3.30	7.23	919.85	0.73	
13	2056.74	8.00	3.30	7.09	923.03	0.73	
14	2063.47	8.00	3.30	7.06	923.49	0.73	
15	2040.69	8.00	3.24	7.21	921.61	0.73	
16	2076.00	8.00	3.30	7.01	924.35	0.72	
17	2080.34	8.00	3.30	6.99	924.65	0.72	
18	2012.49	8.00	3.16	7.41	919.63	0.71	
19	2098.76	8.00	3.30	6.92	925.91	0.71	
20	2123.83	8.00	2.87	7.17	921.91	0.67	
21	2021.32	8.00	3.30	7.24	920.59	0.74	
22	2020.04	8.00	3.30	7.24	920.50	0.74	
23	2017.62	8.00	3.30	7.25	920.34	0.74	
24	2022.61	8.00	3.30	7.23	920.68	0.74	

UMP

APPENDIX G
LIST OF PUBLICATIONS

- Zulhishamuddin, A. R., & Aqida, S. N. (2015). An overview of high thermal conductive hot press forming die material development. International Conference on Automotive Innovation and Green Energy Vehicle. 26 – 27 August 2014 at Swiss Garden and Spa Kuantan. *Journal of Mechanical and Sciences (JMES)* ISSN (PRINT):2289-4659;e-ISSN:2231-8380 volume 9, pp 1686-1694.
- Zulhishamuddin, A. R., Aqida, S. N., & Rahim, E. A. (2016). Optimization of Pulsed Nd:YAG Laser Melting of Gray Cast Iron at Different Spot Sizes for Enhanced Surface Properties. The 19th ESAFORM conference on material forming. 27 -29 April 2016 at Nantes de congress centre. *Journal American Institute of Physics, AIP* (indexed in WoS).
- Zulhishamuddin, A. R., Suffian, R. M., Rashidi, M. M., & Aqida, S. N. (2017). Microstructural Evolution and Phase Transformation in Laser Cladding of Cr and Mo Powder on Grey Cast Iron: Mixture Design of Experiment (DOE). *Journal Material Research Ibero-American Journal of Materials*, p.0-0. ISSN 1516-1439
- Zulhishamuddin, A. R., Aqida, S. N., & Maarof, M. R. (2018). A Comparative Study on Wear Behaviour of Cr/Mo Surface Modified Grey Cast Iron. *Journal Optics and Laser Technology, Elsevier*, volume 104, pp 164 – 169.